Electronic Thesis and Dissertation Repository

5-27-2015 12:00 AM

Application of Polyurethane Products in Accelerated Construction of Innovative Noise Barrier

Bahman Daee, *The University of Western Ontario*

Supervisor: Hesham El Naggar, *The University of Western Ontario*

A thesis submitted in partial fulfillment of the requirements for the Doctor of Philosophy degree in Civil and Environmental Engineering
© Bahman Daee 2015

Follow this and additional works at: https://ir.lib.uwo.ca/etd

Part of the Construction Engineering and Management Commons, Materials Science and Engineering Commons, and the Structural Engineering Commons

Recommended Citation

APPLICATION OF POLYURETHANE PRODUCTS IN ACCELERATED CONSTRUCTION OF INNOVATIVE NOISE BARRIER

(Thesis format: Monograph)

by

«Bahman <u>Daee</u>»

Graduate Program in Engineering Science
Department of Civil and Environmental Engineering

A thesis submitted in partial fulfillment
of the requirements for the degree of
Doctor of Philosophy

The School of Graduate and Postdoctoral Studies
The University of Western Ontario
London, Ontario, Canada

Abstract

Noise barriers (sound walls) are usually constructed along roadways to mitigate the airborne noise emanating from vehicles. They are currently built using various materials including precast concrete panels, masonry, wood and transparent sheets. The main challenge in roadside construction is the obstruction of roadways during the construction, which may result in traffic congestion, public dissatisfaction, car collision and subsequently fatalities. In order to decrease the risk of roadside construction, accelerated and non-obstructive methods are highly preferred by transportation authorities.

An innovative wall system comprised of polyurethane products is proposed, developed and investigated for application in accelerated construction of noise barriers. The proposed sound wall comprises stay-in-place poly-blocks as formwork, two types of polyurethane foam (PF) as structural cores and polyurea as a coating of the wall surfaces. The poly-blocks are stacked layer by layer on the wall footing and form a wall with cylindrical voids. A fast-curing liquid mixture of rigid or light PF is injected into poly-blocks voids to act as the main structural element. Steel rebars connect the PF cores to the wall footing as anchorage system. A polyurea or shotcrete coating is sprayed on both sides of the wall in order to enhance the resistance of poly-blocks surfaces against abrasion, stone impact, weathering, fire development, chemicals and penetration. This construction technique and materials result in less obstruction, faster construction and efficient sound walls in terms of sound attenuation.

A comprehensive experimental program including over 100 specimen and 16 full-scale tests was conducted to determine the materials mechanical properties as well as structural behavior of full-scale walls, which were constructed using different PF and rebar arrangements. In addition, three-dimensional finite element models of the laboratory specimens and the full-scale walls were simulated and verified using the experimental results.

The experimental and numerical results indicated that the structural performance of the proposed wall system is satisfactory for the application of noise barrier according to the relevant building codes. Based on practical observations, the wall system can be

implemented in an accelerated and non-obstructive construction method. Finally, detailed design guidelines are prepared for various practical conditions.

Keywords

Co-Authorship Statement

This thesis has been produced in accordance with the guidelines of the School of Graduate and Postdoctoral Studies. Substantial parts of this thesis have been submitted in peer-reviewed journals. All the experiments, numerical modeling, calibration, interpretation of results and writing the draft and final version of thesis were carried out by the candidate himself, under the supervision of Dr. M. Hesham El Naggar. The supervisor's contribution consisted of providing advice throughout the research program and reviewing the draft and the final thesis and publications results from this research.

Acknowledgments

I would like to express my appreciation to the people who have supported me through this research and have been essential to its completion.

A special thanks to my supervisor Dr. Hesham El Naggar who has been invaluable in providing assistance, guidance and recommendations along the way. His constant technical and motivational supports made these four years unforgettable for me.

Sincere thanks to the manager of Poly-more Canada Inc., Casey Moroschan, for providing the opportunity and funding of this interesting project. I am also grateful to the Poly-more employees, Kevin Moroschan and Jarrod Pare who have tirelessly assisted me in this project.

I am extremely thankful and indebted to Dr. Abbas Samani who shared his feedback, guidance and assistance during this venture.

I would like to thank my friends and staff at Western Engineering for their assistance and support especially Wilbert Logan for all his help in the structural lab.

To my parents, for their unceasing encouragement, support and affections. I am proud to be your son and fully indebted to you because of your dedications and self-sacrifice throughout my life.

Last but certainly not the least, a great gratitude to my lovely wife. She surrounded me with her unconditional love in these years and without her patience, understanding, encouragements, and supports none of my achievements would be possible.

Table of Contents

List of Tables

List of Figures

List of Abbreviations, Symbols, Nomenclature

A_s	Steel area
A_v	Shear area
b	Width of sample
C_e	Wind exposure coefficient
C_g	Gust effect coefficient
C_h	Horizontal drag coefficient
D_b	Diameters of rebar
d	Depth of sample
E	Modulus of elasticity
f_b	bonding strength
f'_c	Compressive strength of concrete
f_y	Yield strength of steel
H	Height
I	Moment of inertia
L	Length of sample
L_b	Lenfth of rebar
M_y	Maximum yield moment

m,n	Material's constants
P	Maximum applied load
q	Mean reference wind pressure
R	Modulus of rupture
t	Time
V_r	Shear resistance
w	distributed load
Δ	Lateral deflection
$\varepsilon(t)$	Strain at the time of t
ν	Poisson ratio
σ_c/σ_t	Compressive/Tensile stress
φ_s	Resistance factor
Φ	Factor of safety

Chapter 1

Introduction

1.1 Overview

This research investigates the application of polyurethane products in construction of noise barriers. The main focuses of the research are to determine mechanical properties of rigid and light polyurethane foams, investigate the structural performance of the proposed wall system and design of the wall in various loading and geometrical conditions. In order to achieve these objectives, an experimental laboratory testing program and extensive numerical analyses were conducted on physical and numerical models. The objectives and outline of the research is described as followings.

1.2 Noise barrier

Noise barriers (sound walls) are usually constructed along roadways to mitigate the airborne noise emanating from vehicles toward residential areas. Sound walls act with different mechanism to reduce the noise intensity. They block and reflect noise, increase noise path and depending on their material can absorb the noise energy to some extent. Noise barrier are designed to reduce 5 to 10 db of noise energy (Federal Highway Administration, 2011).

Transmission loss of noise barriers depends on two factors of height and material. Assuming a sound barrier is solid, sound transmission loss defined as the difference in noise path length before and after the barrier is constructed (I-INCE report, 1999). Based on mathematics involving Fresnel integrals, increasing the noise path from 0.3 to 0.6 m (1-2 ft) will lead to insertion loss from 7-23 db in the frequency range of 31-4000 Hz. This usually can be provided by a 2 m high sound barrier (Paige, 2011).

The barriers material can considerably affect the sound attenuation performance of the wall. While denser barriers such as concrete walls seem to provide more transmission loss, they intensify the noise reflection which ultimately degrades the barrier efficiency.

Hence, sound absorptive materials are found to be more effective where reflection is an issue (I-INCE report, 1999).

Sound barriers are currently built using various materials including precast concrete panels, masonry, wood and transparent sheets. The main obstacle in roadside construction is the obstruction of roadways, which may result in traffic congestion, public dissatisfaction, car collision and subsequently fatalities. Construction vehicles such as truck mixer or mobile crane are required for an extended period of time during the most of roadside constructions. In order to decrease the risks associated with roadside construction, accelerated and non-obstructive methods are highly preferred.

1.3 Proposed noise barrier

Beside the importance of speed of construction technique, superior noise attenuation performance of sound walls is essential, which requires utilizing sound absorbing materials in their construction. Hence, a comprehensive investigation was conducted to examine a speedy construction method utilizing sound absorbing materials for the application of sound barriers. This innovative wall system consists of stay-in-place poly-blocks as formwork, two types of rigid and light polyurethane foam (PF) as structural cores and polyurea as a coating of the wall surfaces. The poly-blocks are stacked layer by layer on the wall footing and form a wall with cylindrical voids. A fast-curing liquid mixture of PF is injected into poly-blocks voids to act as the main structural element. Steel rebars connect the PF cores to the wall footing as anchorage system. A polyurea or shotcrete coating is sprayed on both sides of the wall in order to enhance the surfaces resistance of poly-blocks against abrasion, stone impact, weathering, fire development, chemicals and penetration.

Using these innovative installation technology and materials, the construction of sound walls is faster, less obstructive and more compatible with different geometrical complexities in comparison with common methods and materials. Furthermore, the wall materials are highly sound-resistant and noise absorbing compared to other traditional material.

Sound Transmission Class (STC) rating is defined as an index for the approval of sound barrier materials. The minimum required value of STC is equal to 20 in accordance with Standard Certification of Noise Barrier (CSA-Z107.9, 2003). According to the conducted standard noise transmission tests, STC rating of this wall system is equal to 38 (Acoustic consulting service, 2008). Noise absorbing materials reduce noise reflection more effectively, and thereby perform better where the reflection is an issue.

The proposed wall system can also be employed as a vertical extension to existing sound barriers that are not high enough to block the noise. Most of the provinces across Canada have established a "noise barrier retrofit program", which mainly involves the extension and renewal of the existing sound walls in urban environments, to reduce noise pollution and minimize its impacts on public health. The program also focuses on the sound walls built in the last few decades, which are not high enough and hence are required to be vertically extended 1-2 m to influentially absorb and reflect the vehicles noise.

For this application light polyurethane foam (LPF) was employed rather than rigid polyurethane foam (RPF). LPF is very light, cost-effective and fast-setting foam and it is an appropriate alternative to masonry materials for this application.

The proposed wall system is also easily replaceable and less harmful in vehicular accidents.

1.4 Research objectives

The main objectives of the research conducted as part of this thesis are to:

1- Characterize the mechanical properties of rigid and light polyurethane foams to be employed in the load bearing system of sound barriers.

2- Evaluate the feasibility of employing the proposed wall system as a new or extension of sound barrier.

3- Examine structural performance of the wall system through an experimental program.

4- Determine the wall performance in various design conditions for the investigated application through finite element analyses.

5- Develop a design procedure for the practical implementation of the wall system as a noise barrier.

1.5 Original contribution

To the best of the author's knowledge, the usage of reinforced rigid polyurethane has not been reported in the literatures in the form of this research. Nonetheless, a few attempts have been recently made for the application of polyurethane product in load bearing system of structures. The variety of experiments conducted in this research on polyurethanes for building applications is unique in its own type. The 3D numerical model of the wall including four different materials with various behavioral models is a remarkable feature of this research. This research introduces an innovative construction technique, which can be utilized in accelerated roadside construction and represents the first step towards the usage of polyurethanes in construction of a wall system. It is believed that this study provides a basis for further investigations toward the applicability of polyurethanes in construction of main load-bearing members of structures.

1.6 Thesis outline

Chapter 2 of this thesis presents a comprehensive experimental study on mechanical characteristics of Rigid Polyurethane Foam (RPF) and its application as structural core of the proposed wall system. Mechanical behavior of RPF was characterized by performing tensile, compression, modulus of elasticity, Poisson's ratio, flexural, shear, pull-out, long-term creep and cyclic fatigue tests and the results are presented and discussed. Chapter 2 also describes the outcome of several full-scale static and cyclic tests on wall models, which were fabricated and their lateral performance were established. Applicability of the proposed wall system (poly-wall) in accelerated construction is discussed and preliminary design calculations of poly-wall were also carried out.

Chapter 3 presents numerical investigations on the performance of poly-wall consisting of poly-block, RPF and polyurea coating. The experimental results are used in this

chapter to develop, calibrate and verify 3D finite element (FE) models of poly-wall components including steel rebars, poly-blocks and RPF cores. In this chapter, the verified numerical models are used to conduct a parametric study on the performance of poly-wall models under uniform vertical pressure as well as wind loading. Accordingly, a simplified approach for the design of poly-walls is proposed and discussed.

Chapter 4 presents an experimental and numerical study on structural performance of a noise barrier consisting of poly-block, light polyurethane foam (LPF) and polyurea. This wall system (flexi-wall) is intended to be employed as a vertical extension to existing sound barriers in an accelerated construction method. This chapter entails several mechanical tests conducted on LPF specimens and several full-scale flexi-walls. The results of several static and lateral cyclic loading on full-scale flexi-walls are discussed in this chapter and a preliminary design procedure for the investigated application was also described.

Chapter 5 presents a detailed design procedure for poly-wall and flexi-wall based on the results of the comprehensive experimental and numerical analyses described in previous chapters. The results of the analyses provided a basis for the design of the proposed walls with different heights and under different loading conditions.

Chapter 6 provides general conclusions and some recommendations for future works.

1.7 References

Acoustic consulting service (2008). Sound Attenuation Certification and Report, www.lexiconbuildingsystems.com.

Canadian Standard Association. (2003). CAN/CSA-Z107.9-00, Standard for Certification of Noise Barrier, Ontario, Canada.

Federal Highway Administration. (2011). USDOT (FHWA-HEP-10-025), "Highway Traffic Noise: Analysis and Abatement Guidance." Washington, D.C.

I-INCE report (1999). Technical Assessment of the Effectiveness of Noise Walls, Noise/News International, Vol. 7, pp 137-161.

Tom Paige (2011). Outdoor Noise Barriers, Design and Applications. Report of Kinetic Noise Control Inc. Mississauga, Ontario.

Chapter 2

Application of Rigid Polyurethane Foam in Accelerated Construction of an Innovative Noise Barrier: Experimental Study

2.1 Introduction

Rigid Polyurethane Foams (RPFs) are widely utilized in different industries such as electronic, automotive and aerospace. Versatility, light-weight, fast-curing, high mechanical strength, water and sound resistance etc., are the main attributes that have introduced RPFs as a suitable alternative to conventional materials. In construction, however, they are mainly implemented as non-structural elements of buildings. Sandwich composite panels, claddings and coatings, transparent sheets and insulation boards are most common applications of Polyurethane products. Although some efforts have been recently made to use polyurethanes as structural segments, the supporting academic researches showing their structural performance are rather limited.

Some studies were undertaken to assess structural behaviour of prefabricated composite wall systems and sandwich panels, which incorporate RPF as a structural core (Manalo, 2013; Sharaf et al., 2011; Ruiz et al., 2014). There have been also new interests in adding polyurethanes in concrete mixture to improve its functional properties (Agavriloaie et al., 2012; Ramamurthy et al., 2009). Mechanical properties of RPF exponentially correlate with its density, and the compressive strength of high density RPFs is quite comparable to that of conventional masonry (Chen et al., 2002; Qoods et al., 1998). Application of high-density RPF as a backfill material has been also investigated and its suitability for pavement repairs has been verified in practice (Priddy et al., 2010).

The usage of polymer blocks as stay-in-place formworks has recently become widespread. Verity of polyurethane blocks with different shapes and densities have been manufactured to be employed as a formwork in wall construction. Besides high functionality, sound resistance and heat resistance, polymer encasement provides enhanced curing conditions for cementitious cores of the walls, which ultimately results

in higher quality and strength (Chahrour et al., 2005). Modular construction also reduces construction time and requires less skilled labor which subsequently leads to higher cost-efficiency of projects.

The proposed innovative noise barrier (poly-wall) comprises stay-in-place poly-blocks as formwork, RPF as structural core and polyurea as coating of the wall surfaces. For construction of poly-wall, poly blocks are stacked on the wall footing in order to form a formwork and then liquid mixture of RPF is injected into poly-blocks voids. Rebar dowels connect the RPF cores to the foundation and polyurea is sprayed on the wall surfaces to protect them from abrasion and impact. Detailed characteristics of the mentioned components of poly-wall will be discussed later in this chapter. This research has been also followed by a numerical study described in Chapter 3 and another literature by authors (Daee and El Naggar, 2015).

2.2 Objectives

Two objectives were followed in this part of research. Firstly, the mechanical properties of RPF were determined. For this purpose, an extensive experimental program including tensile, compression, modulus of elasticity, Poisson's ratio, flexural, shear, pull-out, creep tests and cyclic test was conducted on RPF specimens. Secondly, the structural performance of poly-wall as a noise barrier as well as its applicability in accelerated construction was examined. Hence, four full-scale walls were constructed and tested to verify the wall performance under lateral loading. A full scale poly-wall was also subjected to a cyclic loading encompassing 15,000 load cycles in order to determine its fatigue performance. The abrasion resistance of polyurea coating was also examined and finally, a preliminary design of poly-wall according to applicable building standards was performed.

2.3 Components of the poly-wall

2.3.1 Poly-blocks

A poly-block is made of molded low-density polyurethane and weighs approximately 1kg. As shown in Fig. 2.1, this block is 200x200x800 mm and includes four cylindrical

voids with 140 mm diameter. Poly-blocks are modular interlocking blocks, which can be stacked layer by layer and form a wall with cylindrical voids. In essence, the blocks are permanent molds which maintain the structural cores over the curing process. The voids can be filled by any type of building material such as concrete, fiber reinforced grout, etc; however, RPF mixture were used in this research work.

Poly-blocks are light-weight, easy to install, architecturally flexible and fire resistant. Where a continuous wall is not essential, the discrete structural system provided by poly-blocks may lead to less material consumption and subsequently improved cost-efficiency in comparison with other types of formworks such as ICF (Insulated Concrete Forms). Additionally, conducted acoustic tests proved their effective capability to absorb, mitigate and reflect a wide range of noises with unmatched frequency of reflective noise.
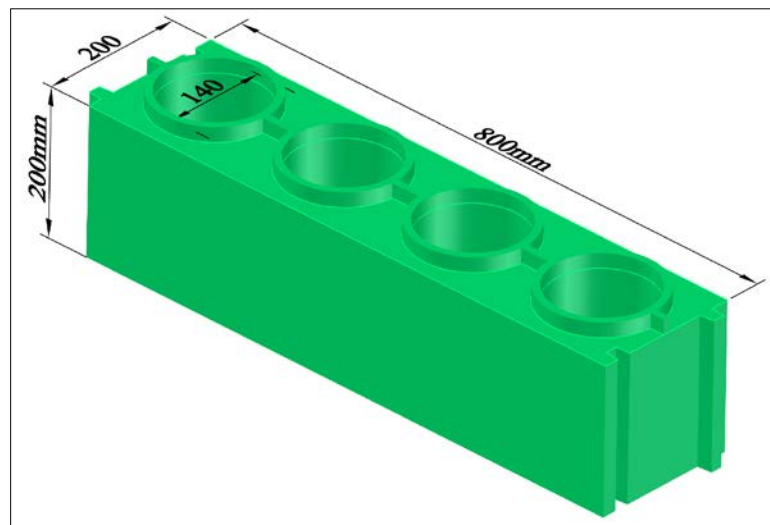
Figure 2.1: Poly-Block shape and dimensions

2.3.2 Rigid polyurethane foam (RPF)

Polyurethanes (PU) are composed of a chain of diisocynates and polyols (Li et al., 2013) and their characteristics vary extensively by changing the mix proportion, additives and processing conditions such as temperature and pressure. Given the versatility and formability of PU, a range of products from seat cushions to protective parts of military aircrafts can be produced. In recent decades, Rigid Polyurethane Foams have been

incorporated in building elements owing to their high strength and durability; however, their application is mainly limited to fabrication of non-structural elements.

In this research, a specific mixture of a high strength RPF with 1100 kg/m^3 density was used and reinforced by steel rebars as a main load-bearing element. The components of this RPF were mixed in liquid form below 60°C and then were injected into poly-blocks voids. This rigid foam usually cures after 6-10 minutes and gradually reaches its maximum strength in less than an hour in ambient temperature. As displayed in Fig. 2.2, RPF posts inside poly-blocks are the structural segments that withstand and transfer applied loads to the footing through the dowels.
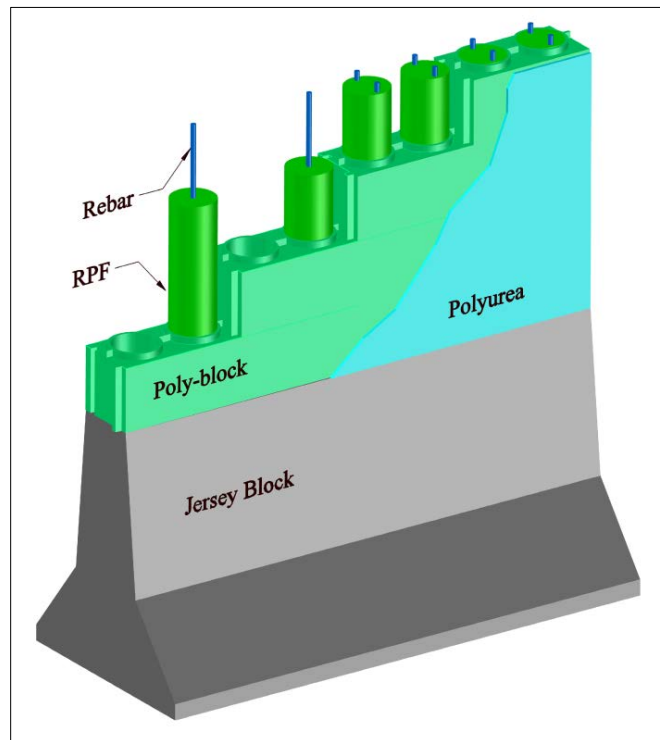
Figure 2.2: Poly-wall made of Polyurethanes

2.3.3 Polyurea coating

Polyurea is a product of a fast-growing technology that involves spraying high-elongation elastomers on different surfaces in order to protect or strengthen them. The chemical structure of polyurea coatings is similar to PU but its mixture contains Polyamin as a resin instead of Polyol. Polyurea coatings are fast-setting, flexible, chemically-stable and

long-lasting material and their characteristics for specific application may be varied by changing the additives. The applications of polyurea in strengthening of concrete members, structural enhancement of cementitious composites as well as improving the blast resistance of masonry walls have been investigated. In theses researches, significant improvements of flexural resistance, ductility and sustainability of elements in large deflections have been reported (Greene et al., 2013; Choi et al., 2013; Irshidat et al., 2011). Some polyurea coatings are corrosion resistant and studies have shown their capabilities as spray-on lining materials in pipeline systems (Motlagh et al., 2013).

In this study, a polyurea coating was sprayed on both sides of the wall panels in order to enhance the surface resistance of poly-blocks against abrasion, stone impact, weathering, fire development, chemicals and penetration. In order to quantify the abrasion resistance of this polyurea coating, four "Taber Abrasion" tests were conducted in compliance with "Standard Test Method for Abrasion Resistance of Coatings" (ASTM D4060-10). In these tests, samples are fixed on a turntable and they rotate in contact with two weighted abrader wheels for usually 1000 cycles. Then, the thickness of the coating is measured and wear indications are calculated. Results of the performed tests revealed that "Wear Cycle per mil" of the samples exceeds 10000 cycles on average which categorizes the polyurea coating as a "highly abrasion-resistant" finish (Fig. 2.3).
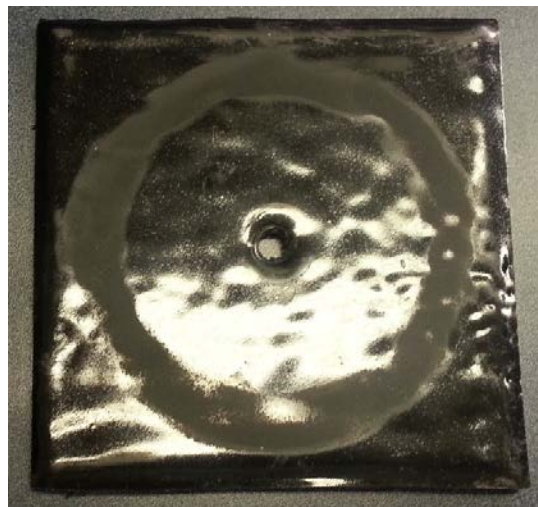
Figure 2.3: Polyurea coating sample after Taber abrasion test

2.4 Construction of sound walls

Sound walls are usually constructed along roadways to mitigate the airborne noise emanating from vehicles. The barriers are designed to reduce the sound level between 5 to 10dB by absorption, reflection and diffraction of the sound waves (FHWA-HEP-10-025). However, road side construction often requires lane closure of roadways for a quite long time, which may cause public dissatisfaction, traffic congestion and even road accidents. Hence, accelerated and non-obstructive methods are more desirable in urban developments and road constructions.

The proposed sound wall (Fig. 2.2), which is composed of aforementioned polymer products, can be employed in accelerated roadside construction. Light-weight poly-blocks, fast-setting RPF and spray-on polyurea all significantly speed up the construction of sound walls. Required equipment for the injection of RPF and spraying polyurea coating such as pumps, hoses and liquid containers are all portable and can be easily unloaded on construction site. Since Poly-wall is comparatively light-weight, a gravity foundation system such as "Concrete Jersey Barriers" would be designed and used as the wall footing. These pre-cast blocks significantly reduce the cost and time of construction, raise the elevation of Poly-wall and protect it from damages caused by vehicles impact.

2.5 Testing environment, machines and procedures

All specimens and full-scale walls were made and tested in laboratory environment where the average temperature was $23^0C\pm2$ and the experimental program commenced two weeks after the samples preparation. All RPF specimens were made of a single batch of polyurethane and resin. Five different testing machines with various capability and capacity ranging from 250 kN to 1600 kN were used depending on the size of specimen and type of the test. Comprehensive efforts were made to identify the proper test procedures specific to high strength RPF as a structural member. However, the extensive literature review revealed a lack of such standards, hence the ASTM procedures recommended for concrete and rigid plastics were followed. Given the lack of standardized specimen size, the specimens' dimensions were selected such that they represented the practical conditions. Loading rates were selected based on some

preliminary trials to induce failure within 45 to 90 seconds in accordance to ASTM procedures (ASTM C39, ASTM D1621 ASTM D3039). The specimen tests were performed on five samples in most of cases however; where results impact on numerical analysis was less significant for the numerical analysis three tests were conducted.

2.6 Tensile test

Uniaxial tensile tests were carried out on dog-bone samples (Fig. 2.4a) using an Instron Mechanical Tester (Fig. 2.4b). Five specimens were cut and machined out of a RPF solid block. The grips cross-section of the test specimen was 22x22 mm and the narrow cross-section was 15x15 mm. An extensometer was installed at mid-length of the narrow section to record the strain within 30 mm. The loading rate was selected as 1 mm/min based on failure duration of sacrificial samples.

The experimental results of five tensile tests on RPF samples are depicted in Fig. 2.5. All the samples illustrate a linear trend up to 40 MPa at which point cracking initiates. The average value of tensile failure stresses (52.2, 57.44, 58.93, 57.03 and 47.45 MPa) was 54.6 MPa corresponding to strain of 3.3%. The results demonstrated a consistent tensile behaviour for all specimens, i.e., all failed within the narrow section in a sudden and brittle manner.
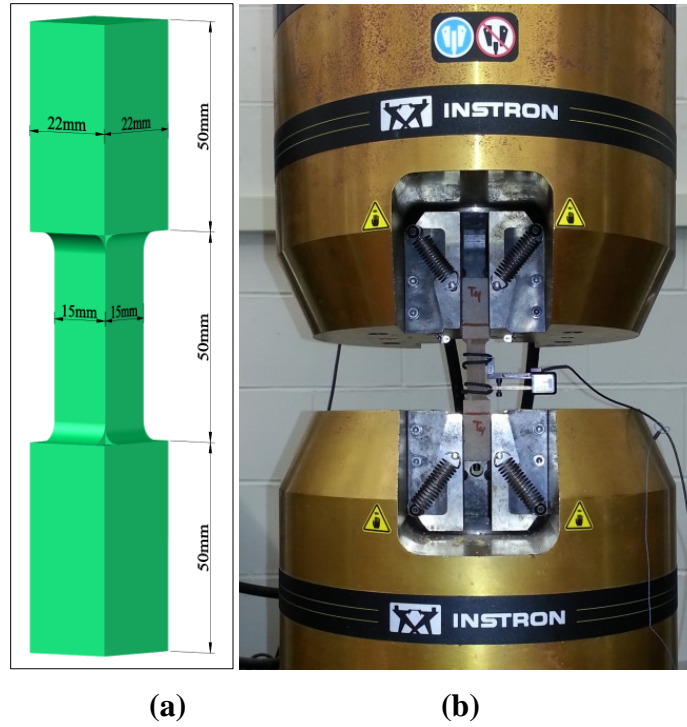
Figure 2.4: Tensile test specimen (a) and testing machine (b)
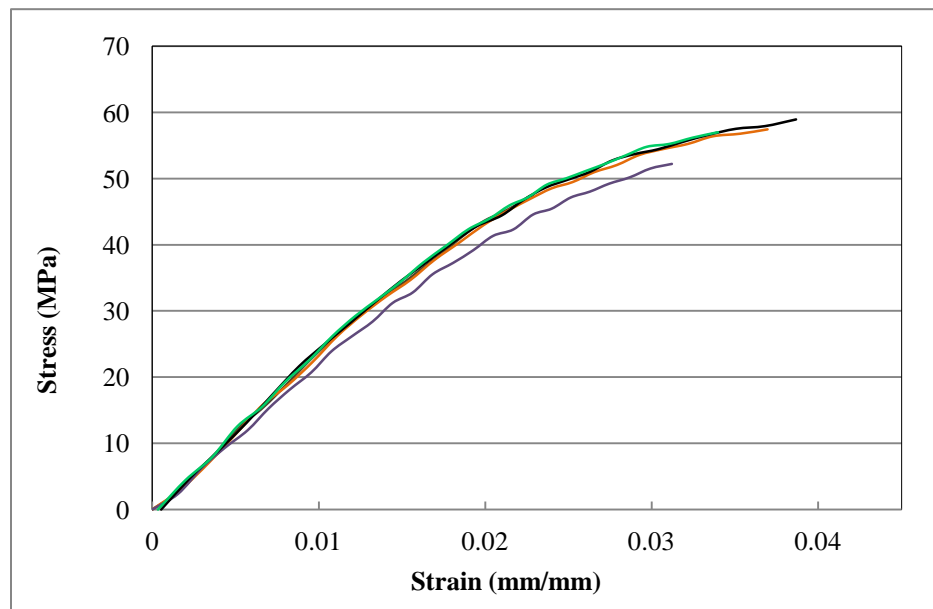
Figure 2.5: Tensile stress-strain relationship of five RPF specimens

2.7 Compression test

To establish compressive behaviour of RPF, five cylinder samples with 280 mm height and 140 mm diameter were made and tested. To make cylinder samples, an assemblage consisted of three poly-blocks was prepared as a mold and the RPF was injected into the voids. After setting of RPF was complete, poly-blocks were broken and the cores were taken out. The samples were then cut in 280 mm long pieces. The top and bottom surfaces of samples were completely grinded and levelled. The samples were loaded at the rate of 2.5 kN/sec through two steel plates in order to uniformly distribute the load (Fig. 2.6). Vertical strain was recorded through 30 mm strain gauges, which were installed on the mid-height of the samples. Load-displacement response of the load cell of testing machine was also acquired at the same intervals. The mix proportion of the RPF components was selected by the supplier to attain a minimum of 20 MPa compressive strength.

The results of compression tests for five specimens are illustrated in Fig. 2.7. All samples demonstrated a semi-linear compressive behaviour up to strain of 0.75-0.8%, at which point the slope slightly varied due to cracking and fracture. The ultimate compressive capacity values were obtained equal to 22.9, 23.2, 24.45, 24.6 and 26.2 MPa with an average of 24.2 MPa. Based on tests observations, all samples failed in a sudden and brittle manner although some cracks appeared on surface of the samples immediately before failure. Such compressive behavior for RPF has been previously reported (Ridha, 2007). According to ASTM C39-12 for concrete specimens, the fracture pattern of all RPF samples was type 1 or 2 which means that at least one cone formed at either end and detached from the sample at the failure moment.

Figure 2.6: Compression test set-up
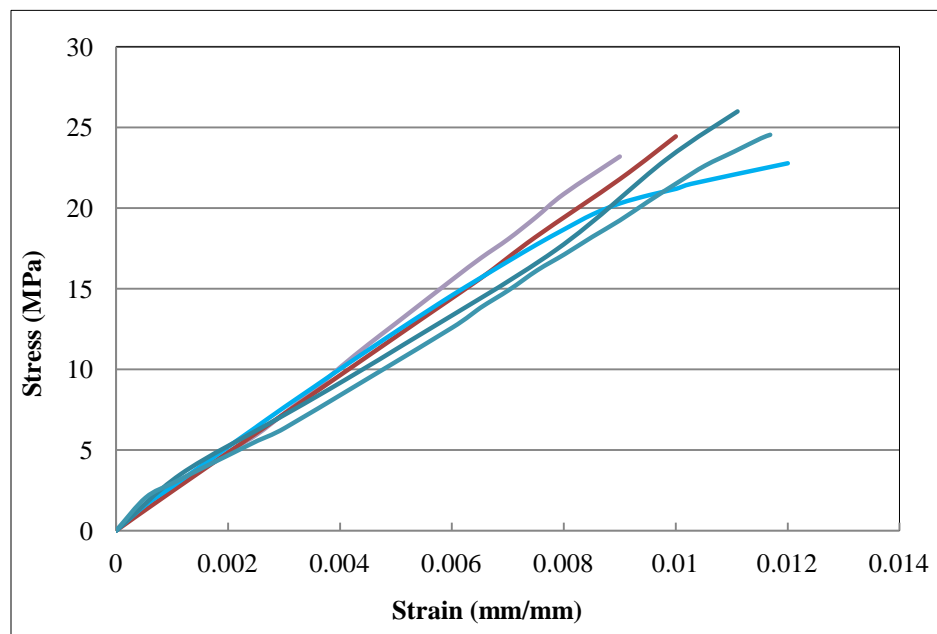
Figure 2.7: Compressive stress-strain relationship of five RPF specimens obtained

from strain gauges

2.8 Modulus of elasticity

Modulus of elasticity in tension and compression (Et & Ec) were calculated using the stress-strain relationship obtained from both tensile and compression tests. RPF samples exhibited a linear behavior in the tests hence; modulus of elasticity was calculated based on stress equal to 40% of ultimate strength in each case. Et and Ec were found identical and equal to 2.3 GPa on average. Since tensile and compressive behaviors of RPF were acquired through a 30 mm part of the samples (i.e. local strain), the fair alignment of the slopes shown in Fig. 2.8 is acceptable, although Et and Ec were achieved from two different tests. This consistency of tension and compression behavior of RPF in the linear range has been previously observed (Rizzi et al., 2000).
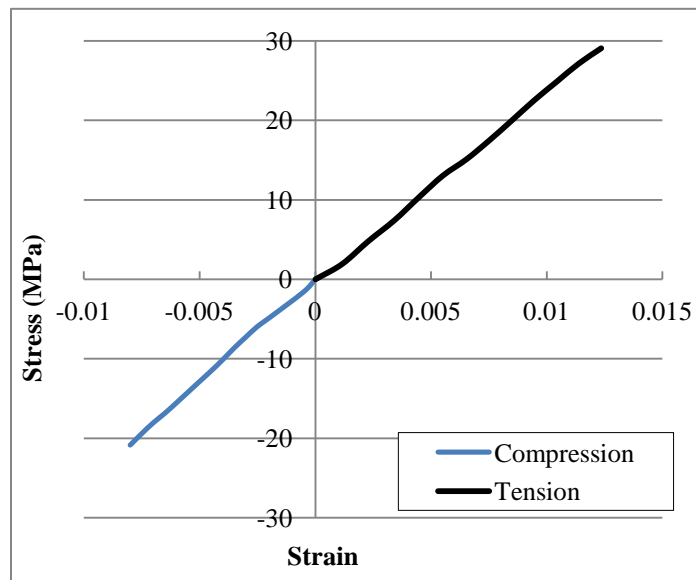
Figure 2.8: Stress-strain relationship obtained from tensile and compression test

2.9 Poisson's ratio

Poisson ratio was established in compliance with described procedure in ASTM C469-10. For this purpose, the cylinder samples were made similar to compressive specimens and the micro measuring apparatus was appropriately mounted on them (Fig. 2.9). Three samples were loaded up to 40% of average compressive strength (9.6 MPa). During loading, longitudinal and lateral strains were recorded and calculations were carried out

as specified in the ASTM standard. The Poisson's ratios of RPF samples were obtained equal to 0.213, 0.224 and 0.226 with the average value of 0.22, which is within the range of values for engineering materials.

Figure 2.9: Poisson ratio test set-up

2.10 Third-Point Loading Flexural Test

The flexural tests were performed on five RPF beams by using the third-point loading method according to specified procedure in ASTM C78-10 standard. The samples were formed in 150x150x530 mm plastic molds. A thick plastic sheet was placed into the molds and was greased to ease demolding of the beams. Liquid mixture of RPF was then poured into the molds, and after a few minutes samples were removed from the molds. Fig. 2.10 illustrates the test set-up for the flexural tests. In addition to actuator readings, two Linear Variable Differential Transducers (LVDTs) were installed at the beam center in order to record the maximum displacement at the top surface.
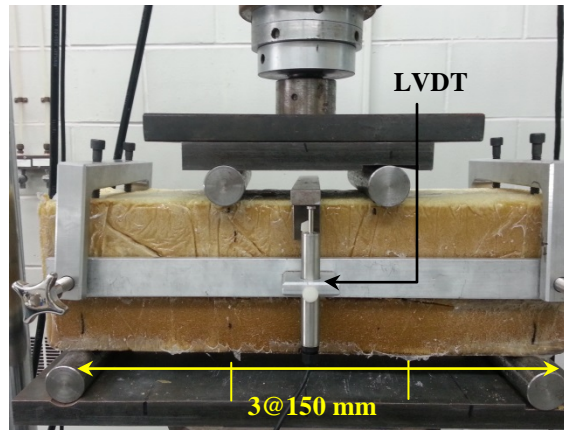
Figure 2.10: Test set-up of three-point flexural test

Load-deformation relationships of five specimens are depicted in Fig. 2.11. It can be seen that all samples displayed a nonlinear flexural behavior with a slight increase in slope at larger displacements. It was observed that all samples experienced sudden and brittle failure in flexural mode. The average resisting force was found to be 72.7 kN (using the obtained values of 64.3, 64.0, 68.99, 82.17and 84.4 kN) and the deflection at failure ranged from 7.54 to 8.77 mm, and modulus of rupture (R) was found to be 9.6 MPa according to Eq. 2.1, i.e.

$$R = \frac{PL}{bd^2}$$
(2.1)

Where L, b and d are respectively span length, width and depth of the beam and P is maximum load.

It is worth mentioning that the only underlying assumption of Eq. 2.1 is that neutral axis coincides with horizontal axis of symmetry regardless of type of stress-strain relationship in a cross-section. Since a consistent behavior in tension and compression was established, Eq. 2.1 is applicable for the RPF beams.
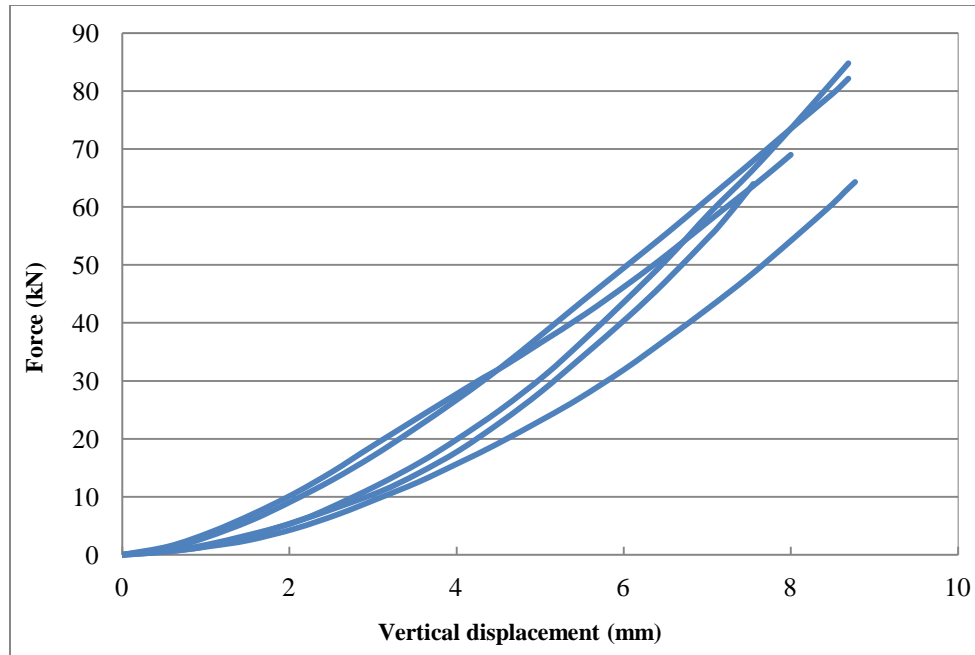
Figure 2.11: Flexural behavior of five RPF samples

2.11 Shear test

The shear strength of RPF is essential to estimate the shear capacity of the full-scale walls. Researchers have attempted to establish suitable test arrangements in order to determine the pure shear strength of different materials (e.g. concrete) as no standard test procedure was available (Bazǎnt et al., 1986; Majdzadeh et al., 2011; Khanlou et al., 2013). In this research, an attempt was made to select a proper specimen shape to minimize the effect of other stresses associated with shear stress during the experiment; and to realistically represent the shear capacity of RPF cores in poly-wall. Thus, five RPF cylindrical test specimens, similar to the compressive samples (140x280 mm), were made. Two 25 mm notches were circumferentially created adjacent to the supporting bars in order to dictate the failure in shear mode (Fig. 2.12). The specimens were loaded at the rate of 0.6 kN/s through two loading points adjacent to pre-defined shear planes. Some sacrificial specimens were tested to ensure that the specimens fail at the notches, and the minimum depth of 25 mm was selected accordingly.

The shear test results depicted in Fig. 2.13 demonstrated that the shear stress is mainly proportional to strain, although an initial stiffening appears in the plots at deflections less than 0.4 mm. The shear capacity values were obtained equal to 4.24, 4.18, 4.48, 4.5and 3.99 MPa with an average of 4.28 MPa. It was observed that all specimens failed through the pre-defined shear plane.
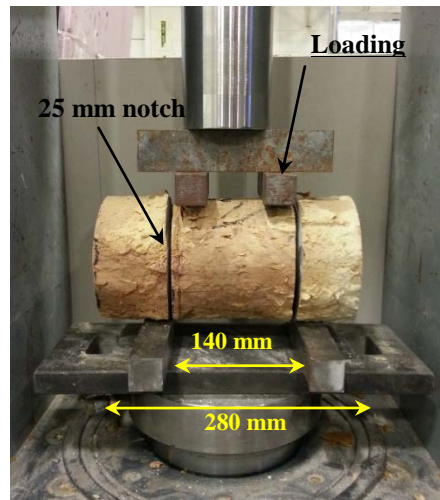
Figure 2.12: Shear test set-up
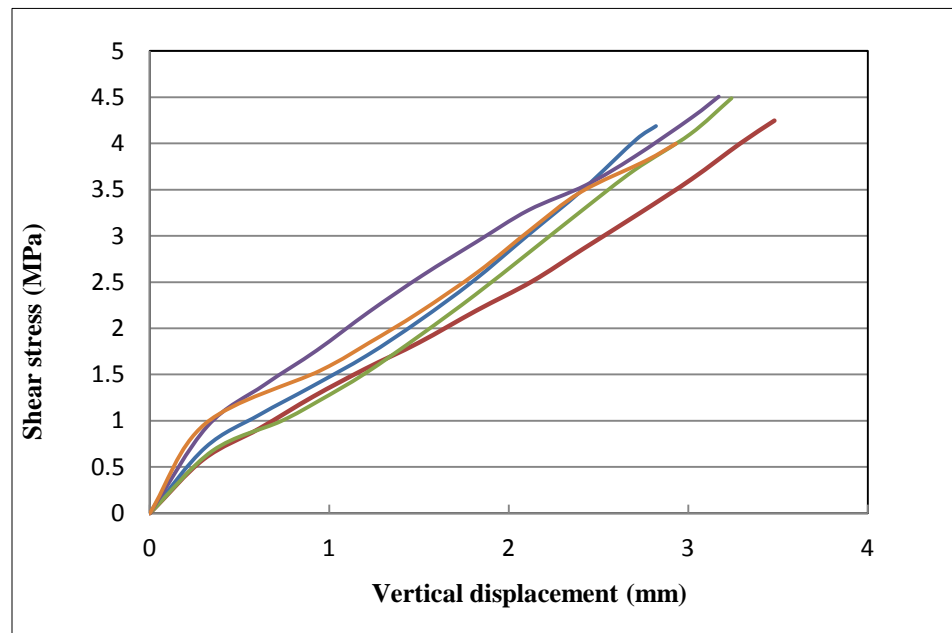
Figure 2.13: Shear stress-strain relationship of RPF

2.12 Pull-out test

The main objective of the pull-out test was to quantify the bond strength of steel rebar to RPF by measuring the required force to pull the embedded rebar out of the RPF core. Rebar dowels in the proposed wall structural system transfer the load to the wall footing and their length influences the wall lateral stiffness. For this test, two wood formworks were made as shown in Fig. 2.14a to hold the rebars at the center of the poly-block voids. RPF was injected into the voids and allowed to harden, the formwork was then demolished and the samples were removed.

Rebar sizes of 10M and 15M with f_y = 400 MPa (Grade 400R of CSA-G30) were selected and the net rebars' embedded length was 380 mm. The samples were assembled in the testing machine as displayed in Fig 2.14b. The rebars were pulled at the rate of 1 kN/s while RPF cores were held by the fixed cross-head of the test machine. The test was repeated for 4 samples of each rebar size. The peak tensile force (P) was recorded to calculate the bonding strength (f_b) assuming that stress is uniformly distributed along the embedment length of rebar, i.e:

$$f_b = \frac{P}{\pi D_b L_b} \tag{2.2}$$

Where D_b and L_b are diameter and embedment length of rebar, respectively. The average results of each four tests for 10M and 15M rebars were found to be 4.8 MPa and 4.29 MPa, respectively. The obtained bond strength values for 10M were equal to 4.86, 4.84, 4.76 and 4.73 MPa and for 15M were equal to 4.19, 4.22, 4.34 and 4.42 MPa, while the standard deviation of all 8 test results was less than 7%. The predominant mode of failure for all specimens was splitting mode and no slip failure occurred.
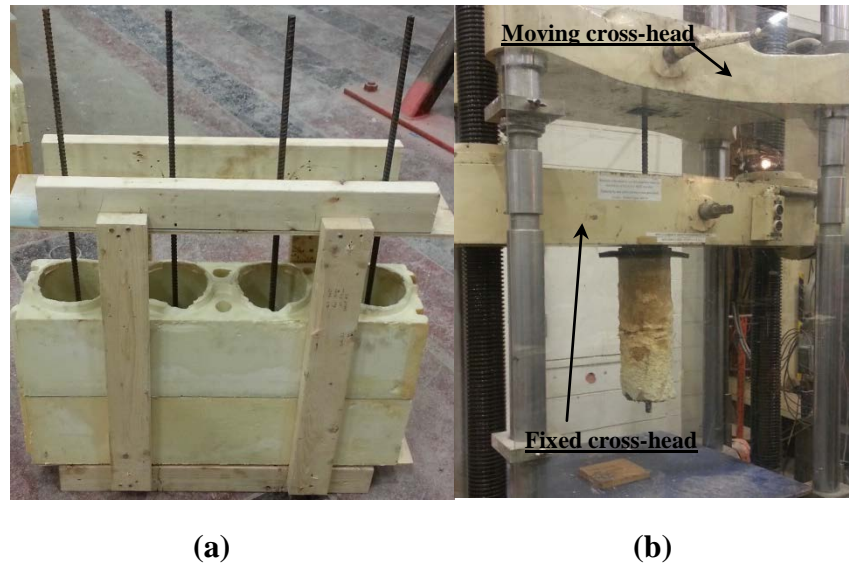
Figure 2.14: Pull-out test arrangements a) Pull-out test formwork, b) Pull-out test set-up

2.13 Creep test

Utilization of new composites in construction has been always a concern for designers. Despite the advantages of new materials, they have not been widely examined in practice and therefore their long-term performance over the life span of buildings is unknown. However, this issue can be addressed by performing short-term tests in laboratory environment and prediction of their long-term behavior by extrapolation of the test data (Behjat et al., 2014; Briodya et al., 2012).

RPF is a "closed-cell" material, which means there are discrete trapped air bubbles in its microstructure. The wall cells bend under pressure and may gradually collapse under long-term loading, which results in densification of the material. Most of polyurethanes show a nonlinear and viscoelastic compressive behavior, which signifies the fact that creep strain increases disproportional to applied stress and advances in constant pressure. The creep response of polyurethanes can be given by (Huang et al., 1991):

$$\varepsilon(t) = \varepsilon_0 + mt^n \tag{2.3}$$

Where ε_0 and $\varepsilon(t)$ are strain values at time zero and t, respectively, m and n are material's constants and t is time. Eq. 2.3 was found to agree with experimental results (Huang et al., 1991).

In this study, creep tests were performed on four specimens to evaluate their viscoelastic behaviour over the time. The specimens' size, loading rate and test set-up were selected identical to the compressive test specimens. However, the load was gradually increased and then held constant for 72 hours at a certain value corresponding to 5, 8, 12 and 14 MPa. For comparison of experimental and empirical results, a power function was fitted for each value of stress based on 48-hour test data using Eq. 2.3. The power regressions were conducted through the "least-squares method" and the fitted curves were extended to 72 hours. The results of creep tests are depicted as dotted lines and Eq. 2.3 predictions are shown as dashed lines in Fig. 2.15.

The results show that the creep strain of all specimens was in secondary stage of creep process in which the strain steadily develops with a negligible rate. The creep rate is slightly higher at greater applied stresses, but in most cases the rate slowed down after one day. The power functions are also in good agreement with the results of the third day.

Vertical loads and creep strain are not key factors for design of noise barriers, as lateral loads mostly govern the design. Nonetheless, the creep test results furthered our understating about RPF behavior since viscoelastic deformations of RPF were found within an acceptable range compared to other types of foams. However, more extended creep tests are essential for estimating long-term creep strains.
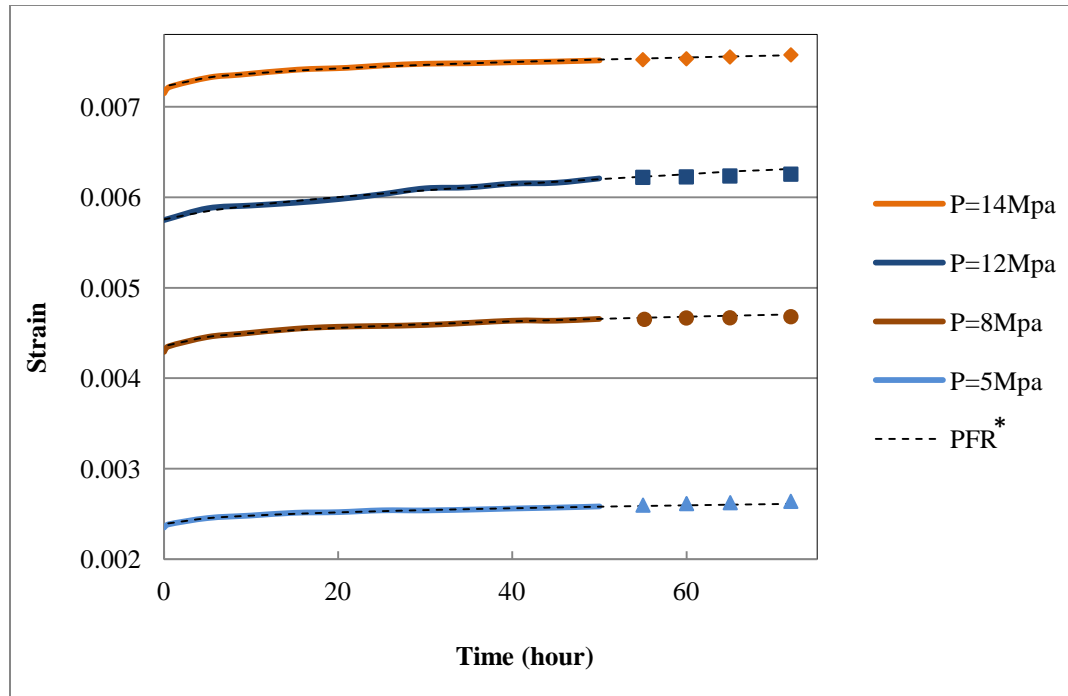
Figure 2.15: Creep compression strain versus time for four values of stress (P)

*The dashed line indicates the curves fitted to 48hr test data using Eq. 2.3. Dots indicate test result within the third day of the creep test.

2.14 Poly-block compression test

Poly-block is made of low-density ($50kg/m^3$) closed-cell polyurethane foam. Under uniform pressure, light foams typically deform linearly until they reach their yield point, which is followed by a plateau with small stress variation. The plateau region is irrecoverable and continues up to large strains at which point densification initiates. As the cell walls of the foam buckle and collapse, air escaping and stiffness hardening continue until the ultimate failure occurs (Schreyer et al., 1994).

To determine the compressive behaviour and particularly the yield strength of poly-blocks, three compression tests were carried out. In practice, the blocks are coated with polyurea which may slightly provide a circumferential confinement for the blocks. Hence, the blocks were coated with polyurea and then tested to account for possible effects of polyurea on the compressive behaviour of poly-block. The load was applied at the rate of 0.5 kN/s through the moving crosshead of the testing machine and was distributed as uniform pressure using steel plates. Since poly-blocks underwent very large

deflections, true strain was calculated rather than less accurate engineering strain. The test was stopped at 50% of deflection as it was beyond the engineering strain range. Two poly-blocks before and after compression test are exhibited in Fig. 2.16.

The dashed lines in Fig. 2.17 illustrate the compressive stress versus true strain of poly-blocks acquired from the experiments. In all cases, a peak was observed at the yield point, and the average strength within the plastic region was about 0.5 MPa. The solid line in Fig. 2.17 is a bilinear representation of the idealized average poly-blocks compressive behaviour, which was calculated based on the test data. It can be observed that the test results are consistent with the typical behaviour of low-density foams.

Figure 2.16: Poly-block before and after compression test
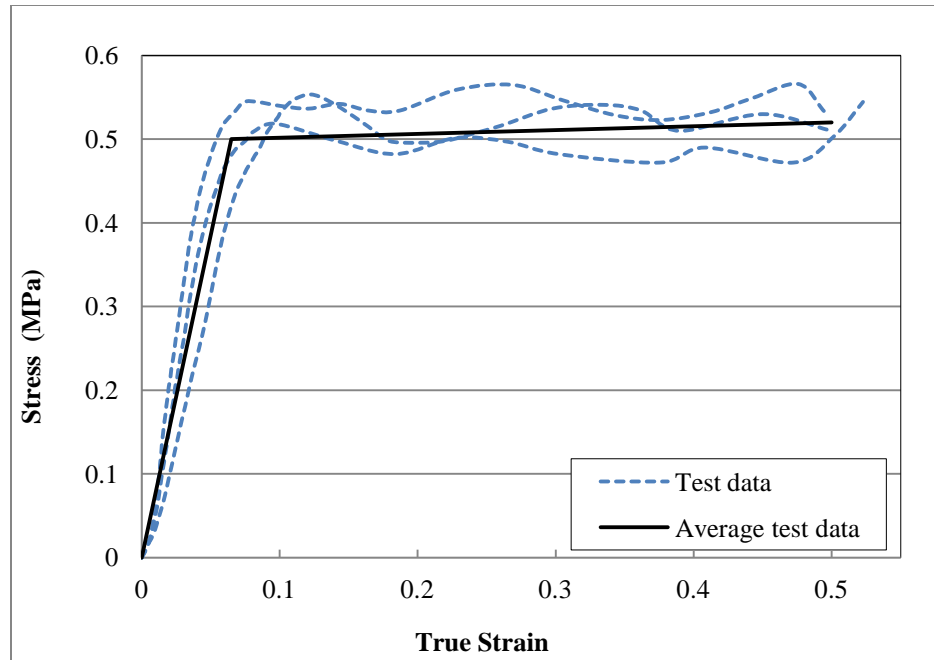
Figure 2.17: Compressive Stress-strain relation of Poly-block

2.15 Full-scale push-over test

Four full scale wall tests were carried out to investigate the performance of the proposed wall system under simulated field conditions. As wind load is the predominant load used in design of noise barriers, the first aim of the full-scale wall tests was to assess the lateral resistance of poly-wall. The experimental results are used to calibrate and verify the finite element model and to demonstrate the feasibility of the poly-wall design. The second aim was to monitor the construction approach for the first time and verify the applicability of the wall system in accelerated constructions.

Initially, wood formworks were made for the wall footings and concrete with f'$_c$=30 MPa was cast in place. The formworks were then disassembled, top surface of footings was leveled and the positions of rebars were marked. Although in actual field applications, the dowels could be inserted into the formwork with specified spacing before the concrete placement, it was easier in the laboratory setup to drill dowel holes after curing the concrete and epoxy the rebars into the holes. Hilty epoxy of HIT-HY150MAX-SD which

provides a bond strength greater than concrete to steel bond was used to ensure that rebars would not slip.

The first course of poly-blocks were positioned on the footings and epoxied in order to prevent dislocation of poly-blocks and leakage of RPF during the injection into the voids. The rest of the blocks were stacked on the first course and epoxied together. To ensure that RPF liquid does not leak out of the block joints, a layer of polyurea was sprayed to seal up all the seams and joints. Figures 2.18, 2.19 and 2.20 show some of the construction steps of the walls.
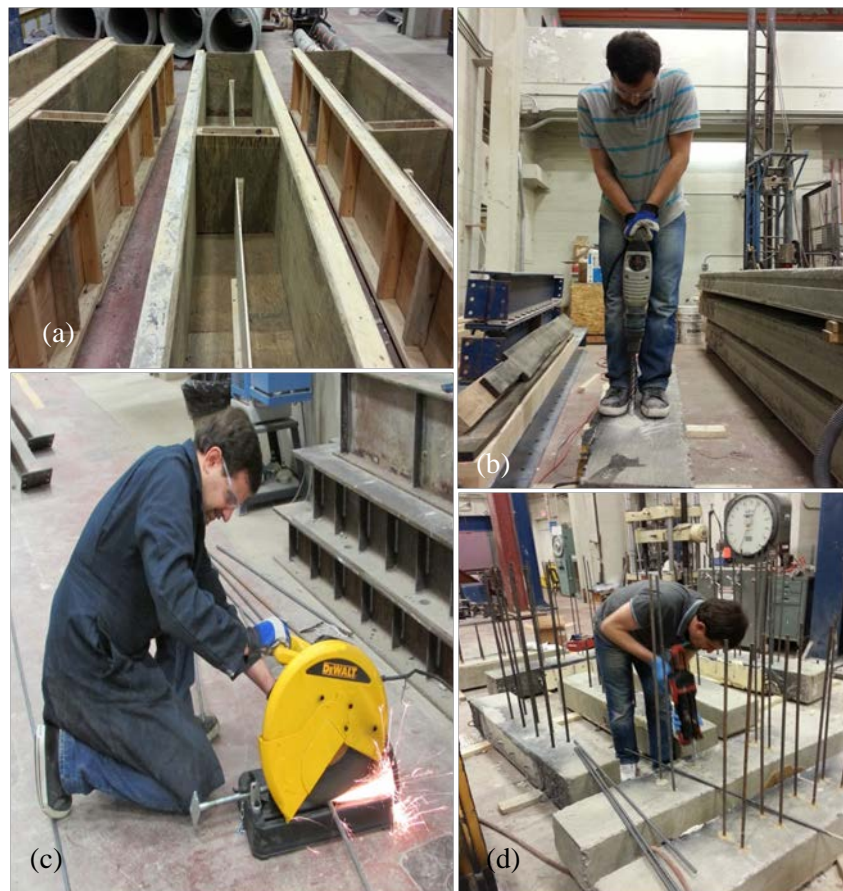
Figure 2.18: Construction steps of the walls, concrete works

(a) Construction of wood formworks for concrete footing, (b) Drilling holes into footings, (c) Rebars cut, (d) Rebars insertion and epoxy

Figure 2.19: Construction steps of the walls, wall assembly

(a) Concrete surface levelling, (b) Stain gauge installation, (c) Poly-block glue, (d) Poly-blocks stacking
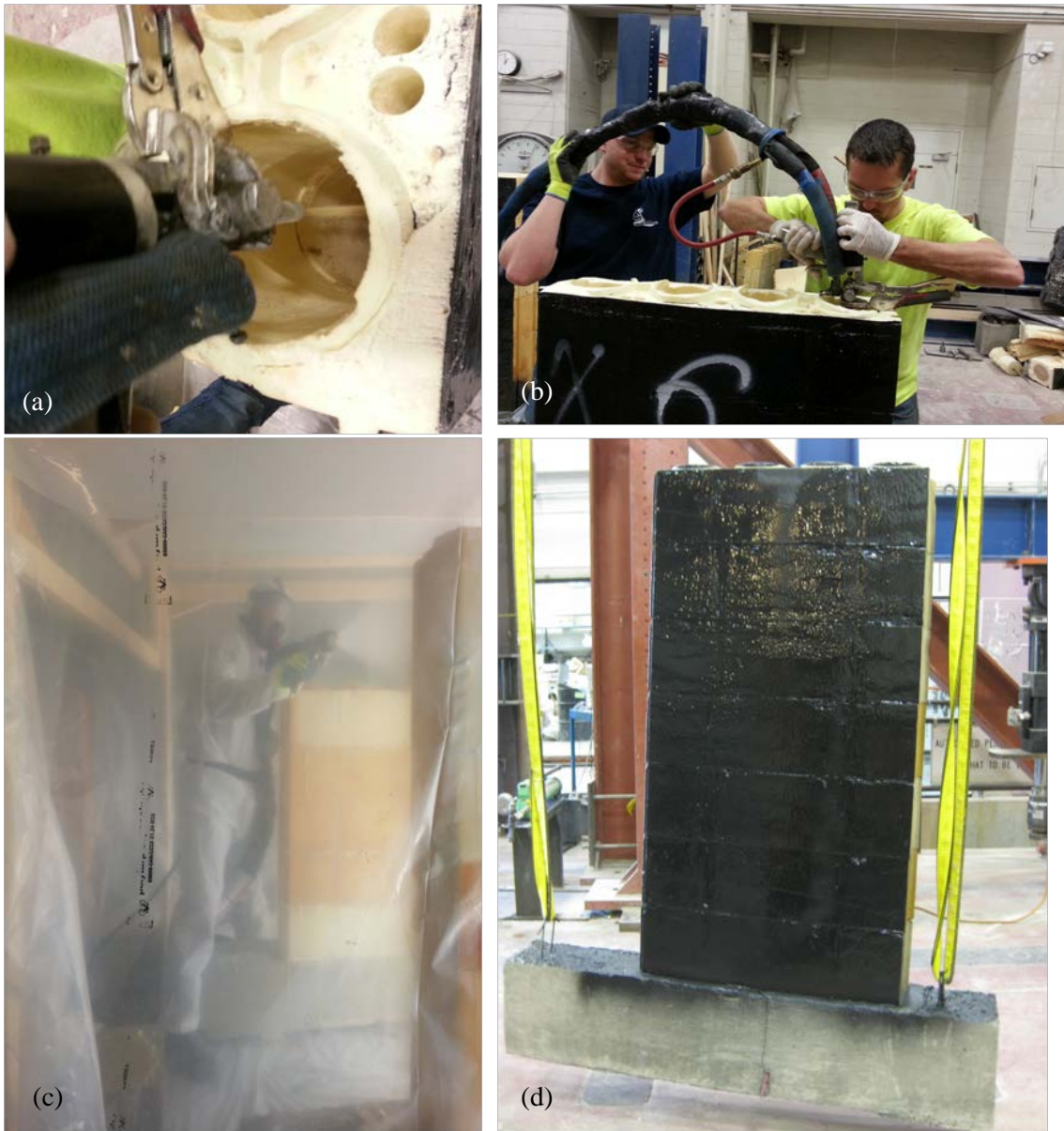
Figure 2.20: Construction steps of the walls, Polyurethane injection and Polyurea spraying

(a) Polyurethane injection, (b) injection apparatus of PU, (c) Poly-urea injection, (d) Wall surface finishing

Fig. 2.21 presents the structural configuration of full scale walls. They consisted of five poly-blocks whose voids were filled up with RPF. Two of the walls were reinforced with 2x10M and the other two were reinforced with 2x15M rebars with 90 mm spacing in each core.
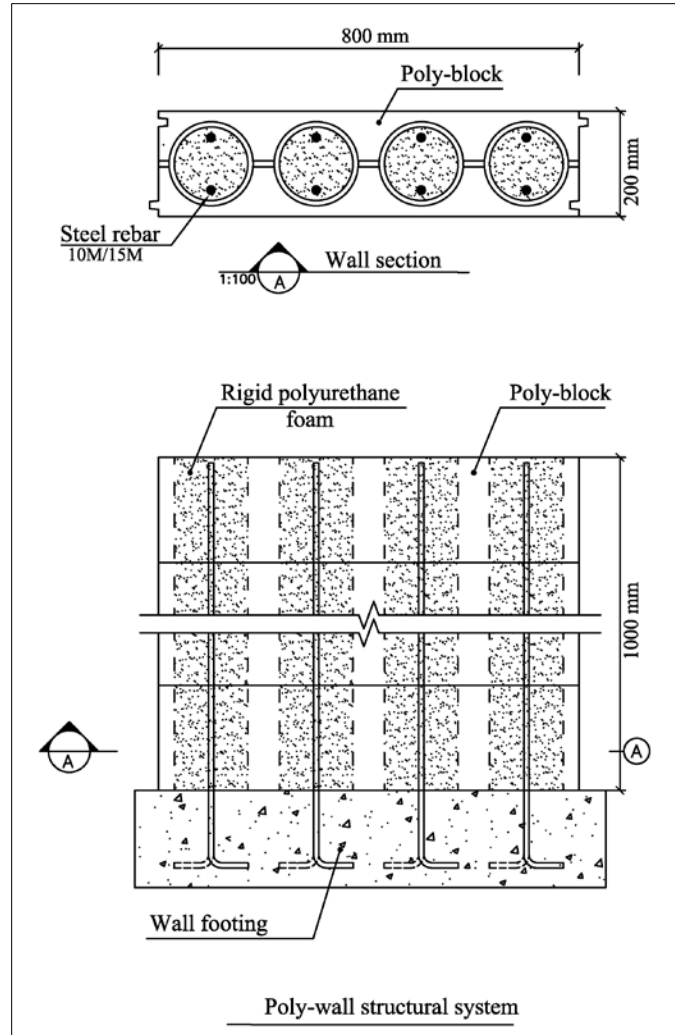
Figure 2.21: Poly-wall structural system and anchoring details

The whole test set-up was designed before the walls construction such that the wall footing properly places between existing anchor holes of the strong floor of the Structural Laboratory at University of Western Ontario while the actuator loading plate meets the wall surface (Fig. 2.22).

A 2 mm layer of Polyurea was sprayed on the wall surfaces as a finishing layer. Although Polyurea does not influence on structural performance of poly-wall, it brings higher surface resistance for the poly-blocks as well as integrity for the entire wall system.

The walls were moved and fixed in front of the actuator as shown in Fig. 2.22. A sophisticated anchoring system consisted of several beams and bolts was utilized to fix the foundations on the floor. Four LVDTs were installed on both sides of each wall to measure its lateral displacement. A load distributer steel plate with the same size of poly-block was used to uniformly distribute the load on the top block. Due to practical difficulties, upper LVDTs were installed behind the loading plate. As a result, a negligible compressive deflection of the loaded poly-block was involved in lateral displacement at the beginning of the loading which was recognized and excluded from the results.
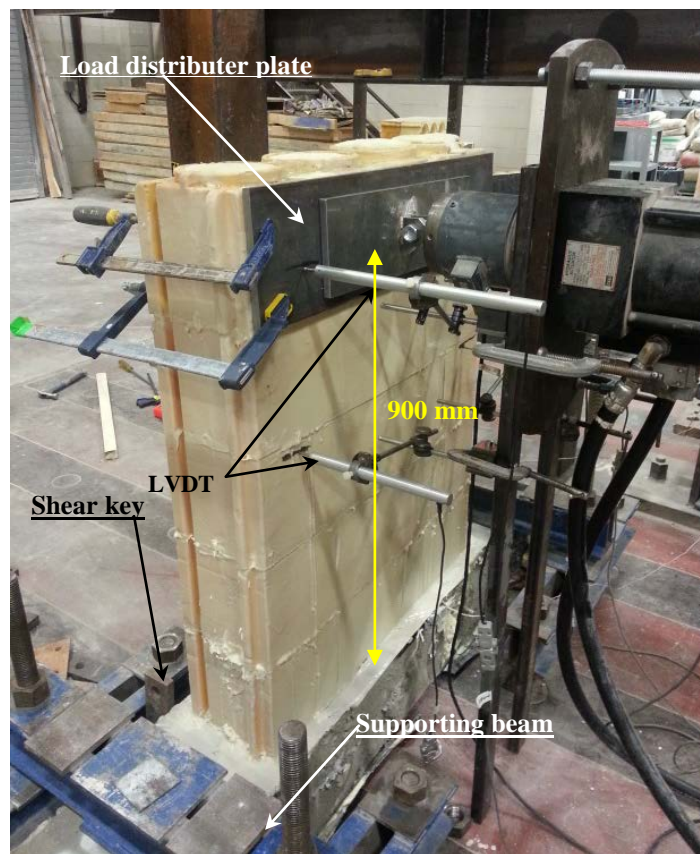
Figure 2.22: Full-scale test arrangements

The walls were preloaded with 0.5 kN to ensure that all surfaces are fully in contact. Walls were laterally loaded at the rate of 0.25 kN/s until the first failure occurred. All walls failed in flexural mode and rupture took place at the RPF cores and inside the

lowest poly-block immediately above the foundation, where all rebars were bent. No torsion took place according to the LVDTs readings installed on both sides of the wall. Figure 2.23a demonstrates the deflected shape of the wall after loading and Figure 2.23b displays cracks in tensile side of the RPF cores.

(a)   (b)
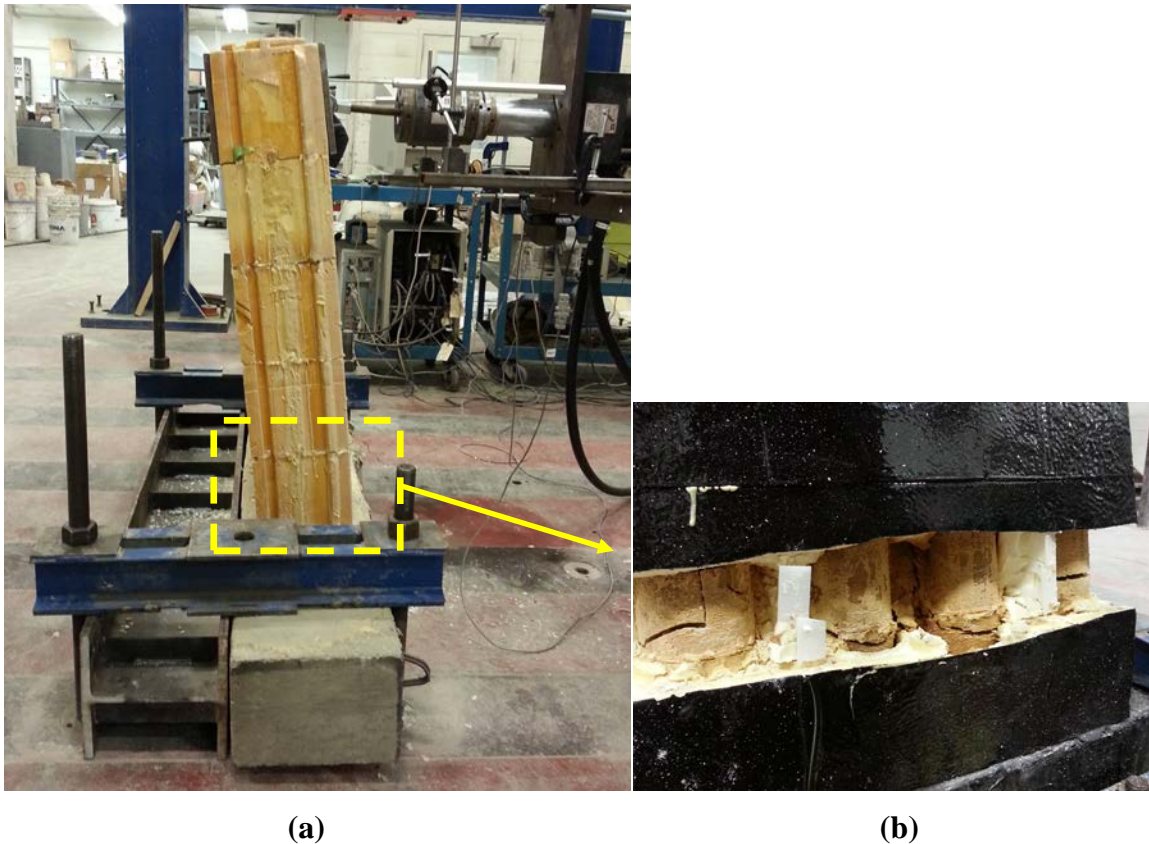
Figure 2.23: a) deflected shape of the wall after application of the lateral load, b) cracks of RPF cores on the tensile face inside the bottom poly-block

The test results of the four poly-walls are depicted in Fig. 2.24. The results are presented in the form of moment-displacement curves with respect to the position of the upper LVDT, which was installed 900 mm above the top of foundation. Fig. 2.24 illustrates that the walls exhibited a fairly linear flexural behavior followed by a brittle failure in all cases. It can also be seen that the behavior of each pair of walls is relatively consistent and their ultimate moment and corresponding deflections are almost identical. The average of ultimate resisting moment of the stronger walls is 28.5 kN.m corresponding to 40.5 mm lateral deflection, while the weaker walls had an average ultimate resisting

moment of 13.8 kN.m and 23.1 mm of lateral deflection. The stronger walls also exhibited higher initial stiffness compared to weaker walls.
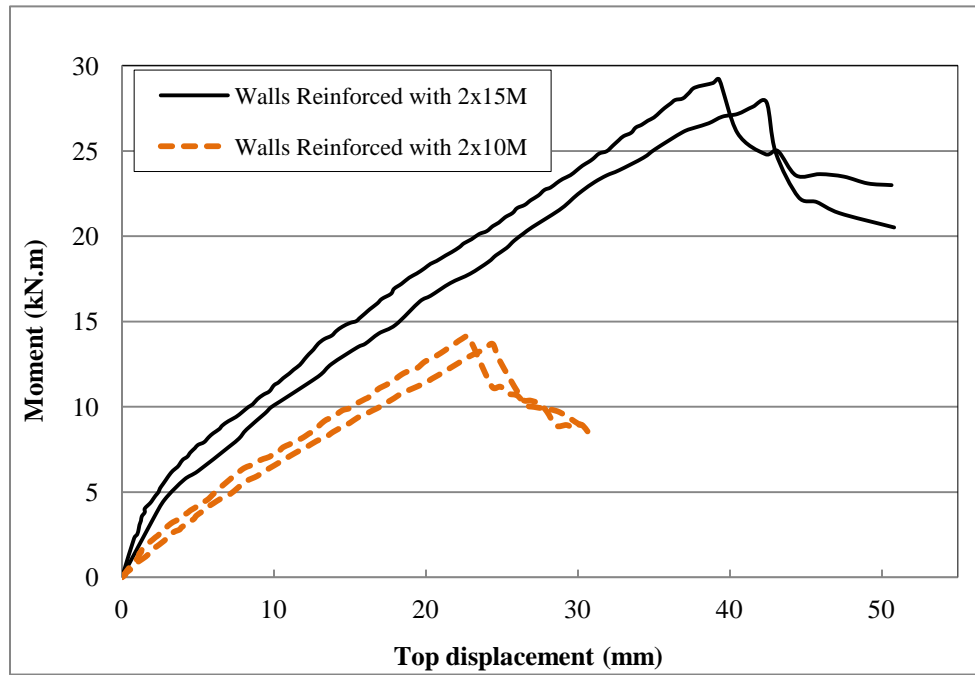
Figure 2.24: Flexural behavior of walls obtained from full-scale tests

The values of ultimate flexural resistance of poly-walls were found close to the resisting yield moment of rebars. The maximum yield moment (M_y) of two rebars at a specific distance can be calculated using Eq.2.4.

$$M_y = (f_y A_s)d \tag{2.4}$$

Where d is effective distance of rebar's centroids, f_y=400 MPa is the yield strength of grade 400R and A_s is rebar area. Considering some approximation, M_y of four RPF cores reinforced with two rebars can be obtained as follows.

For 2x15M reinforcement $M_y = [4(400 \times 201) \times 90] \times 10^{-6} = 28.9 \ kN.m$

For 2x10M reinforcement $M_y = [4(400 \times 78.5) \times 90] \times 10^{-6} = 11.3 \ kN.m$

This indicates that the ultimate strength of poly-wall is primarily controlled by rebars' properties and spacing.

2.16 RPF properties and preliminary design

Table 2.1 presents the strength values of RPF obtained from the experimental data compared with the corresponding concrete values according to the Canadian Standard CSA-A23.3-04. For the sake of comparison, strength values of concrete are divided by $\Phi c=0.65$ to eliminate the safety factor considered in the standard. Table 2.1 reveals that strength values of RPF outperforms concrete strength with the same f'c in most cases and proves the fact that RPF properties are absolutely adequate as a construction material. The main limitation of RPF is its lower modulus of elasticity compared to concrete, which results in lower stiffness and greater deflection. This may constrain the height of walls constructed using RPF where lateral deflections are particularly crucial. However, in the current application, lateral deflection of the poly-wall would be within the acceptable range recommended by codes.

A preliminary design was conducted to evaluate the lateral resistance of a poly-wall considering practical sound wall height and wind loading conditions. The maximum factored moments induced by wind load on 2.2 m and 3 m high sound walls in Toronto area are 8.3 kN.m and 15.2 kN.m according to Canadian standards (CSA-S6-06 & NBCC). Considering factor of safety=0.65 for materials, ultimate moment capacity of poly-walls reinforced with 2x10M and 2x15M with the proposed rebars arrangement are equal to $13.8\times0.65=8.97$ kN.m and $28.5\times0.65=18.52$ kN.m, respectively. These values show the sufficiency of the flexural resistance of poly-wall with the two types of reinforcement. Given the height of Jersey blocks (used as wall foundation), which is typically over 0.8 m, the total wall height would be sufficient as a sound wall in both cases.

Table 2.1: Comparison of mechanical properties of RPF filler and Concrete

Type of test	RPF	Concrete*
Compressive strength (MPa)	24.2	24.2
Density (kN/m³)	11.1	24
Direct tension (MPa)	40	2.8
Modulus of rupture-flexural (MPa)	9.6	4.9
Shear strength (MPa)	4.3	3.2
Bond strength (MPa)	4.5	4.3
Module of elasticity (GPa)	1.27	20
Poisson's ratio	0.22	0.2

The strength values of concrete were divided by $\Phi_c=0.65$ for the comparison.

2.17 Cyclic fatigue test

Utilization of new composites in construction has been always a concern for designers. Despite the advantages of new materials, they have not been widely examined in practice and therefore their long-term performance is relatively unknown once employed in a load-bearing system.

Since noise barriers are exposed to the repetitive wind load over its life span, load-controlled fatigue tests were conducted on a specimen of RPF and a full-scale poly-wall to determine their mechanical degradation under a large number of load cycles.

To approximately simulate the dynamic effects of wind loading, a sinusoidal cyclic loading was applied on both samples within the design stress range that material would experience in practice. The frequency of 0.2 Hz was chosen for the loading since the

predominant frequency of a typical spectrum of wind energy is between 0.15 and 0.3 Hz and its maximum occurs at 0.2 Hz (Liu, 2000).

2.17.1 Specimen fatigue test

A dog-bone shape sample similar to tensile tests was made and properly placed into the Instron testing machine. The test set-up, sample dimensions and data acquisition system were identical to the tensile tests, as shown in Fig. 2.25 and a cyclic tensile loading at the frequency of 0.2 Hz was applied on the sample. For this purpose, the sample was loaded up to 65% of its yield tensile strength (20 MPa) and then unloaded to 6 MPa in a cyclic manner. The tensile stress was recorded by dividing the total tensile force by the narrow area of the sample and strain was obtained directly through the attached extensometer.

The sample was subjected to 15000 load cycles and stress-strain relation of RPF sample was recorded at synchronized intervals. Results of the test are demonstrated in Fig. 2.26 in the form of 16 stress-strain loops, from 1st to 15000th per 1000 cycles. The cyclic response of RPF sample shows no sign of stiffness or strength degradation. The residual strain after 15000th is very minimal and less than 0.00025. Although higher number of load cycles is required for the general conclusion regarding the fatigue behavior of RPF sample, the results indicate a satisfactory fatigue life for the specimen.

Fig. 2.27 presents the hysteresis loops of the cyclic tensile test with respect to the overall tensile behavior obtained from direct tensile tests. The hysteresis loops are fairly matching with RPF tensile behavior indicating consistent performance of the material in both types of loading. It also demonstrates that the response is fairly linear elastic within the loading range considered.

Figure 2.25: Cyclic test set-up of RPF sample
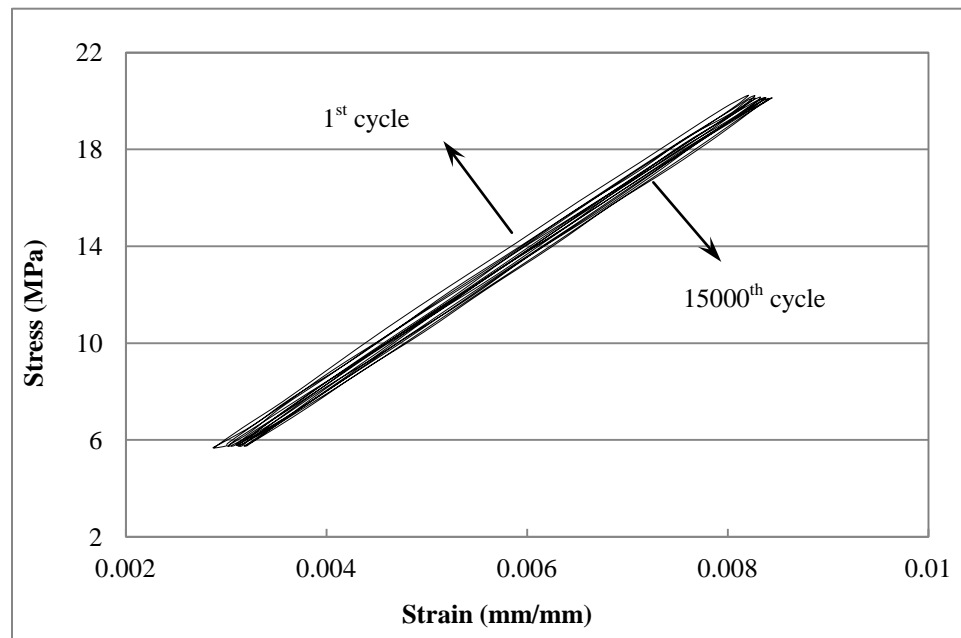
Figure 2.26: Cyclic response of RPF sample from 1 to 15000 cycles
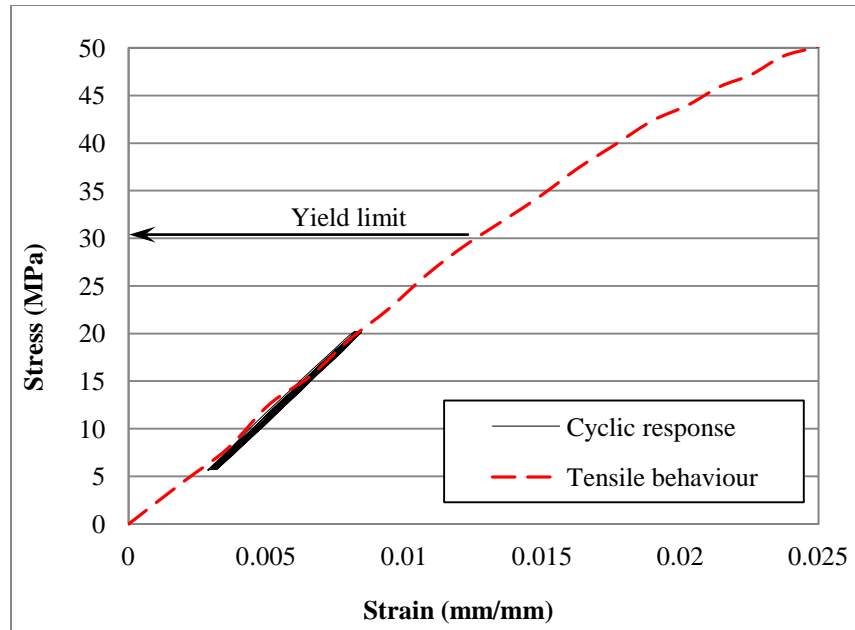
Figure 2.27: Comparison of cyclic response and tensile behavior of RPF

2.17.2 Full-Scale fatigue test

A A poly-wall reinforced with 2x10M in each core was built similar to the walls that were tested under push-over static loading. As displayed in Fig. 2.28, the test assembly was prepared identical to the push-over static test. To push and pull the wall two steel plates were bolted to the both sides of wall and then connected to the hydraulic actuator.

The maximum magnitude of cyclic load was selected corresponding to factored flexural resistance of poly-wall, which is 65% of the ultimate flexural resistance obtained from the static tests. The minimum magnitude corresponds to the maximum magnitude divided by gust factor, which is equal to 2.5 according to Canadian Highway Bridge Design Code (CSA-S6-06). These peaks represent the mean and maximum moment induced by wind load, which are applied on the wall in practice in compliance with the design loads.

The lateral load ramped up to the average value of cyclic load at the rate of 0.2 kN/s and the sinusoidal load was then initiated at 0.2 Hz frequency between a minimum moment of 3.5 kN.m and maximum moment of 8.5 kN.m.

Figure 2.28: Cyclic test set-up of poly-wall

The wall was subjected to 15000 cycles of loading and the test took 21 hours. This number of cycles can be a fairly good representative for the number of occurrence of maximum wind load over 25 years life span of the wall. The lateral load as well as the displacement of the wall top was recorded at synchronized intervals of 0.5 sec using the load cell and two LVDTs, respectively.

The response of the Poly-wall for 16 cycles is depicted in Fig. 2.29, which shows the displacement of the top of the wall versus the base bending moment. Fig. 2.29 displays the hysteresis loops for the cycle of 1 to 15000 for every 1000 cycle. The maximum displacement values in the first and last cycles were equal to 12.5 mm and 14.8 mm respectively, while moment peaks (3.54 kN.m and 8.5 kN.m) were maintained during the experiment with tolerance of 0.15 kN.m. The cyclic response of poly-wall shows no

significant stiffness or strength degradation after 15,000 load cycles. The residual deformation of the wall was only 2.3 mm at most, which could be mainly due to loosening of connections and compressive deformation of poly-blocks. This response of poly-wall confirms the repeatability of the wall behavior under a high-cycle loading. It can be also concluded that the lateral loading within the recommended design range, does not induce residual fatigue stress.
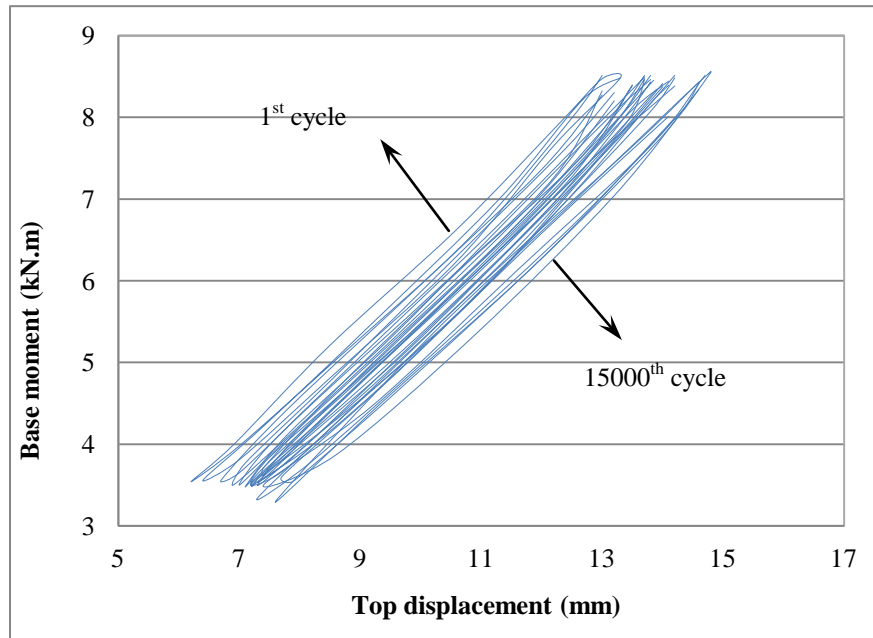
Figure 2.29: Cyclic response of poly-wall from 1 to 15000 cycles

2.18 Conclusion

This study investigates the first known application of RPF in construction of noise barrier. An extensive experimental program was carried out to determine the RPF mechanical properties. The application of poly-wall in accelerated construction as a noise barrier was also experimentally examined and the lateral resistance of four full-scale poly-walls was evaluated.

Based on the experimental results, the mechanical properties of RPF specimens were found quite comparable to conventional construction material such as concrete, and hence are satisfactory to be used as structural core of sound walls. This investigation also

proved the applicability of the proposed wall system in accelerated construction of noise barriers owing to high-strength and easy application of RPF. The results of fatigue cyclic tests confirmed a satisfactory behavior for RPF over an extended period of time.

The combination of poly-blocks and RPF along with polyurea may lead to significantly faster and less obstructive construction compared to conventional masonry or post-and-panel walls. Saving time and reducing the risk of roadside construction will compensate the higher initial cost of RPF.

2.19 Acknowledgements

2.20 References

Agavriloaie L., Oprea S., Barbuta M., and Luca F. (2012)." Characterisation of Polymer Concrete with Epoxy Polyurethane Acryl Matrix." Construction and Building Materials, 37, 190-196.

ASTM Standard D4060-10. (2010)."Standard Test Method for Abrasion Resistance of Organic Coatings by the Taber Abraser." Philadelphia, PA.

ASTM Standard C39/C39M-12. (2012). "Standard Test Method for Compressive Strength of Cylindrical Concrete Specimens." West Conshohocken (PA), ASTM International.

ASTM Standard D1621-10. (2010). "Standard Test Method for Compressive Properties of Rigid Cellular Plastics." West Conshohocken (PA), ASTM International.

ASTM Standard D3039/D3039M-08. (2008). "Standard Test Method for Tensile Properties of Polymer Matrix Composite Materials." West Conshohocken (PA), ASTM International.

ASTM Standard C469/C469M-10. (2010). "Standard Test Method for Static Modulus of Elasticity and Poisson's Ratio of Concrete in Compression." West Conshohocken (PA), ASTM International.

ASTM Standard C78/C78M-10. (2010). "Standard Test Method for Flexural Strength of Concrete (Using Simple Beam with Third-Point Loading)." West Conshohocken (PA), ASTM International.

Bazǎnt Z.P. and Pfeiffer P.A. (1986). "Shear Fracture Tests of Concrete." Materials and Structures,19 (2), 111-121.

Behjat Y., Cheng J., Polak M., and Penlidis A.(2014). "Effect of Molecular Structure on Short-Term and Long-Term Mechanical Behaviour of High Density Polyethylene." Journal of Materials in Civil Engineering. 26 (5), 795-802.

Briodya C., Duignana B., Jerramsb S., and Ronanb S. (2012). "Prediction of Compressive Creep Behaviour in Flexible Polyurethane Foam over Long Time Scales and at Elevated Temperatures." Polymer Testing, 31, (8), 1019-1025.

Canadian Standard Association. (2009). "CAN/CSA-G30.18-09 Carbon Steel Bars for Concrete Reinforcement", Mississauga, Ontario, Canada.

Canadian Standard Association. (2004). "CAN/CSA-A23.3-04 Design of Concrete Structures." Rexdale, Ontario, Canada.

Canadian Standard Association. (2006). "CAN/CSA-S6-06 Canadian Highway Bridge Design Code." Mississauga, Ontario, Canada.

Chahrour A.H., Soudki K.A., and Straube J. (2005). "RBS Polymer Encased Concrete Wall Part I: Experimental Study and Theoretical Provisions for Flexure and Shear." Construction and Building Materials, 19, 550-563.

Chen W., Lu F., and Winfree N. (2002). "High-strain-rate Compressive Behavior of a Rigid Polyurethane Foam with Various Densities." Experimental Mechanics, 42(1), 65-73.

Choi H., Toutanji H., Gilbert J., and Alldredge D. (2013). "Impact Resistance of Polyurea-Coated High Performance Cementitious Composites." Journal of Materials in Civil Engineering, 25(12), 1984-1989.

Daee B., and El Naggar H. (2015). "Application of Polyurethane Products in Accelerated Construction of an Innovative Noise Barrier: Numerical study." (Under Review)

Federal Highway Administration. (2011). USDOT (FHWA-HEP-10-025). "Highway Traffic Noise: Analysis and Abatement Guidance." Washington, D.C.

Greene C., and Myers J. (2013). "Flexural and Shear Behavior of Reinforced Concrete Members Strengthened with a Discrete Fiber-Reinforced Polyurea System." Journal of Composites for Construction, 17(1), 108-116.

Huang J. S., and Gibson L. J. (1991). "Creep of Polymer Foams." Journal of Materials Science, 26(3), 637-647.

Irshidat M., Al-Ostaz A., Cheng A., and Mullen C. (2011). "Blast Vulnerability Evaluation of Concrete Masonry Unit Infill Walls Retrofitted with Nano Particle Reinforced Polyurea: Modelling and Parametric Evaluation." Structures Congress, 2126-2141.

Khanlou A., MacRae G. A., Scott A. N., Hicksand S. J., and Clifton G.C.(2013). "Shear performance of steel fibre-reinforced concrete." Steel Innovations Conference, Christchurch, New Zealand.

Li Y., Kim U.S., Shields J., and Davis R. (2013)."Controlling Polyurethane Foam Flammability and Mechanical Behaviour By Tailoring The Composition Of Clay-Based Multilayer Nanocoatings." Journal of Materials Chemistry A, 1, 12987-12997.

Majdzadeh F., Soleimani S.M., and Banthia N. (2011). "Shear Strength of Reinforced Concrete Beams with a Fiber Concrete Matrix." Canadian Journal of Civil Engineering, 33(6), 726-734.

Manalo A. (2013). "Structural Behaviour of a prefabricated Composite Wall System Made from Rigid Polyurethane Foam and Magnesium Oxide Board." Construction and Building Materials, 41, 642-653.

Motlagh S.G., Jain A., Najafi M. (2013). "Comparison of Spray-on Linings for Water Pipeline Renewal Applications." Pipelines, ASCE, 1113-1125.

NBCC. (2005). "National Building Code of Canada", National Research Council of Canada (NRC), Ottawa, Canada.

Liu P. (2000). "Is the Wind Wave Frequency Spectrum Outdated." Ocean Engineering 27, 577-588.

Priddy L.P., and Newman J.K. (2010)."Full-Scale Field Testing for Verification of Mechanical Properties of Polyurethane Foams for Use as Backfill in PCC Repairs." Journal of Materials in Civil Engineering, 22, 245-252.

Qoods S.H., Neuschwanger C.L., and Whinnery L.L. (1998) "Mechanical Properties of a Structural Polyurethane Foam and the Effect of Particulate Loading." Porous and Cellular Materials for Structural Applications, Materials Research Society, San Francisco, California, U.S.A.1998

Ruiz D., Riveros M., León M., Vacca H., and Jarro S. (2014). "Cyclic and Static Tests to Evaluate the Seismic Strength of Walls and Connections of Prefab Light Weight Panels for Housing Construction Projects." Practice Periodical on Structural Design and Construction, 19(2), 04014004.

Ramamurthy k., Kunhanandan Nambiar E.K., and Indu Siva Ranjani G. (2009). "A Classification of Studies on Properties of Foam Concrete." Cement & Concrete Composites, 31, 388-396.

Ridha M. (2007). "Mechanical and Failure Properties of Rigid Polyurethane Foam under Tension", PhD Thesis, National University of Singapore.

Rizzi E., Papa E. and Coriglian A. (2000). "Mechanical Behavior of a Syntactic Foam: Experiments and Modeling." International Journal of Solids and Structures, 37, 5773-5794.

Schreyer H. L., and Zuo Q. H. (1994). "Anisotropic Plasticity Model for Foams." Journal of Engineering Mechanics, 120, 1913-1930.

Sharaf T., and Fam A. (2011). "Experimental Investigation of Large-Scale Cladding Sandwich Panels under Out-of-Plane Transverse Loading for Building Applications." Journal of Composites for Construction, 15(3), 422-430.

Chapter 3

Application of Rigid Polyurethane Foam in Accelerated Construction of an Innovative Noise Barrier: Numerical study

This Chapter presents a numerical investigation on the performance of an innovative noise barrier (poly-wall) consisting of poly-block, rigid polyurethane foam (RPF) and polyurea. The mechanical characteristics of RPF as well as the flexural resistance of (poly-wall) were established and presented in Chapter 2. The experimental results are used in this chapter to develop, calibrate and verify 3D finite element (FE) models.

3.1 Introduction

Noise barriers (sound walls) are usually constructed along roadways to mitigate the airborne noise emanating from vehicles. The proposed innovative sound wall (poly-wall) comprises stay-in-place poly-blocks as formwork, rigid polyurethane foam (RPF) as structural cores and polyurea as a coating of the wall surfaces. The structural system of poly-wall is displayed in Fig. 3.1.

The mechanical properties of the RPF were determined by performing an extensive experimental program including tensile, compression, modulus of elasticity, Poisson ratio, flexural, shear, pull-out, creep tests and cyclic tests on RPF specimens (Daee and El Naggar, 2014). In addition, four full-scale tests were conducted to assess the lateral resistance of poly-wall reinforced with 2x10M and 2x15M steel rebars in each core as described in Chapter 2.
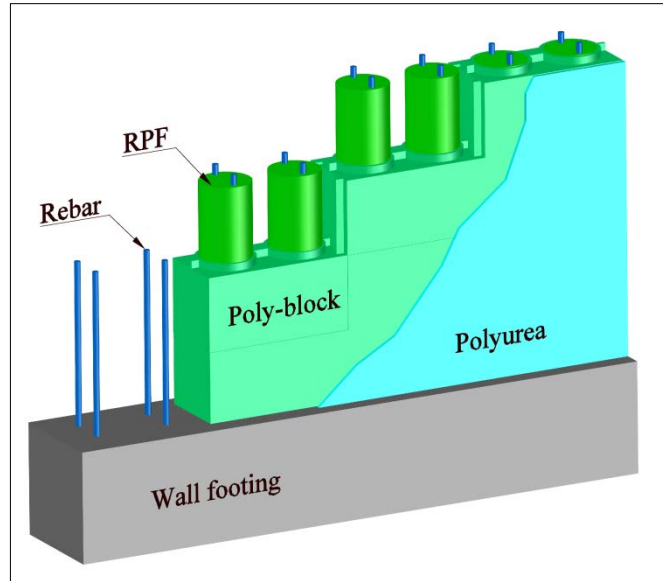
Figure 3.1: Poly-wall made of Polyurethanes

This Chapter is focused on developing a finite element (FE) model of poly-wall employing the commercial FE software, ABAQUS (ABAQUS user manual, 2010). For this purpose, the components of the poly-wall, including poly-block, RPF cores and steel rebars were individually modeled and their stress-strain relations were calibrated using the experimental data. All components were then assembled together and two poly-walls with different reinforcement sizes were simulated according to the conditions of the full-scale tests. The verified numerical models were then used to conduct an investigation on the behavior of poly-wall under lateral wind loading. Based on the results of finite element analysis (FEA), a simplified approach is proposed for the design of poly-wall.

3.2 Verification of finite element models

3.2.1 Steel rebar model

A benchmark FE analysis was carried out to calibrate the behavior of steel rebar model as a structural component of Poly-wall. Hence, a solid 3D model of 16M rebar with f_y=400 MPa (Grade 400R of CSA-G30.18, 2009) and 200 mm length was developed (Fig. 3.2). The top surface of the rebar was subjected to a tensile displacement and the connection of rebar to the concrete foundation was simulated using a tie constraint. The tie constraint

represented the connection of the rebar and foundation well since, in practice, the slip of rebars relative to concrete is prevented by providing a sufficient development length. Therefore, the embedded length of the rebar inside the foundation can be disregarded in the analytical model.

For better discretization of geometry, 6-node linear triangular prism elements (element C3D6 in ABAQUS library) were employed to simulate the inner core of the rebar. The remaining parts of the model were simulated by employing linear hexahedral brick elements (element C3D8R). Using these two types of elements helped to create the most uniform mesh across the entire part, particularly at the center of rebar, which reduced the possibility of stress concentration where it does not exist. The aspect ratio of all elements was kept below 1:3.
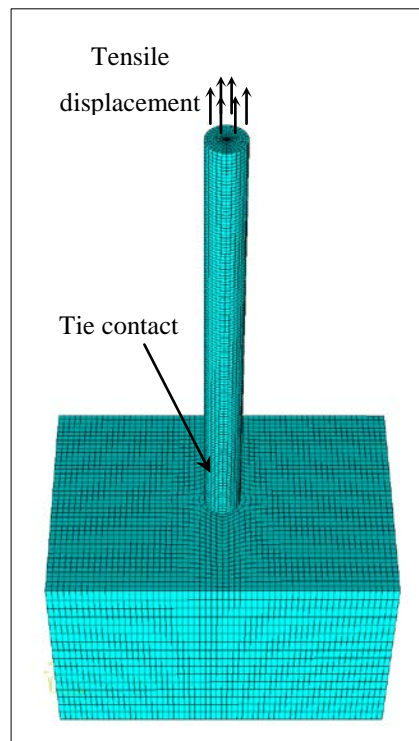
Figure 3.2: FE model of rebar interaction and foundation

All translational and rotational degrees of freedom at the bottom surface of the foundation were restrained. Concrete was modeled as a linear material and its elastic properties (E=25 GPa, v=0.2) were assigned to the foundation. The solid line in Fig. 3.3

displays the typical stress-strain behavior of steel rebar (Lowes, 1999), which was employed in the FE model.

A static displacement-control analysis was conducted and the stress-strain values were directly obtained from the elements that underwent the highest tensile stress. The numerical results are plotted as a dashed line in Fig. 3.3, which demonstrates an excellent agreement with the material properties considered, indicating accurate simulation of the rebar behavior.
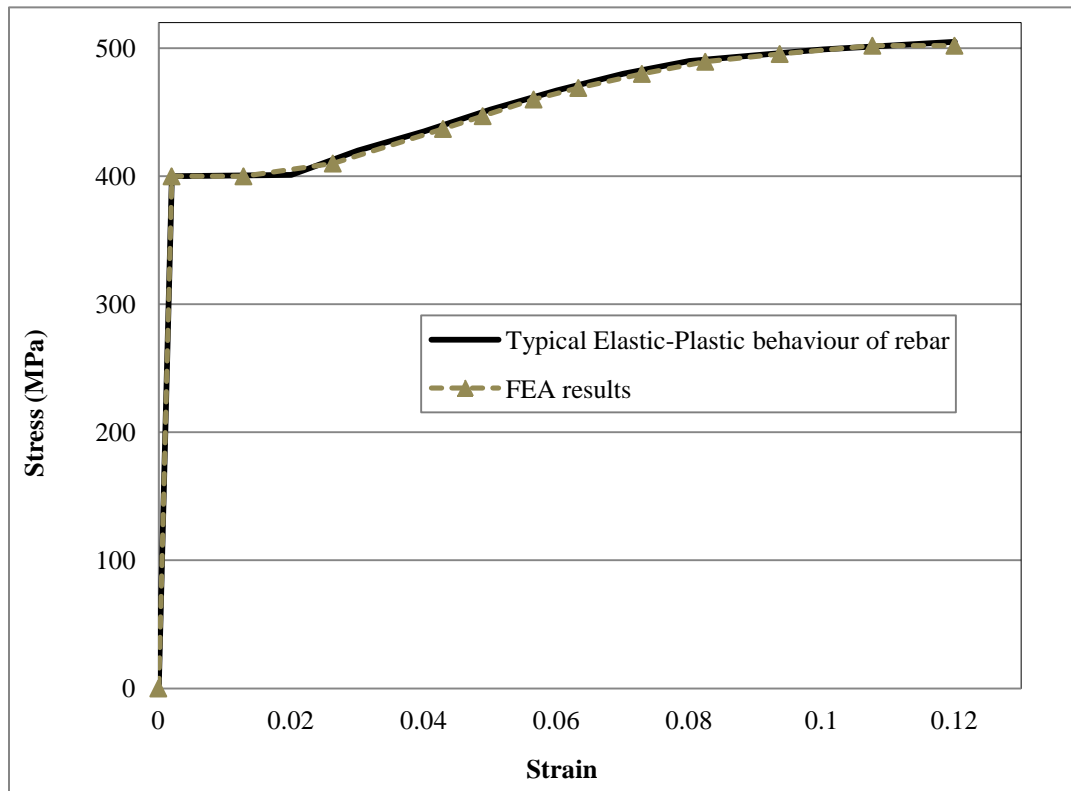
Figure 3.3: Stress-strain relationship of steel rebar and FE results

3.2.2 Poly-Block model

Poly-block is made of low-density (50 kg/m^3) closed-cell polyurethane foam. Under uniform pressure, light foams typically deform linearly until they reach their yield point, which is followed by a plateau with small stress variation. The plateau region is irrecoverable and continues up to large strains at which point densification initiates. As

the cell walls of the foam buckle and collapse, air escaping and stiffness hardening continue until the ultimate failure occurs (Schreyer et al., 1994).

To determine the compressive behavior and particularly the yield strength of poly-blocks, three compression tests were carried out as described in Chapter 2. The dashed lines in Fig. 3.4 illustrate the compressive stress versus true strain of poly-blocks acquired from the experiments. The solid line in Fig. 3.4 is a bilinear representation of the average poly-blocks compressive behavior, which was calculated based on the test data. It can be observed that the test results are consistent with the typical behavior of low-density foams.

The tensile behavior of poly-block was also required for the numerical model. Low-density foams typically demonstrate a linear tensile behavior with a relatively limited plastic region before failure occurs. For the range of 50-60 kg/m^3 density, previous studies have shown that the tensile modulus and strength (E_t, σ_t) are slightly greater than the compressive modulus and strength (E_c, σ_c) (Witkiewicz et al., 2006; Zenkert et al., 2009). However, in the absence of tensile test data, it is common to assume them to be identical. A built-in material model for crushable foams has been developed in ABAQUS assuming a symmetric behavior in tension and compression. In order to define the evolution of the yield surface in this model, only uniaxial compression test data is required (ABAQUS user manual, 2010).

A poly-block model was developed considering the same boundary conditions as the actual tests conducted. All degrees of freedom at the bottom surface of the blocks were restrained and a uniform static pressure was applied on the top surface. The linear hexahedral brick elements along with the hourglass control and reduced integration points were employed in the FE model and the aspect ratio of the elements were kept under 1:3 (Fig. 3.5a). The obtained compressive test data (the solid line in Fig. 3.4) was properly input as the stress-strain relation of the block. Elastic properties of the foam were taken as E=8.33 MPa and ν=0.3 (Witkiewicz et al., 2006) and the plastic region was simulated using the crushable foam model available in ABAQUS. Large-deformation was activated in the software by implementing NLGEOM parameter.

The results of the finite element analysis are demonstrated in Fig. 3.4 in the form of square symbols in comparison with the average test data. The average test data was achieved based on the average yield value and average post yield slope of the test data. The numerical results are in excellent agreement with the average compressive behavior of the blocks across the elastic and plastic regions, indicating satisfactory performance of the numerical model. The undeformed and deformed shapes of the poly-blocks are shown in Fig. 3.5, which are fairly similar to the test observations shown in Fig. 3.6.
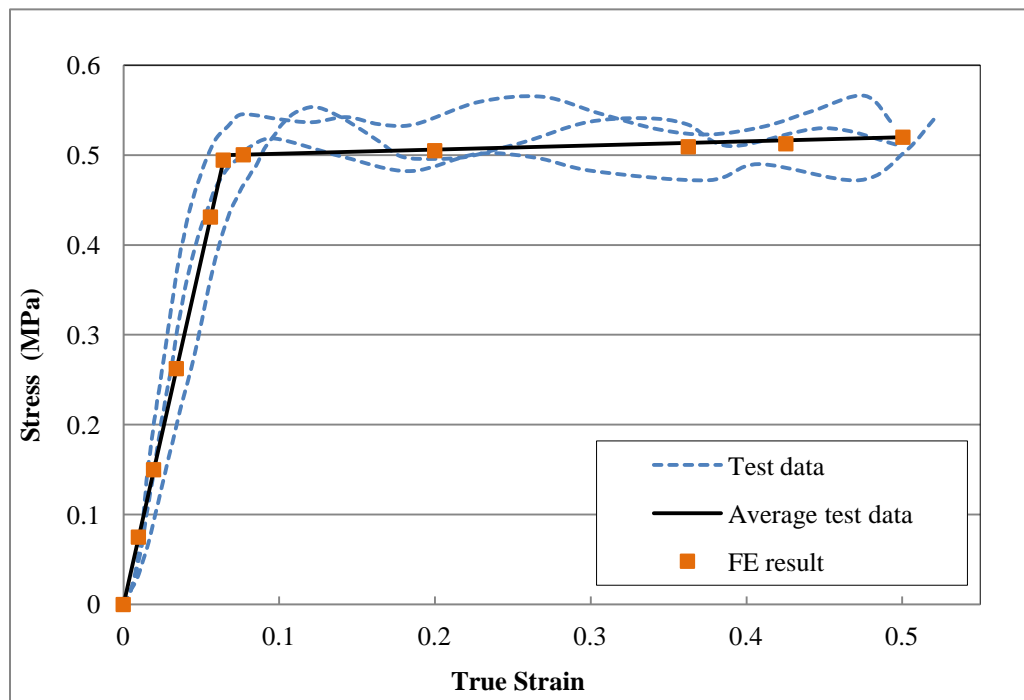
Figure 3.4: Compressive Stress-strain relationship of Poly-block

(a)   (b)
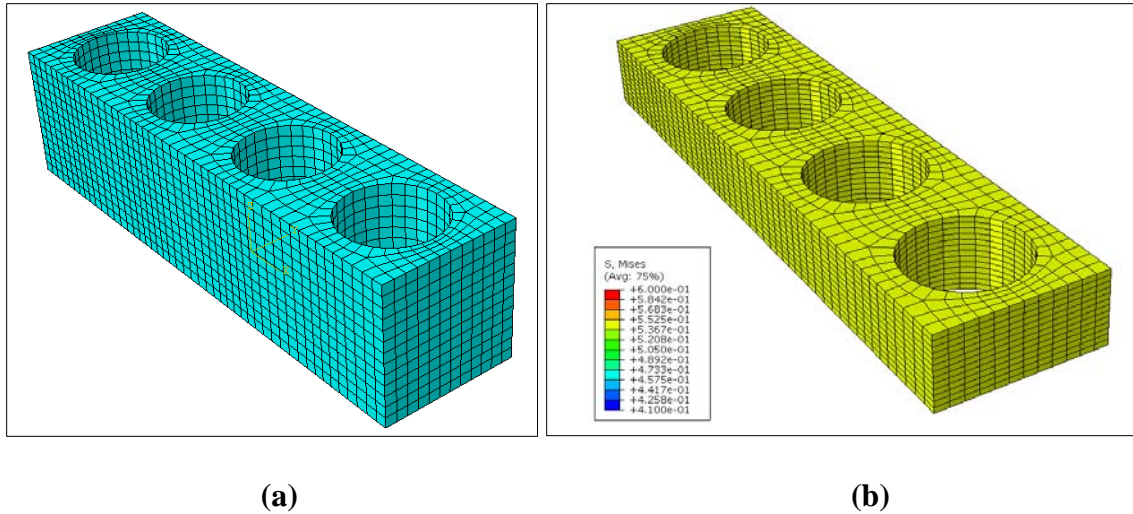
Figure 3.5: Poly-block FE model (a) before loading (b) after loading

Figure 3.6: Poly-block experimental model before and after compression test

3.2.3 Rigid Polyurethane Foam modeling

Compressive stress-strain relations of RPF cylinder samples are shown in Fig. 3.7. These graphs were obtained by relating the load from the load-cell of the testing machine to the overall shortening of the specimen (i.e. global strain). Although the compressive strees-strain relation obtained from strain gauges (local strain) was almost linear (Fig. 2.7), these graphs exhibit a nonlinear behavior with a "toe region" before the linear part of the curves. The toe region which appears in these graphs is an artifact induced by a take-up of slack, loading plates, specimen alignment and so forth (ASTM D1621). This

hyperelastic behavior has been previously reported for the global compressive behavior of RPF samples (Priddy et al., 2010). ASTM D1621-10 suggests a correction method called "toe compensation" in order to zero the strain prior to the linear domain. By employing the described procedures, Ec based on the global strain (i.e. entire specimen length) was found to be 1.27 GPa on average, which is considerably less than the value obtained from local strain (strain gauges).

This discrepancy is attributed to some level of inhomogeneity of RPF samples in addition to the slack effect. It seems that there is a delay in the stress transfer through the length of large samples of RPF which extends the toe region. During a close observation of cylinder samples, some decolorized tiny spots, bubble concentration and hair flaws were found within inner layers of specimens. These factors which may weaken the material at some regions are more pronounced when RPF is injected in a large volume. To resolve this discrepancy, the stress-strain relation of RPF was verified using a 3D FEA which is discussed in Section 3.2.3.1.
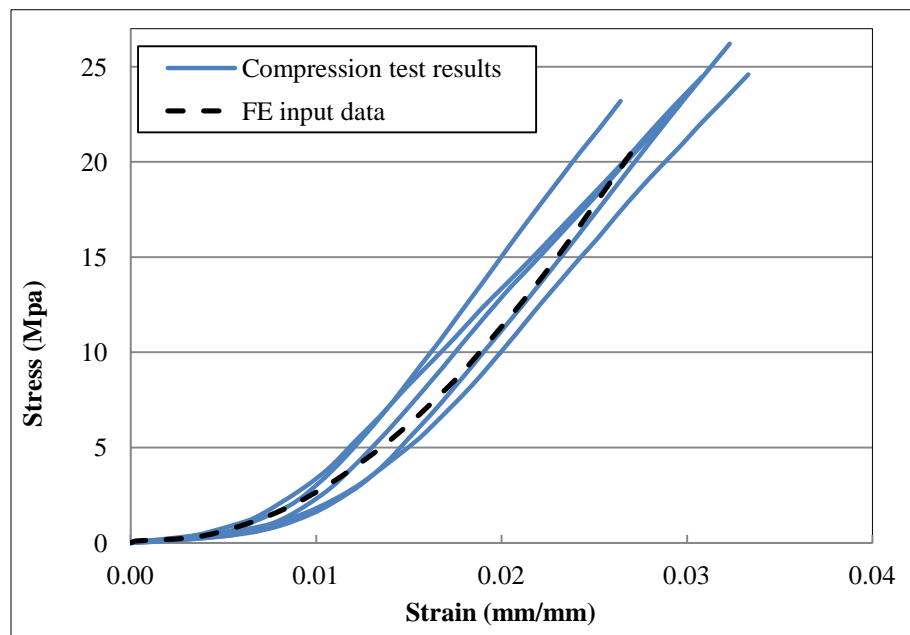
Figure 3.7: Compression stress-strain relation of RPF samples (global strain)

3.2.3.1 Flexural analysis

The non-linear flexural behavior of RPF obtained from the experiments (solid lines in Fig. 3.8) confirms that Hooke's law does not apply throughout the large RPF samples. Since using beam theory and assuming linear behavior with modulus of elasticity equal to 2.3 GPa (obtained from local stress-strain) would result in linear force-displacement relationship with maximum displacement of 1.2 mm at 72 kN of load. This behavior is displayed as dashed line in Fig. 3.8 versus those obtained from the flexural tests.

Therefore, a verification study is conducted herein to establish a stress-strain relationship that represents the behavior of large RPF samples. For this purpose, a 3D finite element model of the flexural test set-up was developed employing 8-node hexahedral elements (C3D8R). Similar to the test arrangement, the beam geometry was modeled as 150x150x530 mm and the contact width of the load and support rollers were taken as 5 mm. The RPF behavior was simulated using a hyperelastic material model to include the effect of toe region. It was also simulated with a symmetric behavior in tension and compression, since uniaxial tests on small RPF specimens demonstrated that the material behavior is almost identical in both compression and tension. The average of compression tests results, shown in Fig. 3.7 as a dashed line, was input in the FEA representing the material properties. For modeling the hyperelastic behavior, a strain energy function was simulated using the third-order Ogden model (Ogden, 1972) (N=3) available in ABAQUS. The Ogden strain energy function fully matched the observed RPF behavior and was also stable throughout the required strain range. The vertical load applied statically in 0.05 increments and the beam deformation was recorded corresponding to the measurement point of the flexural tests.

The dotted curve in Fig. 3.8 represents the FEA result, which perfectly falls within the measured tests data confirming the accuracy of the numerical model. The computational maximum compressive and tensile stresses were found to be +8.9 MPa and -10.9 MPa, respectively as displayed in Fig. 3.9. These values are consistent with modulus of rupture obtained from the experiments. These values are consistent with the calculated modulus of rupture and are less than the ultimate tensile and compressive strength which indicates that failure was dominated by the maximum deflection of the member. As expected, the

maximum tensile stress is slightly greater than the maximum compressive stress due to the effect of supports.

The results of the FEA validated the hyperelastic behavior of RPF as well as the simulated symmetric function for tensile and compressive behaviors.
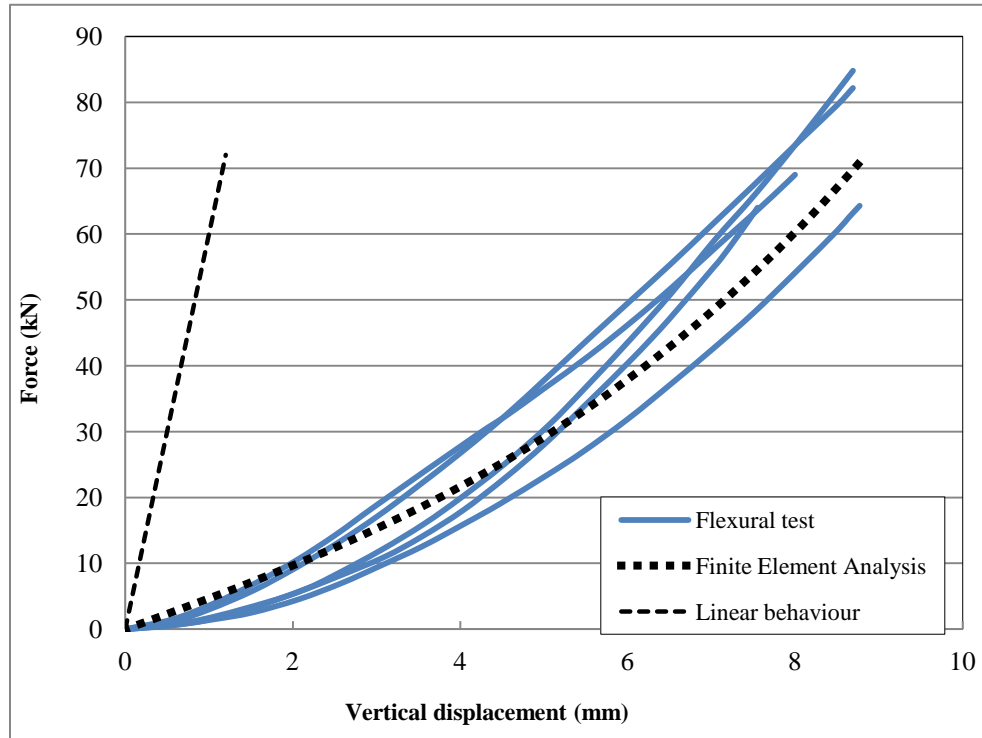
Figure 3.8: Flexural behavior of RPF samples
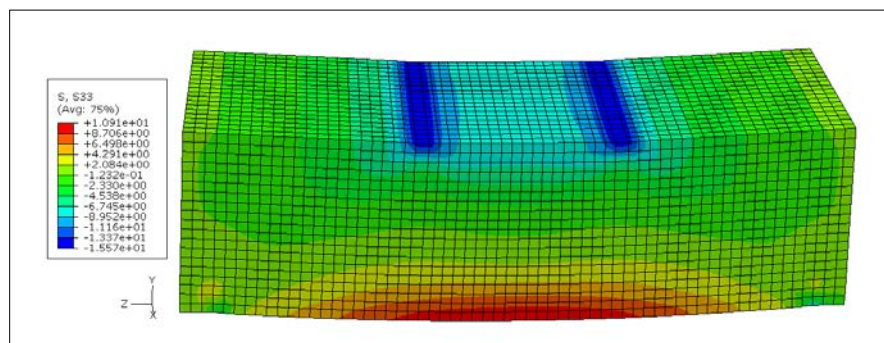
Figure 3.9: Finite Element results of the flexural test

(Not to scale)

3.2.3.2 Uniaxial analysis

A benchmark FE analysis was performed on a cylindrical model of RPF to ensure that the material model is suitable for uniaxial loadings. Hence, a 3D FE model with the same geometric dimensions of the compressive samples (140x280 mm) was simulated as shown in Fig. 3.10a. Material properties, type and aspect ratio of elements were all selected identical to the beam model used in the flexural model. The compressive cylindrical model was subjected to 20 MPa pressure on the top surface and the translational degrees of freedom on the opposite side were restrained. Load-controlled static analysis was performed and the logarithmic (true) strain was recorded at each load step.

The deformed shape of the model (illustrated in Fig. 3.10b) indicates a uniform stress throughout the sample excluding the loaded and constrained faces. The compressive response of RPF and the results of the FEA are exhibited in Fig. 3.11. A fairly good agreement between the two sets of results can be observed and the maximum error of the numerical solution due to the approximation involved in Ogden model was found less than 6.4%. Since the main focus of this research is on the applicability and design of poly-wall, the failure and fracture of RPF was not considered in the numerical analysis.
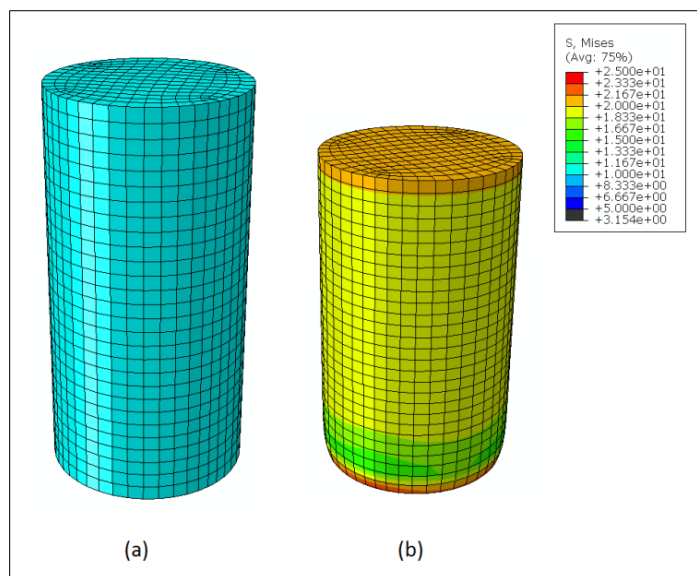
Figure 3.10: FE model of compression test: a) before loading, b) after loading
(Not to scale)
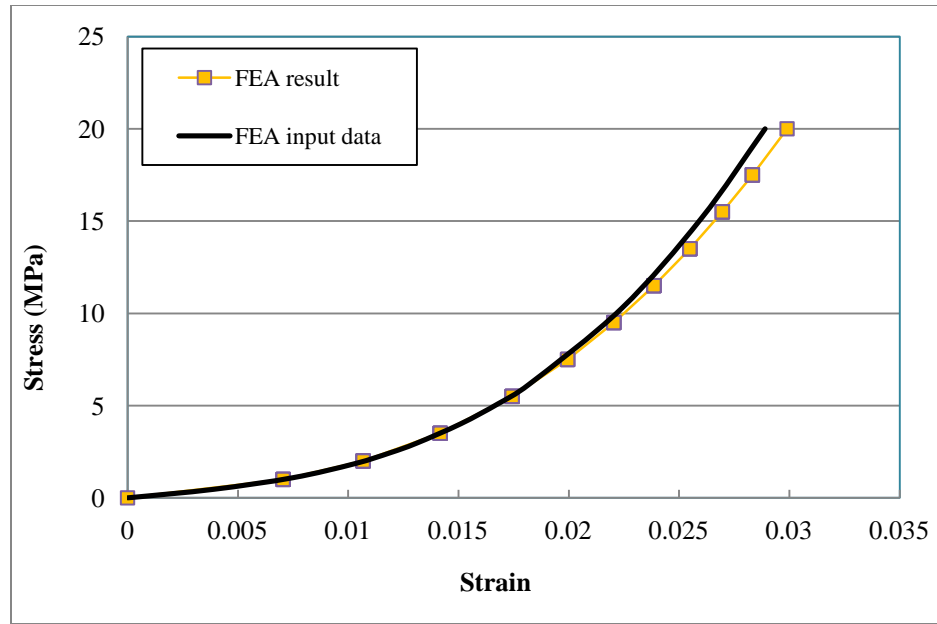
Figure 3.11: Compressive stress-strain relation of RPF and numerical results

3.3 Full-scale wall modeling

The lateral resistance of the poly-wall model was experimentally determined for a single configuration and two types of reinforcement, as discussed in Chapter 2. In order to further our understanding of the performance of full-scale poly-walls, FE analyses are undertaken herein to investigate the response of the wall with different configurations under various loading conditions. Hence, a 3D FE model that corresponds with all the features of the tested poly-wall was developed.

Initially, several preliminary analyses were executed in order to address the computational and convergence issues of the numerical solution. The solid element was selected for the modeling of poly-wall in order to capture all the interactions and contacts of its components. The initial models were verified step by step by adding more features to the geometry, material properties and interactions of the elements. The detailed model was then verified against the experimental results as discussed later.

The full-scale test walls consisted of five stacked poly-blocks, which were filled with RPF and reinforced with either 2x10M or 2x15M rebars in each core. These components

were separately simulated according to the geometric dimensions of the full-scale test walls. As depicted in Fig. 3.12, all parts of the wall were finely meshed using hexahedral brick elements (C3D8R) excluding the inner core of the rebar elements, which were simulated using 6-node triangular prism (C3D6). All elements were employed along with hourglass control and reduced integration points in order to overcome the convergence issues of the full integration.
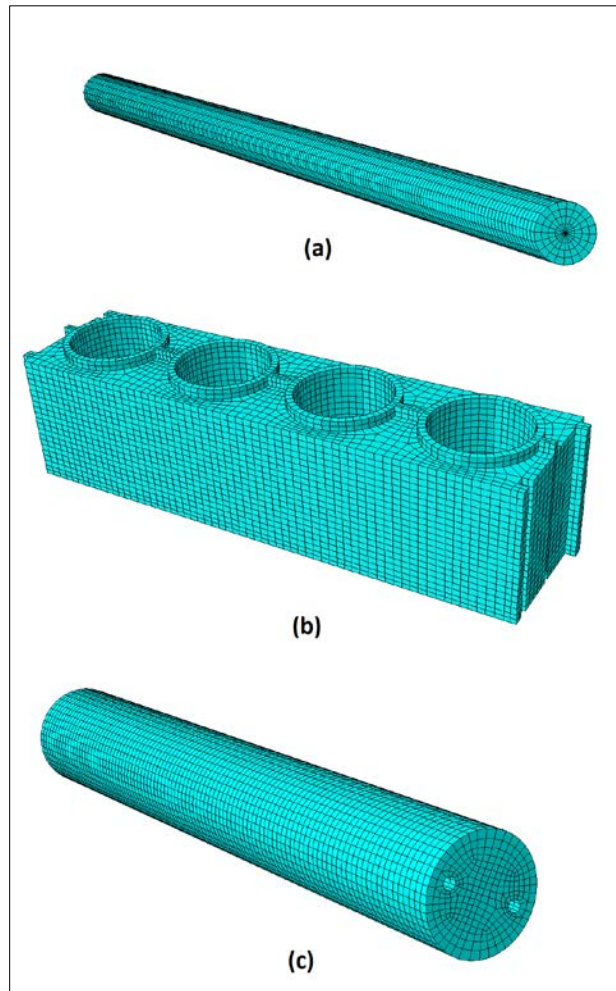
Figure 3.12: meshed parts of Poly-wall, a) rebar, b) Poly-block, c) RPF core

The rebars and RPF cores model were meshed using built-in sweep technique in ABAQUS (ABAQUS user manual, 2010). However, given the detailed geometry of the poly-block, it was discretized by implementing the advanced "bottom-up" meshing

technique. The average aspect ratio of most elements was close to unity, with maximum aspect ratio of less than 3 at regions of complex geometry. The properties of different materials including concrete, steel, RPF and poly-block's crushable foam were defined as described in the previous sections.

Fig. 3.13 displays the assembly sequence of the poly-wall model which consisted of 8 steel rebars, 4 RPF cores and 5 poly-blocks sitting on a concrete block. The contact areas of the different parts were predefined on the top surface of the foundation. Similar to the benchmark example in Section 3.2, the rebars were placed at their positions and connected to the foundation by means of tie constraints (Fig. 3.13a).

The RPF cores were placed on the indicated circular areas and contained the rebars into their cylindrical holes (Fig. 3.13b). The internal surfaces of the holes were tied to the external surfaces of the rebars. The interactions of the RPF cores and the foundation were simulated by tangential contacts between the bottom surfaces of each core and the predefined circular regions on the foundation. The interface was modeled as a "surface to surface" contact and the friction coefficient was assumed as 15%. The adhesion of concrete and RPF cores was disregarded since it cannot be relied on and not possible to measure.

Five poly-blocks model were stacked up and placed on the specified rectangular area on the wall footing (Fig. 3.13c). In the physical test models, the poly-blocks were thoroughly glued together and also to the foundation. Based on the experimental observations during the loading of the wall, no noticeable disconnection between the poly-blocks occurred until the failure of the RPF cores took place. Therefore, the connections of blocks including their contact surfaces and their contact with the wall footing were defined by tie constraints. Due to slight expansion of the RPF liquid during the curing process, it completely sticks to the internal surfaces of the poly-blocks voids. Since there was no relative displacement between the RPF cores and the poly-blocks, they were also tied together. Fig. 3.13d demonstrates the completed numerical model after the assembly and mesh generation.
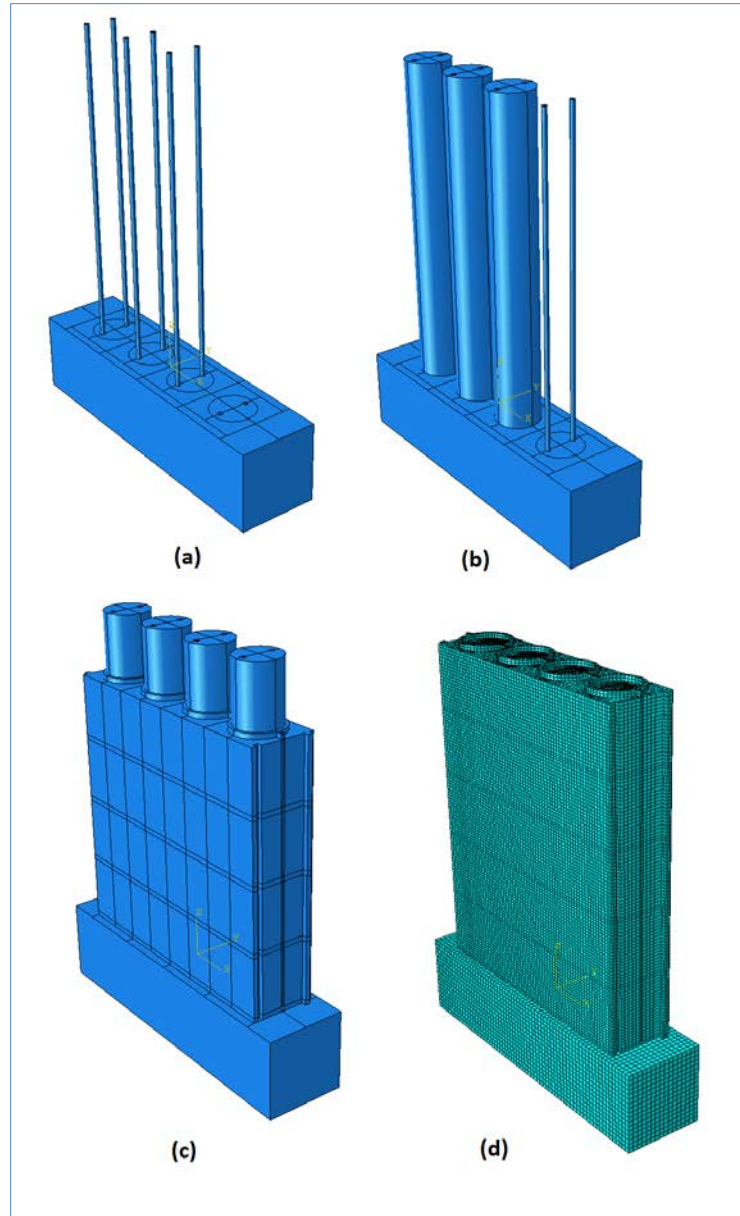
Figure 3.13: Assembly of poly-wall parts, a) rebars, b) RPF cores, c) Poly-blocks, d) completed numerical model

After the assembly stage, the boundary conditions of the FE model corresponding to the experimental test walls were defined. All the translational and rotational degrees of freedom at the bottom surface of the foundation were restrained. As Fig. 3.14 exhibits, the top block was subjected to a distributed load. For the sake of comparison with the measured experimental response, the lateral displacements of the RPF cores were

recorded at the elevation of the linear variable differential transducers (LVDTs) in the experiment (0.90 m above the foundation top surface). The base bending moment was calculated at each loading interval i.e. lateral load times the distance of measurement point from the top of the foundation. The analysis was conducted on two poly-walls, one reinforced with 2x10M and one reinforced with 2x15M rebars. The static analysis was executed and the applied load was increased by increments of 0.05 of the total lateral load.
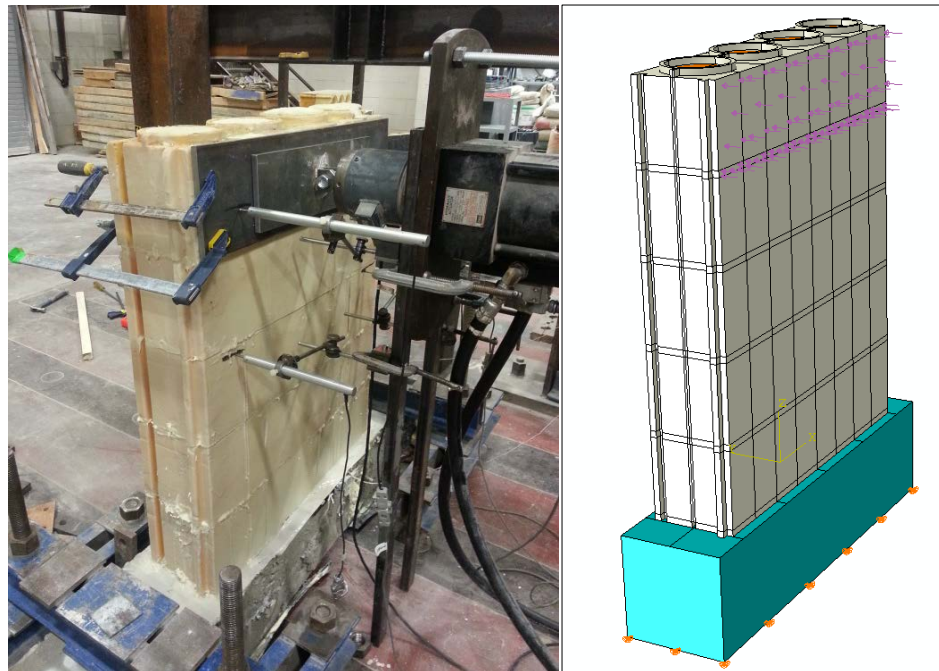
Figure 3.14: Full-scale experimental and corresponding FE model

3.4 Comparison of numerical and experimental results of poly-wall flexural performance

Figure 3.15 compares the flexural behaviour of poly-walls obtained from the numerical and experimental results. The numerical results demonstrate a linear behaviour until the rebars yielded and inelastic deformations initiated. The computed response fairly matched the experimental results up to the yield strength of both walls. The yield displacements were also well predicted by the FEA for both cases however, since the "post-yield" behaviour and fracture of materials were not considered in the numerical

analysis, the numerical results do not match the experimental results past the yield point. This is considered to be acceptable since the design for these walls should not permit yield.

The flexural behaviour of the first wall reinforced with 2x10M rebars obtained from FEA are in good agreement with the test results and form a lower-bound for the experimental lateral resistance. The experimental response of the poly-wall reinforced with 2x15M exhibited a greater initial stiffness in comparison with the FEA results. This could be attributed to some experimental factors such as tensile strength of polyurea, non-alignment of rebars and the test set-up. Also, this initial flexural stiffness was observed for the applied bending moments below 5 kN.m where non-structural elements could contribute to the load resisting system. This discrepancy was not clearly noticeable in the behaviour of the first wall.

Regardless of the higher initial stiffness, it can be seen in Fig. 3.15 that the slopes of the measured and calculated responses for the second wall are slightly unmatched, particularly for lateral displacements greater than 25 mm. This is due to the fact that the properties of RPF cores may marginally vary along the height of the wall due to slight densification of RPF during the curing time. This causes more expansion in higher elevations and subsequently less stiffness. It must also be noted that since there was a slight variation in the compressive behaviour of RPF plotted in Fig. 3.7, a low-average stress-strain relations was selected for the RPF properties in the FE model. This was done to include some level of conservatism in the design of poly-wall and to ensure that the FEA results always form a lower-bound for the lateral resistance. Considering a design moment capacity equal to 65% of the ultimate resisting moment, the flexural behaviour of the poly-walls achieved from the numerical models would be on the safe side for design purpose.
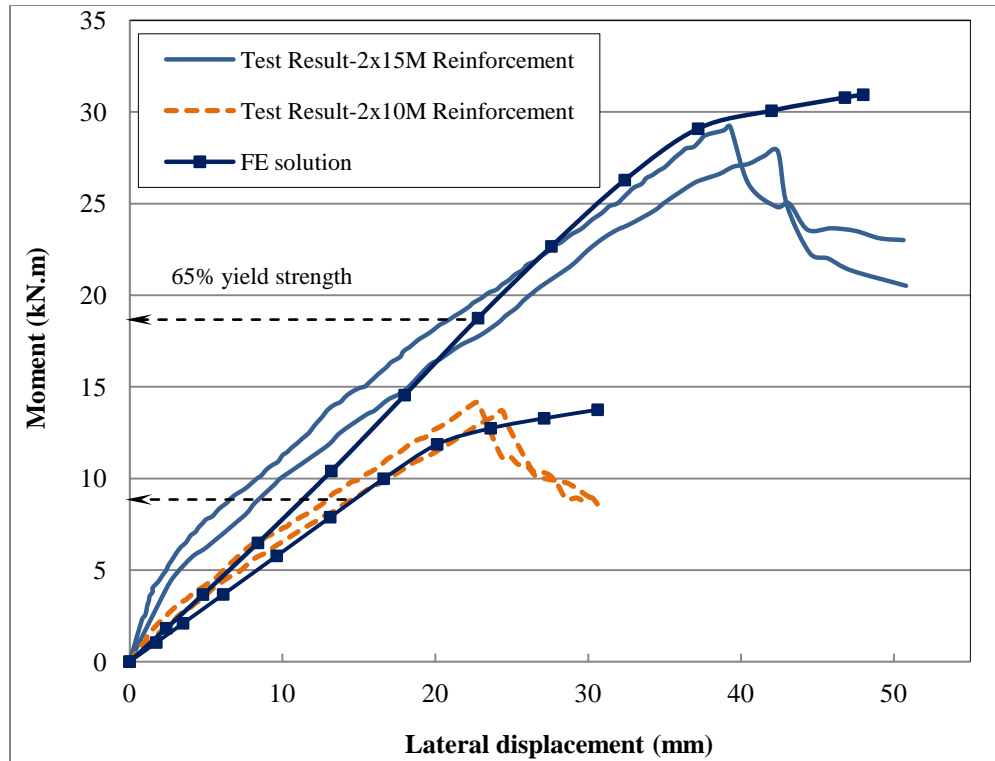
Figure 3.15: Comparison of flexural behavior from load tests and numerical analyses

3.5 Stress contour of poly-wall connection

The stress contour at the interface of the poly-wall and the foundation is illustrated in Fig. 3.16. As expected, the RPF cores have "toe" and "heel" regions associated with the compressive and tensile sides. The maximum compressive stress of the core took place at the toe region, where it contributes to the load bearing mechanism by transferring the compressive forces to the foundation. Close examination of Fig. 3.16 reveals that both tensile and compressive rebars play a major role in the anchorage system due to a significant difference between the stiffness of steel and RPF. It can be also observed that the tensile and compressive stresses in the rebars exceed the yield strength.

The stresses in the poly-blocks were minimal due to their negligible stiffness. The maximum tensile stress in the RPF elements was equal to 10 MPa and occurred in the vicinity of the tensile rebar immediately above the foundation. This value well matched

with the modulus of rupture obtained from the flexural tests specified earlier in Chapter 2. Also, this maximum stress occurred at the same location where the RPF cores cracked and failed in the full-scale experiments according to the test observations.
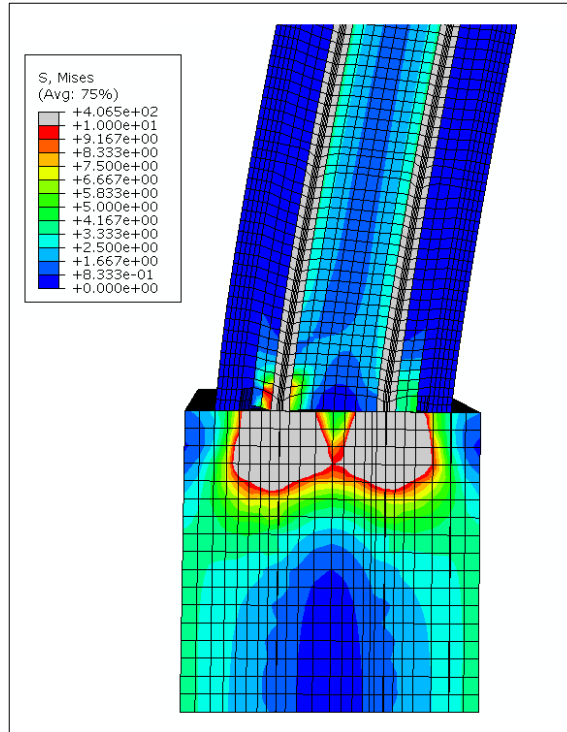
Figure 3.16: Stress contour at the connection of Poly-wall and foundation
(Not to scale)

3.6 Discussion on the finite element analysis

Several attempts were made to improve the accuracy and efficiency of the analyses because the computation time for analysis of a finely meshed poly-wall with all geometrical features using load-controlled analysis exceeded 70 hours. To optimize the time of the numerical solution, the results of displacement-controlled and load-controlled analyses were compared and the former was found to be superior in terms of convergence rate in the nonlinear domain.

To ensure that the mesh density has no impact on the accuracy and the solution convergence, sensitivity analysis was conducted considering different element size of poly-wall components. It was concluded that finer mesh of the rebars and to some extent

of the RPF cores resulted in higher accuracy. On the other hand, no effect on the results was observed by refining the poly-blocks mesh.

The effect of the number of tie constraints on the computations time was also evaluated. In this case, the poly-blocks, RPF cores and the rebars were assembled as a single part with different properties and the tie constraints between them were removed. However, their interfaces with the foundation were kept unchanged (i.e. tie constraints of rebars and contact surfaces of RPF cores). These changes significantly reduced the computation time to less than 11 hours and no noticeable change in the accuracy of the results was observed. The only disadvantage of this method is that discretization of a single part with a sophisticated geometry is more complicated and time-consuming than several independent parts.

It was also found that the effect of poly-blocks stiffness on the performance of the poly-wall model is trivial. Therefore, the details of poly-block geometry were reduced by removing its edges and grooves. Thus, the detailed model of poly-block shown in Fig. 12b was replaced with a simplified poly-block model similar to that shown in Fig. 6a. This modification reduced the solution time to 3 hours with no impact on precision of the results.

3.7 Wind load on poly-wall

In this section, the structural performance of poly-wall is investigated for application as a sound wall. In this case, its design is mostly dominated by the response to wind loading. Hence, in order to evaluate the response of the poly-wall to wind loading, the two FE models of the poly-wall that were verified using the experimental results are employed in the analysis. However, the applied loads were replaced with a uniform lateral load on one surface of the wall to represent the wind loading. Since, the total height of the wall is less than 4m, the wind load was uniformly distributed along the height. Similar to previous analyses, the load was increased gradually by increments of 0.05 of the total load.

Fig. 3.17 compares the behaviour of poly-walls under uniform lateral load with that due to semi-concentrated loads for two types of reinforcement. The plots in Fig. 3.17 show the resultant applied lateral load versus the displacement at the wall top. Since, the resultant of the uniform load acts at the mid-height of the wall, the base bending moment produced by this load is almost half of that produced by the concentrated lateral load applied at the top block. Given that response is dominated by bending deformations, the lateral yield load in the case of uniform loading is twice the yield load for concentrated loading at the top.

(a)   (b)
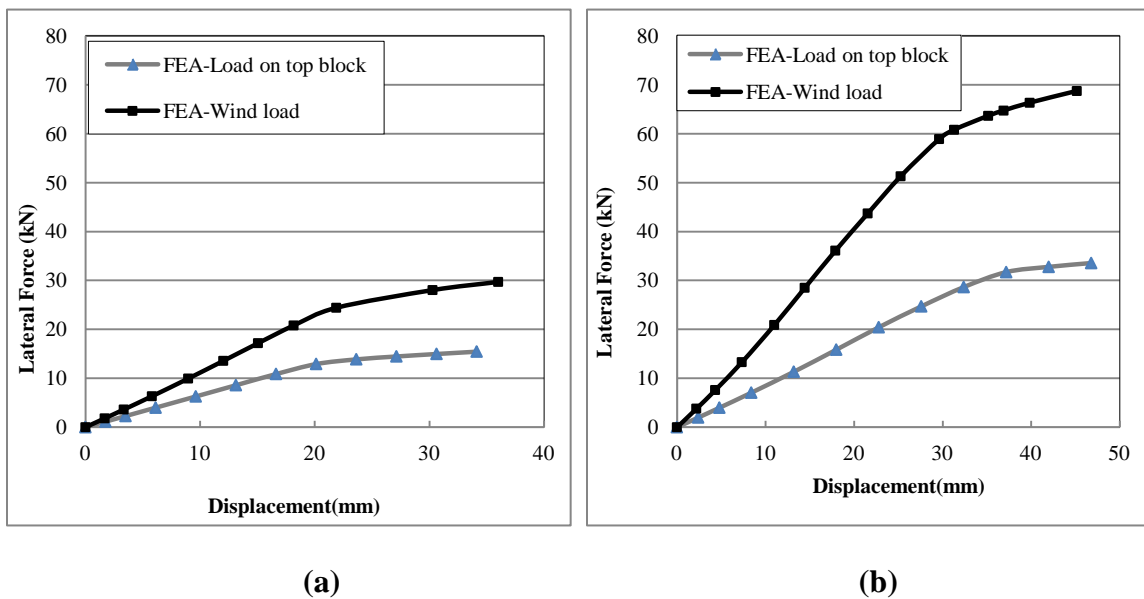
Figure 3.17: Comparison of lateral load-displacement relationship of poly-wall in concentrated and distributed loading, wall reinforced with a) 2x10M, b) 2x15M

The walls deflections due to both types of loadings were also obtained from "linear elastic solution". The poly-wall was simplified with a cantilever beam as shown in Fig. 3.18. Assuming identical flexural stiffness and equal total load, the ratio of end displacements of beams 1 and 2 is obtained as $\Delta_2/ \Delta_1 =2.16$.

The same ratio was calculated for the poly-walls using the numerical results shown in Fig. 3.17. For the poly-walls reinforced with 2x10M and 2x15M, the deflection ratios

were 2.24 and 1.96, respectively, i.e. difference of 3.7% and 9.2% relative to the equivalent beam results.

This comparison demonstrates the possibility of employing an equivalent flexural stiffness (EI) for the design of poly-walls with different load distributions and heights. It is believed that the equivalent cantilever beam can reasonably estimate the lateral displacement of poly-walls. On the other hand, the maximum factored moment induced by wind loading can be calculated according to the building codes and then compared with the flexural yield capacity of the anchoring system of the wall (i.e. RPF cores with reinforcing bars), which was experimentally established. Hence, this equivalent approach may be employed as a replacement of the rigorous FEA for the preliminary design of poly-walls under different lateral load profiles.
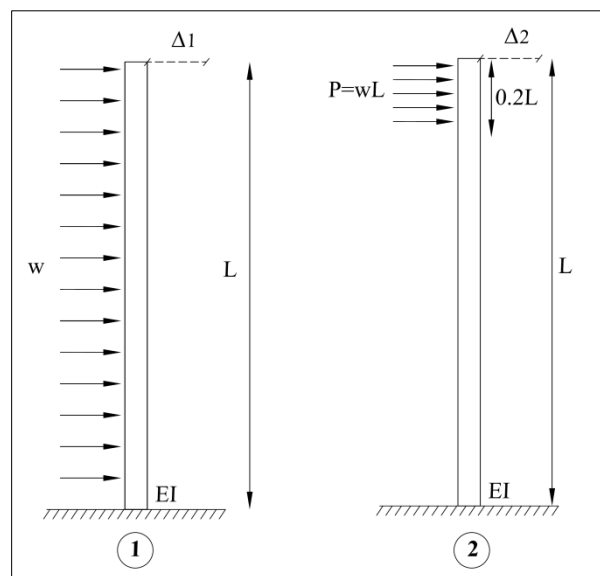
Figure 3.18: Equivalent model of poly-wall

3.8 Effect of external vertical load on the lateral resistance of the poly-wall

Poly-wall can be used as a load bearing wall system and carry vertical load in addtion to lateral load. Sound barries sometimes have attachments, which may apply external gravity loads on the wall. Also, poly-wall can be employed as a perimeter walls of

buildings which carry the vertical loads besides wind load. This combined loading was investigated herein assuming that the vertical load is applied on the cores of the wall to be transferred to the the foundation. The vertical load path should be accurately designed in order to achieve the best lateral performance of the poly-wall.

A parametric study was conducted to determine the effect of vertical load on the lateral resistance of poly-walls reinforced with 2x10M and 2x15M rebars. For theses analyses, the total vertical (dead) loads were uniformly distributed on the RPF cores at the wall top and a uniform lateral wind load was then gradually applied to the surface of the wall. The analyses were performed for 0, 0.5, 1, 1.5 and 2 MPa vertical pressure on each core and the total lateral resistance of the poly-wall was obtained in each case. The numerical model is demonstrated in Fig. 3.19 representing the applied loads on the wall.

The numerical analyses results for poly-walls reinforced with 2x10M and 2x15M rebar under combined loading are illustrated in figures 3.20 and 3.21. For both walls, it is noted that up to 0.5 MPa vertical pressure, lateral yield resistance remained almost constant. However, the yield resistance decreased proportional to the increase in vertical loads beyond 0.5MPa. This is due to the fact that the rebars, which are the main load-bearing component of the wall become preloaded before the lateral load application. This results in some reduction of their load bearing capacity. Tables 3.1 and 3.2, show the percentage of the reduction in lateral resistance of the wall. For the first poly-wall reinforced with 2x10M, reduction of lateral resistance due to vertical pressure is negligible up to 0.5 MPa and is 20% up to 1MPa. For the wall reinforced with 2x15M, the reduction of lateral resistance up to 2 MPa is limited to 10.7%. Design of Poly-wall shall be in compliance with the reported values considering the effect of vertical loads, if applicable.
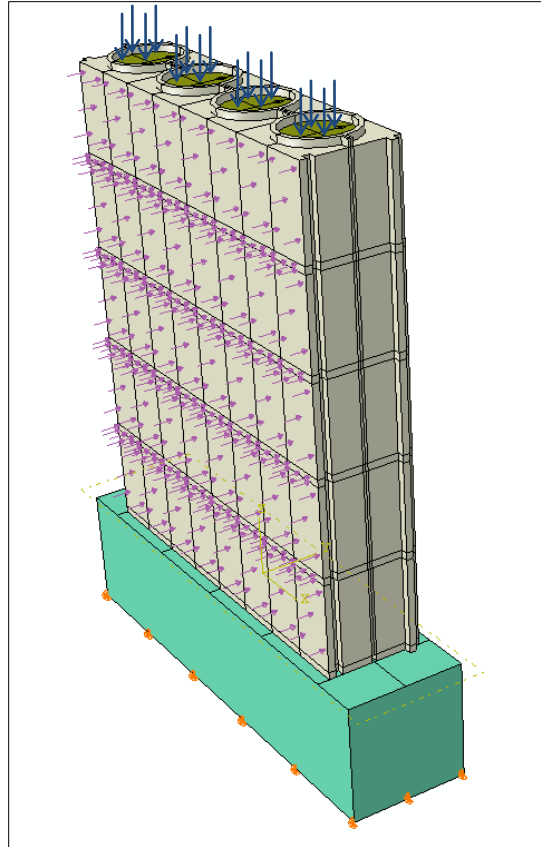
Figure 3.19: Numerical model of the Poly-wall under simultaneous loading
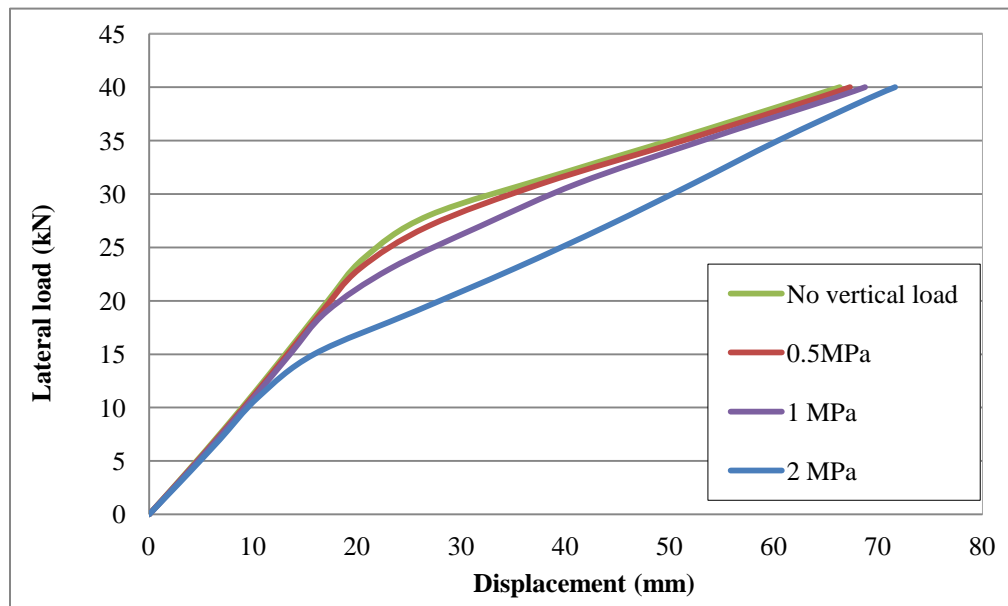
Figure 3.20: Lateral behavior of Poly-wall reinforced with 2x10M under simultaneous loading
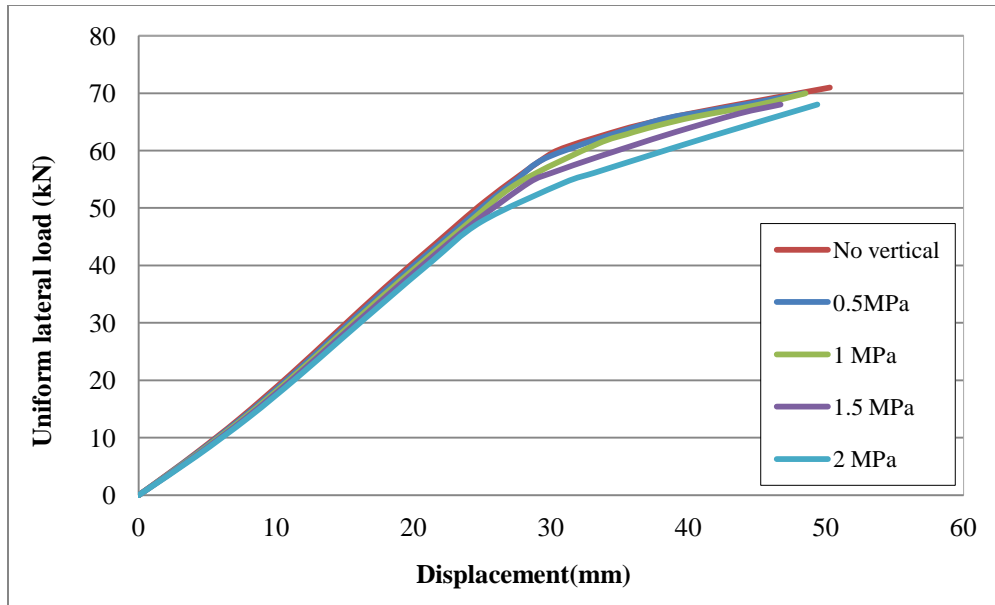
Figure 3.21: Lateral behavior of Poly-wall reinforced with 2x15M under simultaneous loading

Table 3.1: Effect of vertical load on lateral resistance of poly-wall reinforced with 2x10M

Vertical pressure on each core (MPa)	Total vertical load for a unit length (kN)	Reduction % of lateral resistance
0	0.0	0
0.5	38.5	-1.9%
1	76.9	-20.2%
2	153.9	-44.4%

Table 3.2: Effect of vertical load on lateral resistance of poly-wall reinforced with 2x15M

Vertical pressure on each core (MPa)	Total vertical load for a unit length (kN)	Reduction % of lateral resistance
0	0.0	0
0.5	38.5	0.0%
1	76.9	-4.6%
1.5	115.4	-7.5%
2	153.9	-10.7%

3.9 Conclusions

A comprehensive 3D Finite Element model was developed to investigate the structural performance of the proposed sound wall (poly-wall) under lateral loading. For this purpose, 3D FE models of the wall components were calibrated using test data. Numerical models of the entire poly-wall was then established and verified using the experimental results. Finally, the lateral performance of the poly-wall model was assessed under wind loading and a simplified equivalent model was proposed for the design applications. The effect of vertical load on lateral strength of poly-wall was established for different levels of pressure. According to the results of this study, the following conclusions can be drawn:

1. An excellent agreement was achieved between the numerical predictions and the experimental observations of the poly-wall components including steel rebar, poly-block and RPF cores which indicates high accuracy of FE modeling.

2. The Ogden hyperelastic model was capable to accurately simulate the behaviour of RPF under uniaxial and flexural loading.

3. The calculated responses using the numerical model of the full-scale poly-walls were in reasonable agreement with the measured responses during the experiments. The calculated responses formed a lower bound for the observed lateral resistance during the physical experiments within the desired range of design requirement.

4. The equivalent beam model of the poly-wall was verified with the numerical outcomes. It may be employed to calculate the lateral displacement of the wall with reasonable accuracy.

5. Results of parametric studies indicated that vertical loading has negligible effects on lateral strength of Poly-wall up to 0.5 MPa for both types of reinforcement. The reduction factor of lateral strength due to vertical load is more pronounced for the wall with 2x10M reinforcement however, the stronger wall is less sensitive to the vertical pressure.

3.10 References

ABAQUS analysis user's manual (2010). Version 6.9-1, Dassault Systemes Corp, Providence, RI.

ASTM Standard C39/C39M-12. (2012). "Standard Test Method for Compressive Strength of Cylindrical Concrete Specimens." West Conshohocken (PA), ASTM International.

Canadian Standard Association (2009). "CAN/CSA-G30.18-09 Carbon steel bars for concrete reinforcement." Mississauga, Ontario, Canada.

Daee, B. and El Naggar, M.H. (2014). "Application of Polyurethane Products in Accelerated Construction of an Innovative Noise Barrier: Experimental study." (Under review).

Lowes L.N. (1999). "Finite Element Modeling of Reinforced Concrete Beam-Column Bridge Connections." Doctor of Philosophy in Civil Engineering, University of California, Berkeley.

Ogden R. W. (1972). "Large Deformation Isotropic Elasticity on the Correlation of Theory and Experiment for Incompressible Rubberlike Solids." Proceedings of the Royal Society of London. Series A, Mathematical and Physical Sciences, 326(1567), 565-584.

Priddy L.P. and Newman J.K. (2010). "Full-Scale Field Testing for Verification of Mechanical Properties of Polyurethane Foams for Use as Backfill in PCC Repairs." Journal of Materials in Civil Engineering, 22, 245-252.

Schreyer H. L. and Zuo Q. H. (1994). "Anisotropic Plasticity Model for Foams." Journal of Engineering Mechanics, 120, 1913-1930.

Witkiewicz W. and Zieliński A. (2006). "Properties of the Polyurethane (Pu) Light Foams. "Advances in Materials Science, 6(2), 35-52.

Zenkert D. and Burman, M. (2009). "Tension, Compression and Shear Fatigue of a Closed Cell Polymer Foam." Composites Science and Technology, 69, 785-792.

Chapter 4

Application of Flexi-wall in Noise Barriers Retrofitting

This chapter presents an experimental and numerical study on structural performance of an innovative noise barrier consisting of poly-block, light polyurethane foam (LPF) and polyurea. This wall system (flexi-wall) is intended for application as a vertical extension to existing sound barriers using an accelerated construction method. Experimental and numerical analyses performed on the wall system and results were discussed in this chapter.

4.1 Introduction

Noise barriers reduce and block the noise waves traveling toward residential areas. With development of urban areas, some of the existing sound walls are required to be vertically extended since most often they are not high enough to efficiently attenuate the noise pollution.

Some provinces across Canada have established a "noise barrier retrofit program", which mainly involves extending and renewing of the existing sound walls in urban environments, to minimize sound pollution impacts on public health. According to the published policy of ministries of transportation of several provinces (e.g. Ontario, Alberta and British Columbia), accelerated and cost-efficient construction techniques, which do not alter the structural system and foundation of the existing walls are desired. The program also focuses on the sound walls built in the last few decades which are not high enough and are required to be vertically extended 1-2 m to influentially absorb and reflect the vehicles noise.

An innovative sound wall system was developed at the Western University, and was examined to serve as a vertical extension to the existing sound walls. The wall system (denoted as flexi-wall) consists of stay-in-place poly-blocks as formwork, light polyurethane foam (LPF) reinforced with steel rebars as structural cores and polyurea as

a coating of the wall surfaces (Fig. 4.1). Poly-blocks are interlocking light-weight blocks which are stacked up layer by layer and act as formwork for the LPF cores. The poly-block is 200×200×800 mm and includes four cylindrical voids with 140 mm diameter. It is made of molded low-density polyurethane and weighs approximately 1kg. The poly-blocks are fire-resistant blocks and have an excellent capability to absorb, mitigate and reflect a wide range of noises with unmatched frequency of reflective noise. Polyurea coating is an abrasion-resistant finishing layer, which is sprayed on the surfaces of the wall and sets within 2-3 minutes. This layer also enhances the surface resistance of poly-blocks against stone impact, weathering, fire development, chemicals and penetration. LPF is an expanding liquid mixture which is injected into the poly-block voids and cures within 10 minutes. Steel rebars are epoxied into holes drilled in the existing sound wall and connect the wall extension to its base.
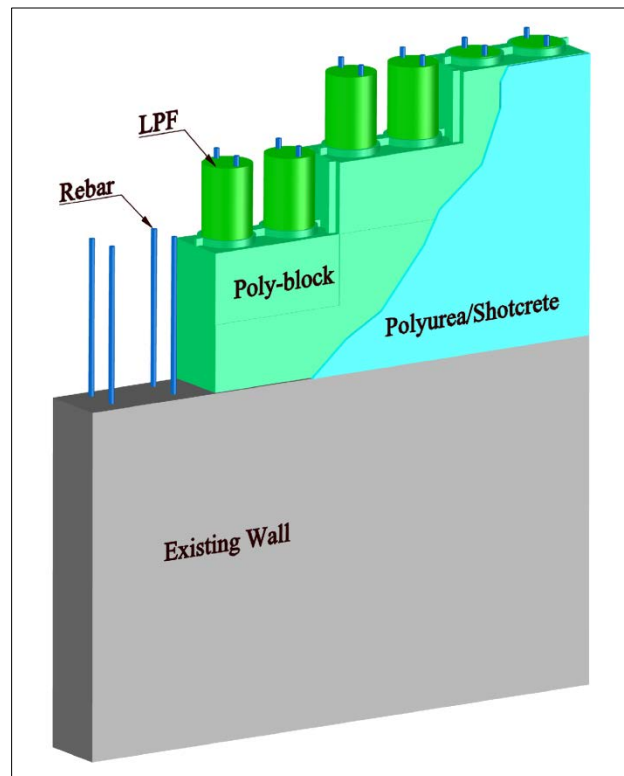
Figure 4.1: Extending an existing sound wall using flexi-wall

In comparison with conventional masonry walls, conducted acoustic experiments show that such a wall system consisting of polyurethane products are highly noise-absorbing (Acoustic consulting service, 2008). The construction of flexi-wall along roadways is also faster and less obstructive since there is no need for construction vehicles and mobile cranes, which usually block or constrict the roads during roadside construction. This accelerated technique also reduces traffic congestion, construction noise and risk of road accidents during the construction period which results in lower cost of the project.

To investigate the structural performance of flexi-wall, several mechanical experiments on specimens and full-scale walls were conducted. Five compression tests were carried out on cylindrical samples of LPF and its stress-strain behavior was established. The bond strength of LPF to steel rebars was also obtained through four pull-out tests. Two full-scale flexi-walls were constructed and their lateral resistance was experimentally determined. A full-scale flexi-wall was subjected to 15000 cycles of lateral loading in order to investigate its mechanical degradation during cyclic loading events (e.g. wind loading). Finally, 3D numerical model of the wall components as well as full-scale flexi-wall were developed and verified using experimental results. The finite element model was then employed for further investigation of the wall behavior under different loading condition.

4.2 Light polyurethane foam

Light polyurethanes foams (LPF) are composed of a chain of diisocynates and polyols and their mechanical strength completely correlates with their density, which ranges from 3 to 50 lb/ft^3 (48-800 kg/m^3) (Li et al., 2013). By changing manufacturing techniques, chemical formulation or production process, different polyurethane with various characteristics can be produced. Polyurethanes are currently being used in different industries such as, aerospace, automotive, furniture and medical equipment due their light-weight, formability and durability.

The application of LPF in buildings constructions is mainly limited to thermal insulation in sandwich panels and prefabricated walls. Some attempts have been recently made in order to incorporate light foams in load-bearing structural elements. For instance, the

application of LPF in lightweight mortar has been examined and results indicated that LPF improves workability and consistency of mortar while its flexural and compression strength remain unaffected (Junco et al., 2012). There is also a growing interest in the use of expanding polyurethane foam to remediate expansive soil and differential settlement of concrete slabs and foundations (Buzzi et al., 2010).

Deformation of light foams under a uniform pressure is typically linear before the yield point, which is followed by a plateau with small stress variation (Fig. 4.2). The plateau region is irrecoverable and continues up to large strains at which point densification initiates. Locking stage takes place as the cell walls of the foam buckle and collapse and air escaping and stiffness hardening continue until the ultimate failure occurs (Buzzi et al., 2010).
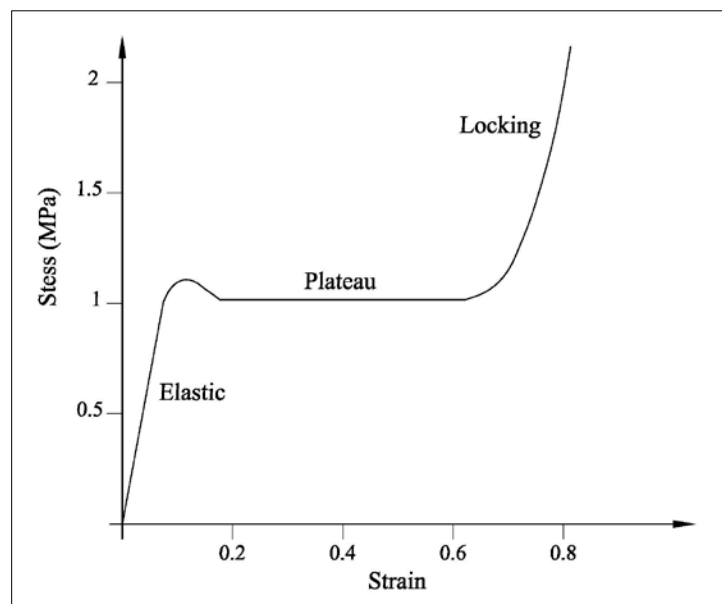
Figure 4.2: Typical compressive behavior of LPF

In this research, a specific mixture of closed-cell light polyurethane foam with 140 kg/m^3 density was employed. The components of this LPF were mixed in liquid form below 60°C and then were injected into poly-blocks voids. This foam usually cures within 6-10 minutes and gradually reaches its maximum strength in less than an hour in ambient temperature.

4.3 Flexi-wall structural system

The flexi-wall structural system comprises poly-blocks, LPF and reinforcements. Poly-blocks can distribute lateral loads almost equally to the LPF cores. As displayed in Fig. 4.1, the LPF cores inside poly-blocks are reinforced with steel rebars and form the structural cores of flexi-wall. Rebars connect and anchor the wall to its base and since the stiffness of rebars is considerably greater than LPF, they also provide lateral stiffness for the entire walls system. A layer of shotcrete may be also applied on the surfaces of the wall to provide more structural integrity and consistency with the existing wall.

4.4 Compression test of light foam specimens

To determine the compressive behavior and particularly the yield strength of LPF, compression tests were carried out on five cylindrical specimens with 100 mm diameter and 150 mm height. To make the specimens, LPF liquid mixture was injected to the plastic cylindrical molds and after some minutes they were taken out to completely set. The bottom and top surfaces of the sample were then cut to provide a flat surface for loading.

Figure 4.3 illustrates the compression test set-up of the LPF specimens. Two steel plates and a revolving joint were used to ensure that the load is uniformly distributed on the top surface of specimen. The load was applied at the rate of 0.2 kN/s through the loading cell of the testing machine. The compressive load and the total deflection of samples were recorded using the load cell. Since the specimens underwent very large deflections during the tests, true strain was calculated rather than less accurate engineering strain.

The tests were stopped once samples started to distort between 25% and 35% of strain since it is beyond the engineering strain range. Two LPF specimens before and after compression test are exhibited in Fig. 4.3a and 4.3b and results of the test are illustrated in Fig. 4.4.

(a) **(b)**
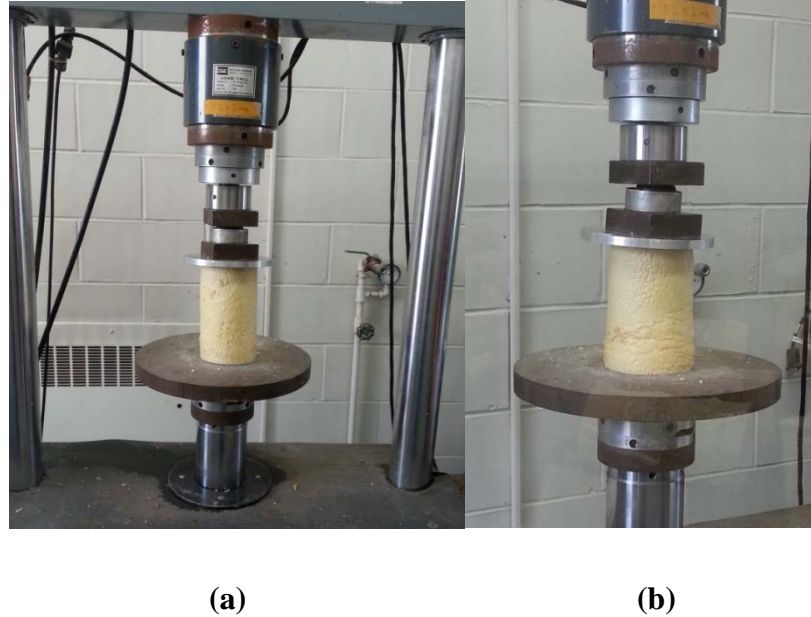
Figure 4.3: Compression test on LPF samples, a) before loading, b) after loading

The solid lines in Fig. 4.4 display the compressive stress versus true strain of LPF specimens acquired from the experiments. In all cases, a peak was observed at the yield point, and the average strength within the plastic region was found to be 1.3 MPa. The dashed line in Fig. 4.4 is a bilinear representation of the average of idealized compressive behavior of LPF specimens, which is consistent with the typical compressive behavior of low-density foams. The average test data was achieved based on the average post yield values and slopes regardless of the peak occurs after yield point.

4.5 Pull-out test

The main objective of the pull-out test was to quantify the bond strength of steel rebar to LPF by measuring the required force to pull the embedded rebar out of the LPF core. The rebar dowels in the proposed structural system transfer the load to the wall footing and their length influences the wall lateral stiffness.

For this test, two wood formworks were made as shown in Fig. 4.5a to hold the rebars at the center of the poly-block voids. The LPF was injected into the voids and allowed to harden, the formwork was then demolished and the samples were removed.
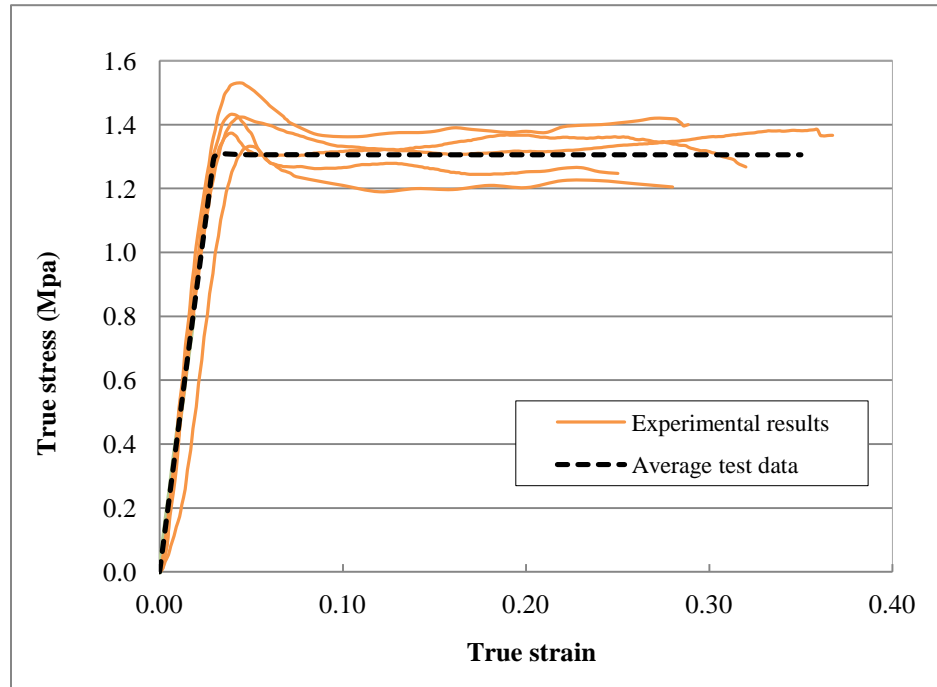
Figure 4.4: Compressive Stress-strain relation of LPF samples

Rebar sizes of 10M and 15M with f_y=400 MPa (Grade 400R of CSA-G30.18-0) were selected and the net rebars' embedded length was 380 mm. The samples were assembled in the testing machine as displayed in Fig. 4.5b. The rebars were pulled at the rate of 0.2 kN/s while LPF cores were held by the fixed cross-head of the test machine. The test was performed for 2 samples of each rebar size. The peak tensile force (P) was recorded to calculate the bonding strength (f_b) assuming that stress is uniformly distributed along the embedment length of rebar, i.e:

$$f_b = \frac{P}{\pi D_b L_b}$$

(4.1)

where D_b and L_b are diameter and embedment length of rebar, respectively. The bond strength of each test and the average results for 10M and 15M rebars are shown in Table 4.1. These values are used for design of the wall and determination of development length of rebars inside LPF cores.

| (a) | (b) |
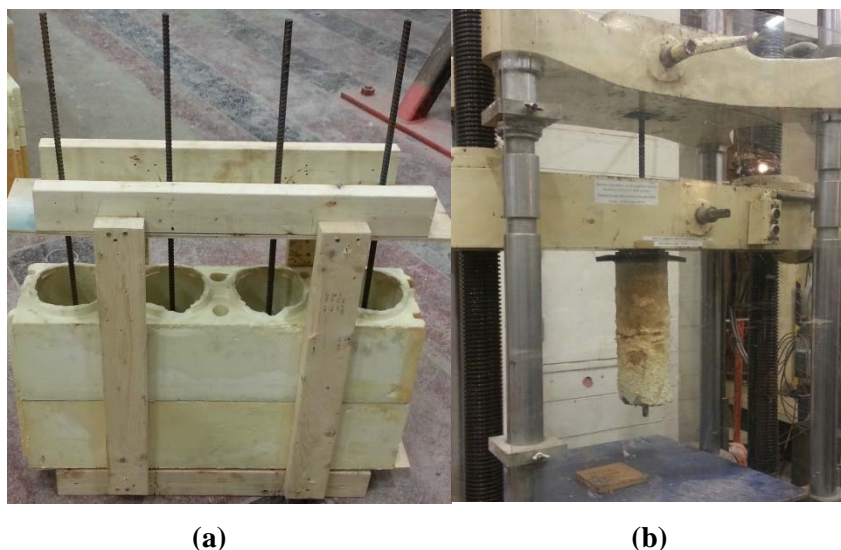
Figure 4.5: Pull-out test arrangements a) Pull-out test formwork, b) test set-up

Table 4.1: Bond strength of LPF to steel rebar

Test No.	Rebars Size	
	10M	15M
Test-1 (MPa)	0.74	0.83
Test-2 (MPa)	0.76	0.87
Average bond strength (MPa)	0.75	0.85

4.6 Full-scale static test of flexi-wall

Two full-scale wall tests were carried out to investigate the performance of flexi-wall as an extension to existing noise barriers. The first aim was to monitor the construction approach for the first time and verify the applicability of the wall system in accelerated constructions. As wind load is the predominant load used in design of noise barriers, the second aim of the full-scale wall tests was to determine the lateral resistance of flexi-wall. Initially, wood formworks were made for the wall footings and concrete with f'$_c$=30 MPa was cast in place. The formworks were then disassembled, top surface of footings

was leveled and the positions of rebars were marked. The dowels were inserted and epoxied into the drilled holes after curing the concrete using Hilty epoxy of HIT-HY150MAX-SD which provides a high-strength bond.

The first course of poly-blocks was positioned on the footings and epoxied in order to prevent dislocation of poly-blocks and leakage of LPF during the injection into the voids. The rest of the blocks were stacked on the first course and epoxied together. To ensure that LPF liquid does not leak out of the block joints, a layer of polyurea was sprayed to seal up all the seams and joints.

Fig. 4.6 demonstrates the structural configuration of full scale walls. They consisted of five poly-blocks whose voids were filled up with LPF. The walls were reinforced with 2×15M and with 90 mm spacing in each core.
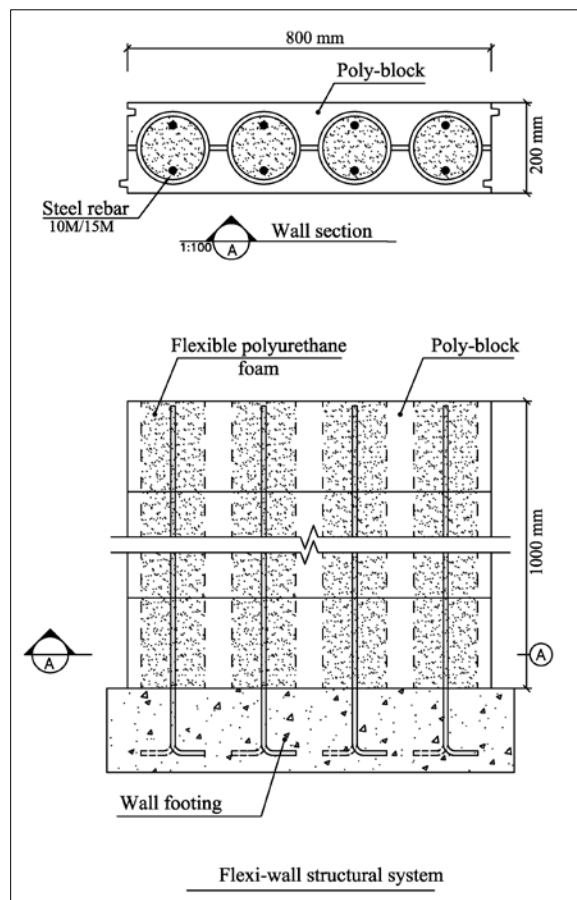
Figure 4.6: Flexi-wall structural system and anchoring details

The whole test set-up was designed before the walls construction such that the wall footing properly places between existing anchor holes of the strong floor of the Structural Laboratory at Western University while the actuator loading plate meets the wall surface (Fig. 4.7).

A 2 mm layer of Polyurea was sprayed on the wall surfaces as a finishing layer. Although Polyurea does not influence on structural performance of flexi-wall, it brings higher surface resistance for the poly-blocks as well as integrity for the entire wall system.
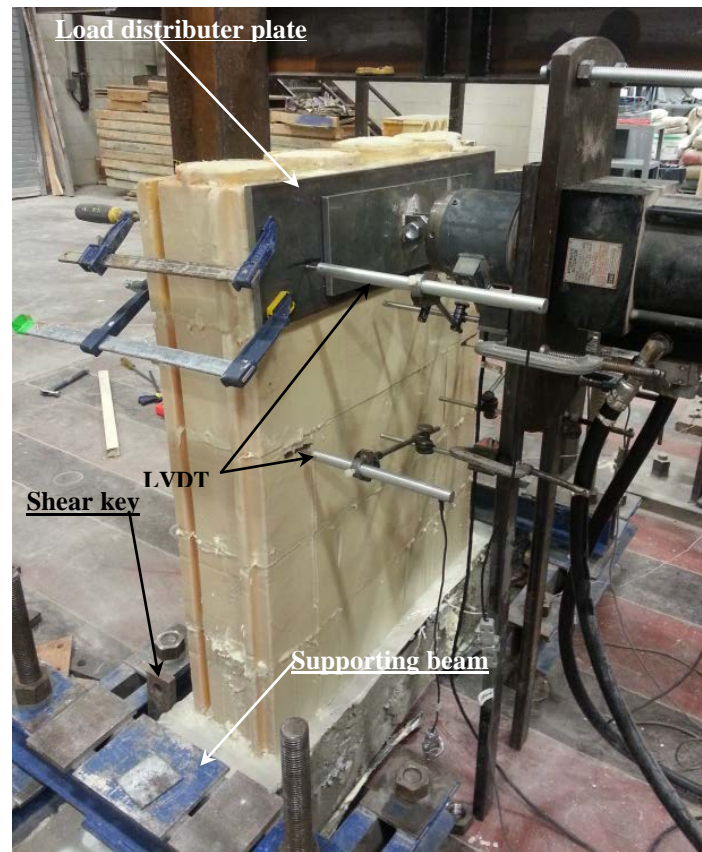
Figure 4.7: Full-scale test arrangements of flexi-wall

The walls were moved and fixed to the floor in front of the actuator as shown in Fig. 4.7. A sophisticated anchoring system consisting of several beams and bolts was utilized to fix the foundations to the strong floor. Four Linear Variable Differential Transducers (LVDTs) were installed on both sides of each wall to measure its lateral displacement. A load distributer steel plate with the same size of the poly-block was used to uniformly

distribute the load on the top block. The walls were preloaded to 0.5 kN to ensure that all surfaces are in full contact. The walls were laterally loaded at the rate of 0.2 kN/s until the first failure occurred. All walls failed in flexural mode and rupture took place at the LPF cores and inside the lowest poly-block immediately above the foundation, where all rebars were bent. No torsion took place according to the LVDTs readings installed on both sides of the wall.

The test results of the two flexi-walls are depicted in Fig. 4.8. The results are presented in the form of moment-displacement curves with respect to the position of the upper LVDTs, which was installed 900 mm above the top of foundation. Fig. 4.8 illustrates that the walls exhibited a fairly linear flexural behavior followed by a sudden strength degradation and failure in both cases. It can also be noted that walls' stiffness, ultimate base moment and its corresponding deflections are almost identical and the overall behavior of the walls is consistent. The average of ultimate resisting moment of the walls is 16 kN.m corresponding to 48 mm lateral deflection.
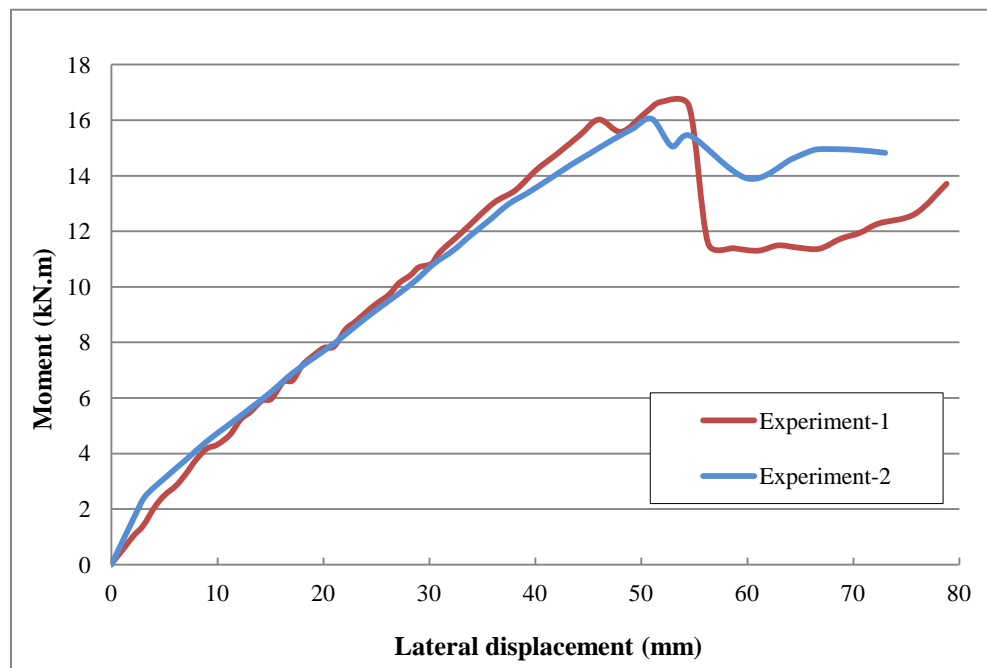
Figure 4.8: Full-scale test results of flexi-wall

4.7 Cyclic test of the flexi-wall

Utilization of new composites in construction has been always a concern for designers. Despite the advantages of new materials, they have not been widely examined in practice and therefore their long-term performance is relatively unknown once employed in a load-bearing system. Since noise barriers are exposed to the repetitive wind load over its life span, a load-control fatigue test was conducted on a full-scale flexi-wall to determine its mechanical degradation under a high-cyclic loading.

To reproduce the dynamic effects of wind load, a sinusoidal cyclic loading at 0.2 Hz frequency between a minimum moment of 4 kN.m and maximum moment of 10 kN.m was applied on the wall. The frequency of 0.2 Hz was chosen since the predominant frequency of a typical spectrum of wind energy is between 0.15 and 0.3 Hz and its maximum occurs at 0.2 Hz (Liu, 2000). The maximum magnitude of cyclic load corresponds to factored flexural resistance of flexi-wall which is 65% of the ultimate flexural resistance obtained from the static tests. The minimum magnitude corresponds to the maximum magnitude divided by gust factor which is equal to 2.5 according to Canadian Highway Bridge Design Code (CSA-S6, 2006). These peaks basically represent the mean and maximum moment induced by wind load which can be applied on the wall in practice based on the maximum flexural resistance.

A flexi-wall reinforced with 2x15M in each core was built similar to the walls that were tested under a push-over static loading. The wall was assembled as shown in Fig. 4.7, however, to push and pull the wall two steel plates were bolted to both sides of the wall and then connected to the hydraulic actuator.

The lateral load ramped up to the average value of cyclic load at the rate of 0.2 kN/s and the sinusoidal load was then initiated. The wall was subjected to 15000 cycles of loading and the test took 21 hours. This number of cycles can be a fairly good representative for the number of occurrence of maximum wind load over 25 years life span of the wall .The lateral load as well as the displacement of the wall top was recorded at synchronized intervals of 0.5 Hz using the load cell and two LVDTs, respectively.

The response of the flexi-wall for 16 cycles is depicted in Fig. 4.9, which shows the displacement of the top of the wall versus the base bending moment. Fig. 4.9 displays the hysteresis loops for the cycle of 1 to 15000 for every 1000 cycle. The maximum displacement in the first and last cycles is equal to 26.5 mm and 29.4 mm respectively, while moment peaks (4 kN.m and 10 kN.m) were maintained during the experiment with the tolerance of 0.15 kN.m. Since the response of the wall is in the linear domain, cyclic loss percentage can be calculated using the stiffness degradation of the wall which is equal to 5.71%. This value indicates that the repeatability of the wall behavior is quite sustainable over 15000 cycles of loading. It can also be concluded that the cyclic response of flexi-wall is mainly controlled by the steel rebars since the residual deformation of the wall is only 2.9 mm at most after a high-cyclic loading.
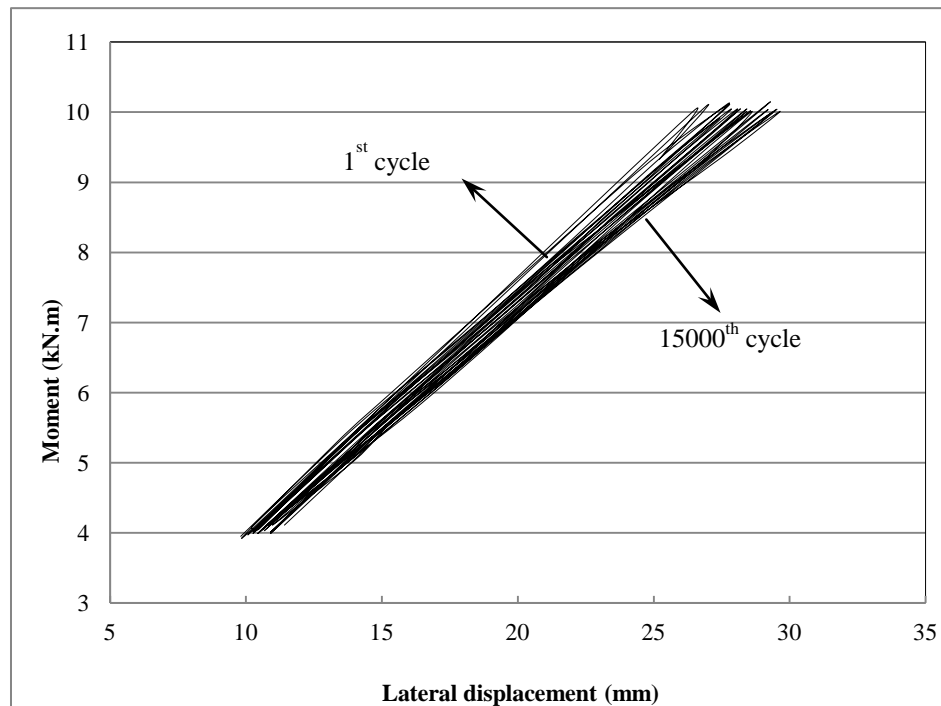
Figure 4.9: Cyclic response of flexi-wall from 1 to 15000 cycles

4.8 Preliminary design of flexi-wall

A preliminary design was conducted to evaluate the lateral resistance of a flexi-wall in practice based on Canadian standards (CSA-S6, 2006; NBCC, 2005). The factored flexural resistance for design of flexi-wall is selected equal to 65% of the yield strength

of the wall achieved from the full-scale static experiments. As a result, the ultimate moment capacity of a unit length of flexi-walls reinforced with 2x15M steel rebars with the proposed arrangement is equal to 13 kN.m. This value is equal to the maximum factored moment induced by a uniform wind pressure on a 2.5m high sound wall in Toronto area. The height suffices the required height of extension to an existing noise barrier.

4.9 Numerical model

The behavioral models of flexi-wall components including steel rebar, poly-block and foundation were assumed to be identical to poly-wall elements as described in Chapter 3 in the Sections of 3.3, 3.4. As discussed, the numerical models of these components were all individually calibrated and verified using experimental results and the results of FEA illustrated a good agreement with experimental data. Therefore, the same FE models were employed for the simulation of flexi-wall. The numerical model of LPF though, which is employed only in flexi-wall is explained in details as followings.

4.9.1 Numerical model of LPF

Finite element model of light polyurethane foam (LPF) was developed using behavioral model of crushable foam built in ABAQUS (ABAQUS FE package and user manual, 2010). To put the behavior of light foams in perspective, the average compression test results of LPF and poly-block are superimposed in Fig. 4.10 which indicates that both types of foam behave similarly under compression with different level of load-bearing capacity. Their compressive response is linear up to yield point followed by a perfectly plastic trend. This similarity is due to the fact that the density of both types of foam is relatively close (60 and 140 kg/m^3) and as a result, the same behavioral model can be employed for their numerical model.

A cylindrical FE model of LPF was developed considering the same boundary conditions as the actual tests conducted. Linear hexahedral brick elements along with the hourglass control and reduced integration points were employed in the FE model and the aspect ratio of the elements were kept under 1:3 (Fig. 4.11a). The average compressive test data (the dash line in Fig. 4.10) was properly input as the stress-strain relation of the cylinder.

Elastic properties of the foam were taken as E=45 MPa and ν=0.3 (Witkiewicz et al., 2006) and the plastic region was simulated using the crushable foam behavioral model built in ABAQUS. Large-deformation was activated in the software by implementing NLGEOM parameter. All degrees of freedom at the bottom surface of the RPF model were restrained and a uniform static pressure was applied on the top surface. Compressive stress and strain of model was recorded and compared with the input data.
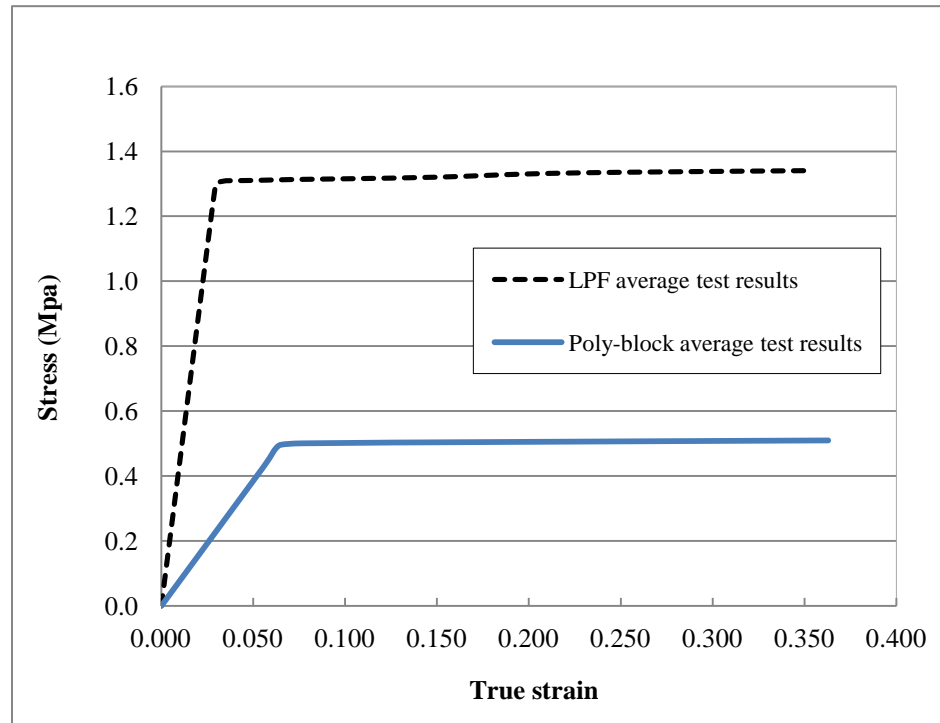
Figure 4.10: Comparison of compression behavior of LPF and poly-block

The results of the finite element analysis are demonstrated in Fig. 4.12 in the form of square dots. It can be observed that the numerical results are in excellent agreement with the average compressive behavior of the blocks across the elastic and plastic regions, indicating satisfactory accuracy of the numerical model. The undeformed and deformed shapes of the poly-blocks are shown in Fig. 4.11a and 4.11b, which are fairly similar to the test observations.
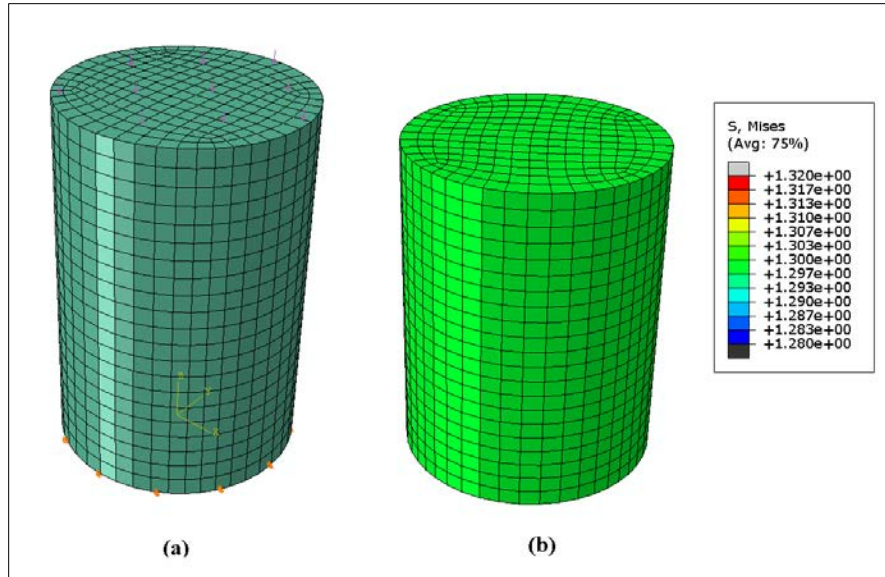
Figure 4.11: FE model of compression test of LPF, a) before loading b) after loading

(Not to scale)
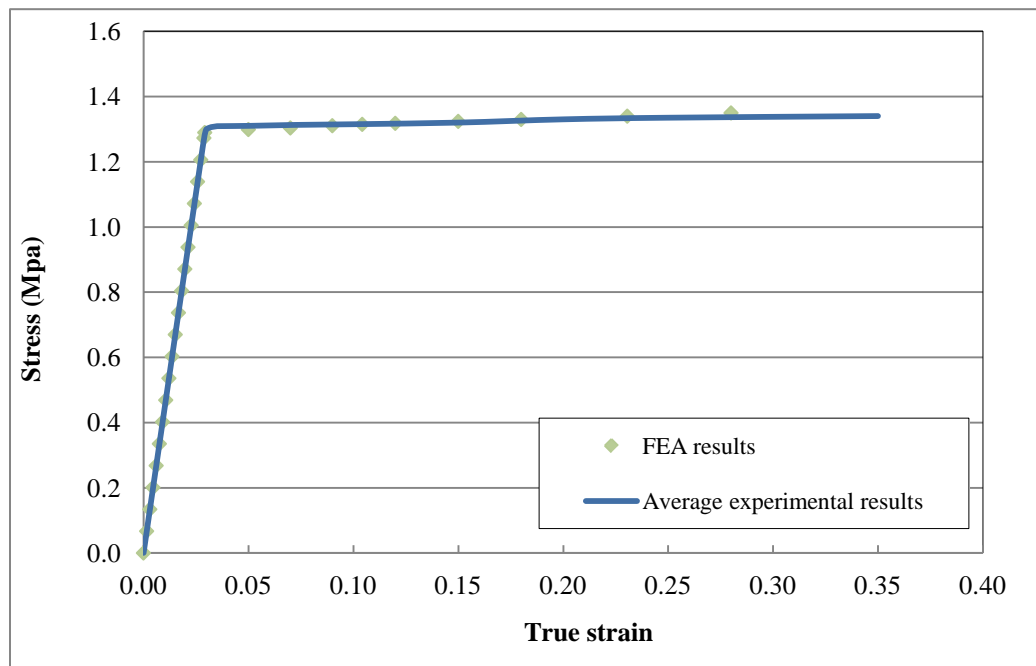
Figure 4.12: Compressive stress-strain relation of LPF

The tensile behavior of LPF was also required for the numerical modeling. In contrast to the plastic compressive behavior, tensile behavior of low-density foams is typically linear with a relatively limited plastic region (Shen et al., 2013) as demonstrated in Fig. 4.13. For the low density foams, previous studies have shown that the tensile modulus and strength (Et,σt) are slightly greater than the compressive modulus and strength (Ec,σc) (Witkiewicz et a., 2006; Zenkert et al., 2009). However, in the absence of tensile test data, it is common to assume them to be identical. In the behavioral model of crushable foams in ABAQUS, tension and compression behavior of low density foam is assumed symmetric. It is stated that in order to define the evolution of the yield surface in this model, only uniaxial compression test data is required (ABAQUS user manual, 2010).
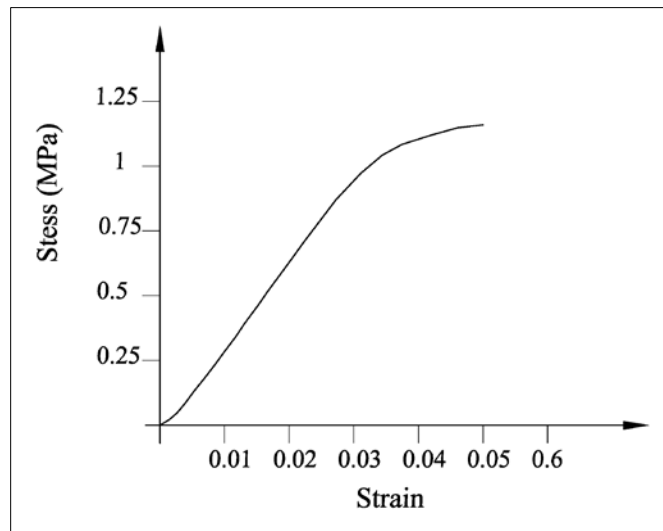
Figure 4.13: Typical tensile behavior of LPF

4.9.2 Full-scale wall modeling

As described in Section 4.6, the lateral resistance of the flexi-wall model was experimentally determined for a single configuration and 2x15M reinforcement. FE analyses were carried out to investigate the response of the wall with different configurations under various loading conditions in order to get deeper insight about the performance of full-scale flexi-walls. Hence, firstly a 3D FE model that corresponds to all the features of the tested flexi-wall was developed.

Solid brick element was utilized for the modeling of flexi-wall in order to include all the interactions and contacts of its components. The initial models were verified step by step by adding more features to the geometry, material properties and interactions of the elements. To address the computational and convergence issues of the numerical solution, several preliminary analyses were executed. The detailed model was then verified with the experimental results as discussed later.

Experimental full-scale models consisted of five stacked poly-blocks, which were filled with LPF and reinforced with 2x15M rebars in each core. These components were separately simulated according to the geometric dimensions of the full-scale test walls. As depicted in Fig. 4.14, all parts of the wall were finely meshed using hexahedral brick elements (C3D8R) excluding the inner core of the rebar elements, which were simulated using 6-node triangular prism (C3D6). All elements were employed along with hourglass control and reduced integration points in order to overcome the convergence issues of the full integration.

The rebars and LPF cores model were meshed using built-in sweep technique in ABAQUS. However, given the detailed geometry of the flexi-block, it was discretized by implementing the advanced "bottom-up" meshing technique. The average aspect ratio of most elements was close to unity, with maximum aspect ratio of less than 3 at regions of complex geometry. The properties of different materials including concrete, steel, RPF and poly-block's crushable foam were defined as described in Chapter 3.

Fig. 4.15 displays the assembly sequence of the flexi-wall model. The contact areas of the different parts were predefined on the top surface of the foundation. Similar to the simulation approach of poly-wall, the rebars were placed at their positions and connected to the foundation by means of tie constraints (Fig. 4.15a).

The LPF cores were placed on the indicated circular areas and contained the rebars into their cylindrical holes (Fig. 4.15b). The internal surfaces of the holes were tied to the external surfaces of the rebars. The interactions of the LPF cores and the foundation were simulated by tangential contacts between the bottom surfaces of each

core and the predefined circular regions on the foundation. The interface was modeled as a "surface to surface" contact and the friction coefficient was assumed as 15%. The adhesion of concrete and LPF cores was disregarded since it cannot be relied on and not possible to measure.
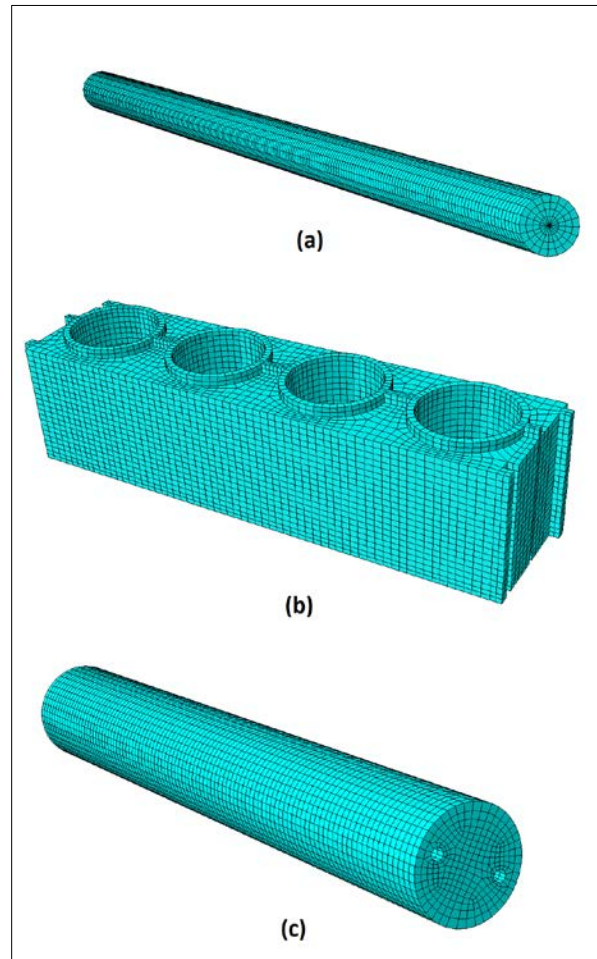
Figure 4.14: Meshed parts of flexi-wall, a) rebar, b) poly-block, c) RPF core

Five poly-blocks model were stacked up and placed on the specified rectangular area on the wall footing (Fig. 4.15c). In the physical test models, the poly-blocks were thoroughly glued together and also to the foundation. Based on the experimental observations during the loading of the wall, no noticeable disconnection between the poly-blocks occurred until the failure of the RPF cores took place. Therefore, the connections of blocks including their contact surfaces and their contact with the wall footing were defined by tie constraints. Due to expansion of the LPF liquid during the

curing process, it completely sticks to the internal surfaces of the poly-blocks voids. Since there was no relative displacement between the RPF cores and the poly-blocks, they were also tied together. Fig. 4.15d demonstrates the completed numerical model after the assembly and mesh generation.
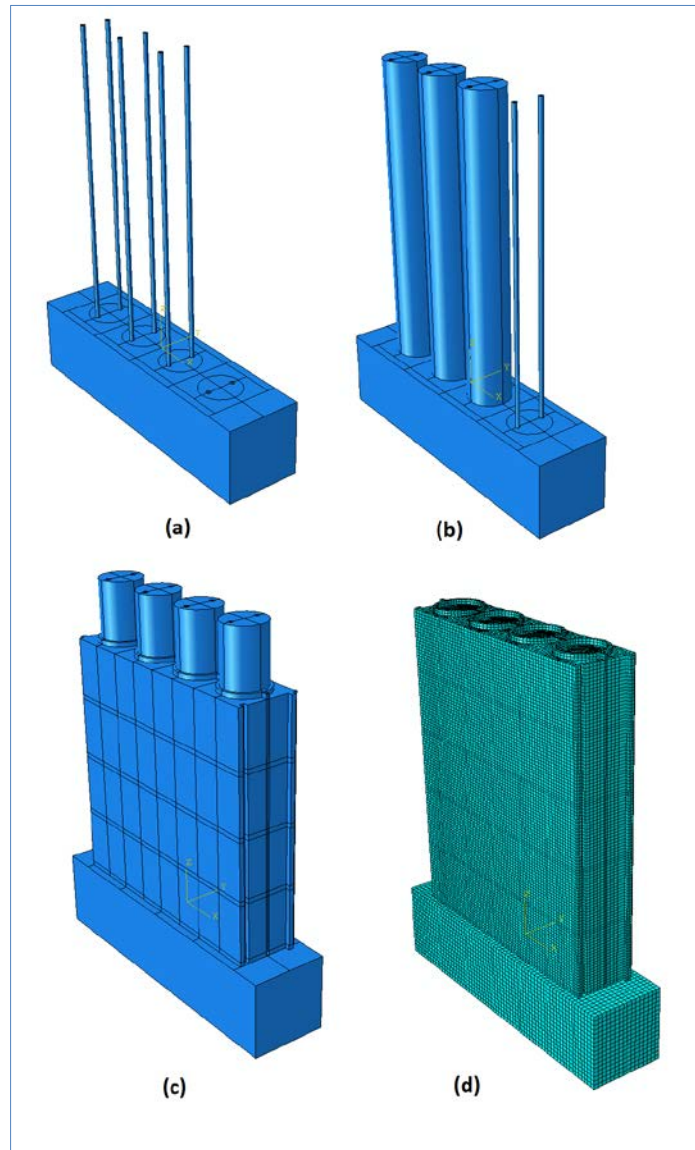
Figure 4.15: Assembly of flexi-wall parts, a) rebars, b) RPF cores, c) Poly-blocks, d) completed numerical model

The boundary conditions of the FE model corresponding to the experimental walls models were defined. All the translational and rotational degrees of freedom at the bottom surface of the foundation were restrained. As Fig. 4.16 exhibits, the top block was subjected to a distributed load. For the sake of comparison with the measured experimental response, the lateral displacements of the LPF cores were recorded at the elevation of the linear variable differential transducers (LVDTs) in the experiment (0.90 m above the foundation top surface). The base bending moment was calculated at each loading interval i.e. lateral load times the distance of measurement point from the top of the foundation. A static push-over analysis was executed and the applied load was increased by increments of 0.05 of the total lateral load.
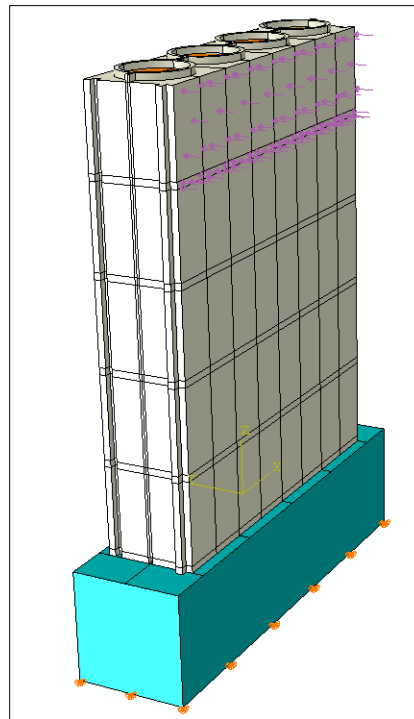
Figure 4.16: Full-scale FE model of flexi-wall

4.10 Comparison of numerical and experimental results of flexi-wall flexural performance

Fig. 4.17 compares the flexural behavior of flexi-walls obtained from the numerical and experimental results. The numerical results (dotted line) demonstrate a linear behavior until the rebars yielded and inelastic deformations initiated. The computed response fairly

matches with the experimental results up to the yield strength. The yield displacements were also well predicted by the FEA, however, since the "post-yield" failure of materials were not considered in the numerical analysis, the numerical results do not match the experimental results past the yield point. This is considered to be acceptable since the design for these walls should not permit yield.

The flexural behavior of the flexi-walls reinforced with 2x15M rebars obtained from FEA, form a lower-bound for the experimental lateral resistance. Considering a design moment capacity equal to 65% of the ultimate resisting moment, the flexural behavior of the flexi-walls achieved from the numerical analyses would be on the safe side for design purpose.
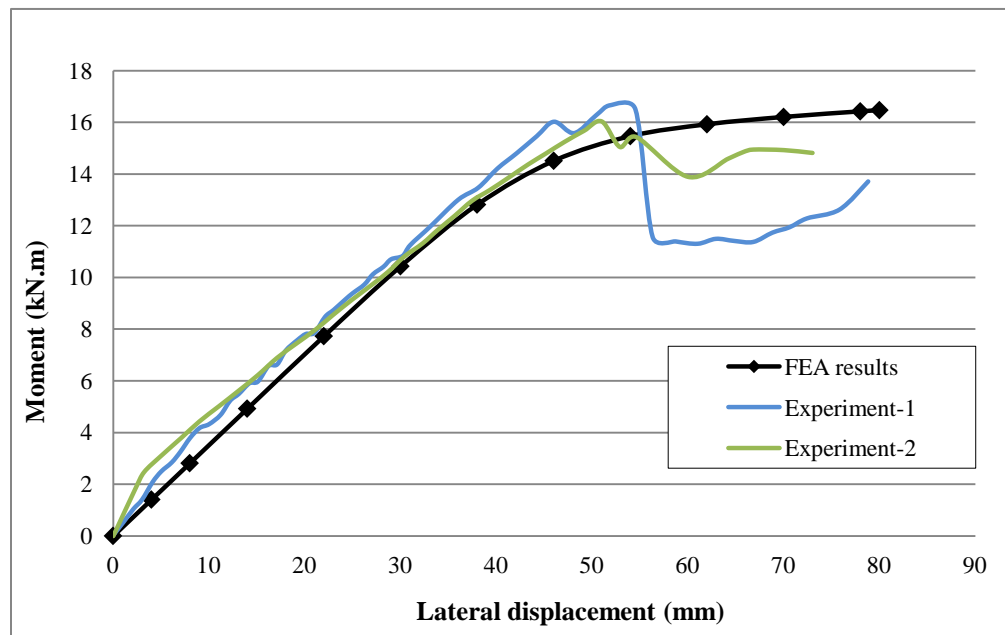
Figure 4.17: Comparison of flexural behavior from load tests and numerical analyses

4.11 Discussion on finite element analysis

A close observation of FEA results indicates that the main load-bearing elements in the structural system of flexi-wall are steel rebars and thereby LPF cores do not provide significant lateral stiffness for the wall system. However, LPF cores play a key role in structural integrity of the wall through holding the rebars in their position to act

effectively in the anchorage system. In essence, LPF cores equally distribute the internal forces to the rebars while controlling their excessive deflection.

Owing to huge difference between the strength of LPF core and rebars, stress in the cores is almost negligible in comparison with the yield strength of rebars. Similar to poly-wall, FEA reveals that the stresses in the poly-blocks were minimal due to their negligible stiffness. The failure mechanism of the walls was flexural where steel rebars yield and the LPF cores crush in compressive area, alike the experimental observation.

As noted in Chapter 3, the numerical models must have been optimized to resolve the convergence issues associated with FEA of a rigorous solid FE model combined with several interface elements. For this purpose, displacement-controlled and load-controlled analyses were initially compared and the former was found to be superior in terms of convergence rate in the nonlinear domain.

To ensure that the mesh density has no impact on the accuracy and the solution convergence, sensitivity analysis was conducted considering different element size of flexi-wall components. It was concluded that finer mesh of the rebars and to some extent of the LPF cores might result in higher accuracy. On the other hand, no effect on the results was observed by refining the poly-blocks mesh.

Alike the poly-wall model the poly-blocks, LPF cores and the rebars were assembled as a single part with different properties in order to reduce the computation time. In this case, the tie constraints between the components of the wall were removed. However, their interfaces with the foundation were kept unchanged (i.e. tie constraints of rebars and contact surfaces of RPF cores). These changes significantly reduced the computation time to less than 8 hours and no noticeable change in the accuracy of the results was observed. The only disadvantage of this method is that discretization of a single part with a sophisticated geometry is more complicated and time-consuming than several independent parts.

As reported before, the effect of poly-blocks stiffness on the performance of the flexi-wall model is trivial. Therefore, the details of poly-block geometry were reduced by

removing its edges and grooves. This modification reduced the solution time to 2 hours with no impact on precision of the results.

4.12 Wind load on flexi-wall

Design of sound wall is mostly dominated by its response under wind loading. Hence, the structural performance of flexi-wall as an extension of sound wall was investigated under lateral uniform loading. The FE models of flexi-wall that was verified using the experimental results in previous section, was employed in the analysis.

As shown in Fig. 4.18, a uniform lateral load representing the wind loading was applied on one surface of the wall. Since, the total height of the wall is less than 4m in practice; the wind load was uniformly distributed along the height. Similar to previous analyses, the load was increased gradually by increments of 0.05 of the total load. The output of analyses was recorded and the results were then plotted in the form of lateral load versus top displacement of the wall. The FE analyses were performed for two rebar size of 2x10M and 2x15M.

Fig. 4.19 displays the behavior of flexi-walls under uniform lateral load for two types of reinforcement. Both walls demonstrate a linear behavior up to yield point followed by a ductile behavior. The ultimate lateral resistance of walls (for 800 mm width) is respectively 10 and 14.4 kN before first yield occurs. The slope of plots in Fig. 4.19 also indicates that the stronger wall reinforced with 2x15M is considerably stiffer than the wall reinforced with 2x10M owing to higher size of rebar. It is worth mentioning that the fracture of material after yield points was not in the scope of this research and thereby were not simulated. Theses obtained values were used for design of flexi-wall which is discussed in Chapter 5 in more details.

Given the fact that the response of flexi-wall is dominated by flexural mode, the lateral yield load produced by uniform loading is twice the yield load produced by concentrated loading because, resultant of the uniform load acts at the mid-height of the wall and therefore the produced base bending moment is almost half of that produced by the concentrated lateral load applied on the top block.
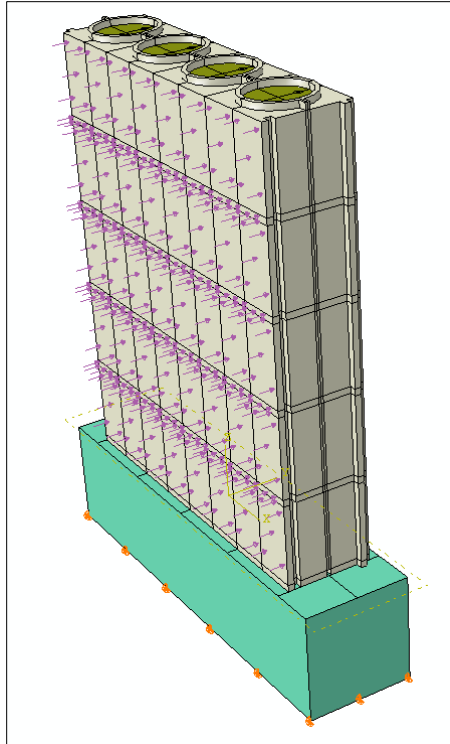
Figure 4.18: Wind loading on flexi-wall numerical model
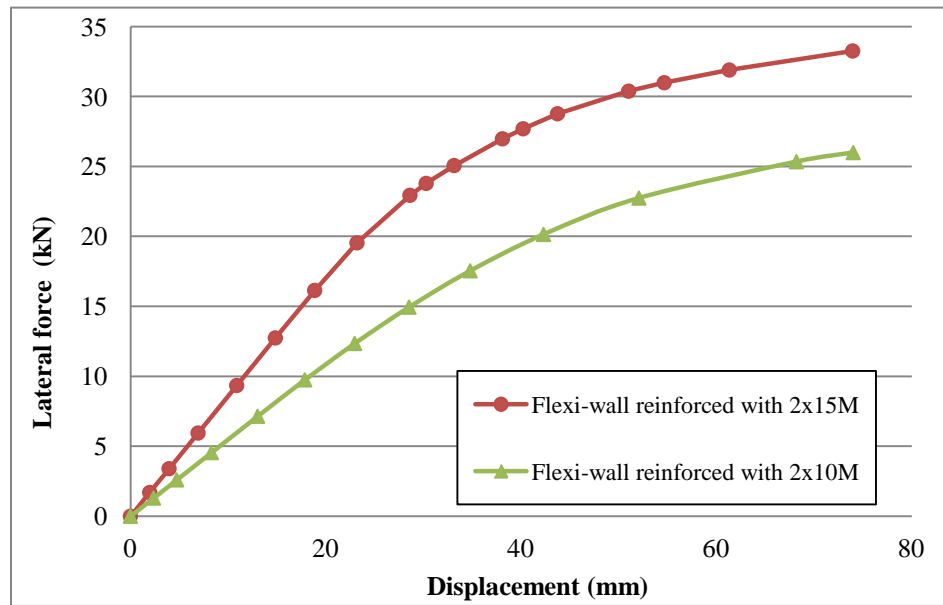
Figure 4.19: Lateral load-displacement relation of flexi-wall reinforced with 2x10M and 2x15M under wind loading

The design of the wall should be conducted based on the elastic linear part of the wall behavior. Hence, an equivalent cantilever beam can be utilized to approximate the lateral deflection of the wall in the linear range. Similar to poly-wall, the linear behavior of flexi-walls with two types of reinforcement was simplified by an equivalent cantilever beam and accuracy of the method was verified using conducted numerical analysis.

On the other hand, the maximum factored moment induced by wind loading can be calculated according to the building codes and then compared with the flexural yield capacity of the wall obtained experimentally. This equivalent approach may be employed as a replacement of the rigorous FEA for the preliminary design of flexi-walls under different lateral load profiles. Results of this simplified method were summarized in Chapter 5.

4.13 Conclusions

This study investigates the application of light polyurethane foam (LPF) in construction of an extension to existing noise barriers. An experimental program was carried out to determine the LPF mechanical properties as well as the lateral resistance of the entire wall system. A fatigue test was also performed on a flexi-wall in order to evaluate its long-term performance under a repetitive loading. 3D finite element models of the wall components as well as the entire wall system were established and verified using experimental results. According to the results of this study, the following conclusion can be drawn:

1. The construction of flexi-wall is faster, less obstructive and more economic than conventional method for the investigated application. The outcomes of the experiments showed that flexi-wall exhibited a linear behavior up to yield point and its lateral resistance was satisfactory as a short extension for existing noise barriers.

2. The results of cyclic loading test confirmed the reliability of flexi-wall behavior in the range of design loading. The cyclic loading yielded only 5.7% stiffness loss after 15000 cycles which is quite comparable to fatigue characteristics of other engineering materials.

3. The mechanical performance of flexi-wall is mainly governed by the steel rebars and as LPF is lighter and less expensive than cementitious material, flexi-wall can be a good alternative to other types of extension for sound walls renewal.

4. The achieved responses using the numerical model of the full-scale flexi-walls were in reasonable agreement with the measured experimental responses. The ultimate flexural strength of flexi-wall under a uniform wind loading is found completely acceptable for the investigated application.

Even though not examined in the current study, but it is expected that applying a layer of shotcrete on the wall surfaces could enhance the flexural resistance, surface resistance and fatigue characteristics of the wall.

4.14 References

ABAQUS Analysis User's Manual (2010). Version 6.9-1, Dassault Systemes Corp., Providence, RI.

Acoustic Consulting Service (2008). Sound Attenuation Certification and Report, www.lexiconbuildingsystems.com.

ASTM Standard D4060-10. (2010)."Standard Test Method for Abrasion Resistance of Organic Coatings by the Taber Abraser." Philadelphia, PA.

Buzzi O., Fityus S., Sloan S.W. (2010). "Use of expanding Polyurethane Resin to Remediate Expansive Soil Foundations." Canadian Geotechnical Journal 47(6), 623-634.

Canadian Standard Association. (2009). "CAN/CSA-G30.18-09 Carbon steel Bars for Concrete Reinforcement", Mississauga, Ontario, Canada.

Canadian Standard Association. (2006). "CAN/CSA-S6-06 Canadian Highway Bridge Design Code." Mississauga, Ontario, Canada.

Choi H., Toutanji H., Gilbert J., and Alldredge D. (2013). "Impact Resistance of Polyurea-Coated High Performance Cementitious Composites." Journal of Materials in Civil Engineering, 25(12), 1984–1989.

Greene C., and Myers J. (2013). "Flexural and Shear Behavior of Reinforced Concrete Members Strengthened with a Discrete Fiber-Reinforced Polyurea System." Journal of Composites for Construction, 17(1), 108–116.

Irshidat M., Al-Ostaz A., Cheng A., and Mullen C. (2011). "Blast Vulnerability Evaluation of Concrete Masonry Unit Infill Walls Retrofitted with Nano Particle Reinforced Polyurea: Modeling and Parametric Evaluation." Structures Congress, 2126-2141.

Junco C., Gadea J., A. Rodríguez, S. Gutiérrez-González, V. Calderón. (2012). "Durability of Lightweight Masonry Mortars Made with White Recycled Polyurethane Foam." Cement & Concrete Composites, 34, 1174-1179.

Li Y., Kim U.S., Shields J., and Davis R. (2013)."Controlling Polyurethane Foam Flammability and Mechanical Behavior by Tailoring the Composition of Clay-Based Multilayer Nanocoatings." Journal of Materials Chemistry A, 1, 12987-12997.

Motlagh S.G., Jain A., Najafi M. (2013). "Comparison of Spray-on Linings for Water Pipeline Renewal Applications." Pipelines, ASCE, 1113-1125.

NBCC. (2005). "National Building Code of Canada", National Research Council of Canada (NRC), Ottawa, Canada.

Paul C. Liu (2000). "Is the wind wave frequency spectrum outdated." Ocean Engineering 27, 577-588.

Schreyer H. L., and Zuo, Q. H. (1994). "Anisotropic Plasticity Model for Foams." Journal of Engineering Mechanics, 120, 1913-1930.

Shen S.Y., Masters F.J., Upjohn H.L., Ferraro C.C. (2013). "Mechanical Resistance Properties of FRP/Polyol–Isocyanate Foam Sandwich Panels." Composite Structures, 99, 419–432.

Witkiewicz, W., and Zieliński, A. (2006). "Properties of the Polyurethane (Pu) Light Foams. "Advances in Materials Science, 6(2), 35-52.

Zenkert, D., and Burman, M. (2009). "Tension, Compression and Shear Fatigue of a Closed Cell Polymer Foam." Composites Science and Technology, 69, 785-792.

Chapter 5

Design Guidelines for Poly-wall and Flexi-wall

An innovative wall system comprised of polyurethane products, which is proposed for application in accelerated construction of noise barriers has been developed and investigated in the University of Western Ontario. The proposed sound wall (denoted poly-wall and flexi-wall) consists of stay-in-place poly-blocks as formwork, rigid or light polyurethane foam (RPF/LPF) as structural cores and polyurea as a coating of the wall surfaces. Poly-blocks are interlocking light-weight blocks, which are stacked up layer by layer and act as formwork for the polyurethane cores. RPF and FPF are fast-curing liquid mixtures, which are injected to the poly-block voids and reach to their maximum strength within 10 minutes. The RPF/LPF cores are reinforced with one or two steel rebars depending on the design load and height of the wall. Steel rebars are epoxied into the drilled holes in the wall base and connect the two parts of the wall to the foundation. The polyurea coating is an abrasion-resistant finishing layer, which is sprayed on the surfaces of the wall and set within 2-3 minutes.

In this chapter, a design procedure for poly-wall and felxi-wall is developed and elaborated based on the results of the comprehensive experimental and numerical analyses described in previous chapters. The comprehensive experimental program which was conducted at the Structural Lab of Western University included over 80 specimen tests and 16 full-scale tests in order to evaluate the mechanical properties and structural performance of the wall system. The performed numerical analyses included several nonlinear finite element models that were validated employing the experimental results and were then used to analyze the structural behavior of the wall system. The results of the analyses provided a basis for the design of poly-walls with different heights and under different loading conditions, which are discussed in this chapter.

5.1 Application

Text Poly-wall and flexi-wall can be constructed as a new sound barrier or as a vertical extension of an existing wall. As a new sound barrier, it can be constructed on a strip footing (e.g. grade beam) or paved surface if the base provides the stability and strength requirements. Reinforcements can be inserted into the foundation at their pre-determined positions before casting the foundation or alternatively epoxied into drilled holes after curing the foundation. As shown in Fig. 5.1, the wall may be built on the concrete Jersey block to protect it from vehicular collision.
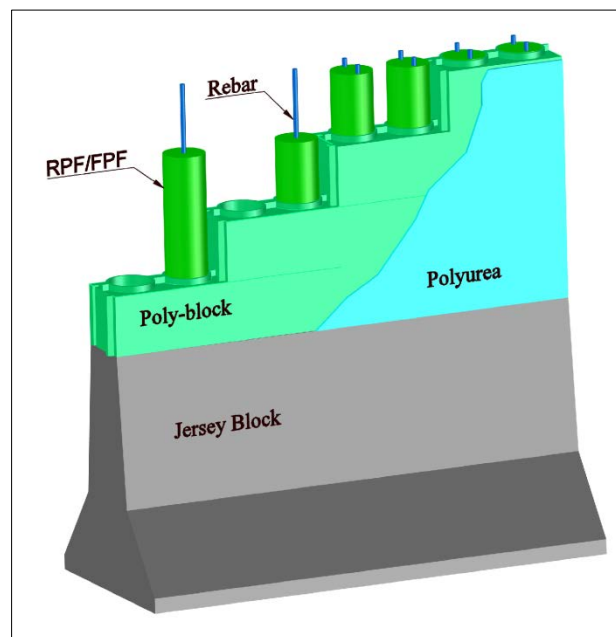
Figure 5.1: Poly-wall/flexi-wall structural system built on concrete block

Poly-wall and flexi-wall can also be constructed as a vertical extension of an existing wall where the sound wall is not high enough to effectively reflect the traffic noise. Most of the provinces across Canada have established a "noise barrier retrofit program" to regulate noise pollution and minimize its impacts on public health using a cost-effective renewal technique. The program focuses on sound walls built in the last few decades, which are required to be vertically extended 1-2 m to effectively absorb and reflect the vehicles noise.

The proposed light-weight wall system can be readily built on top of a cementitious or concrete sound wall. The construction of poly-wall and flexi-wall can be less obstructive for traffic and much faster than conventional methods.

For vertically extending an existing sound barrier, a layer of shotcrete instead of polyurea can be applied on the entire wall surfaces. The layer provides a more consistent appearance and further enhances the structural integrity of the entire wall. This will retrofit the old wall, properly connect the new and old parts of the wall and will provide a suitable finishing layer for the wall. Fig. 5.2 displays the construction of poly-wall/flexi-wall on an existing noise barrier.
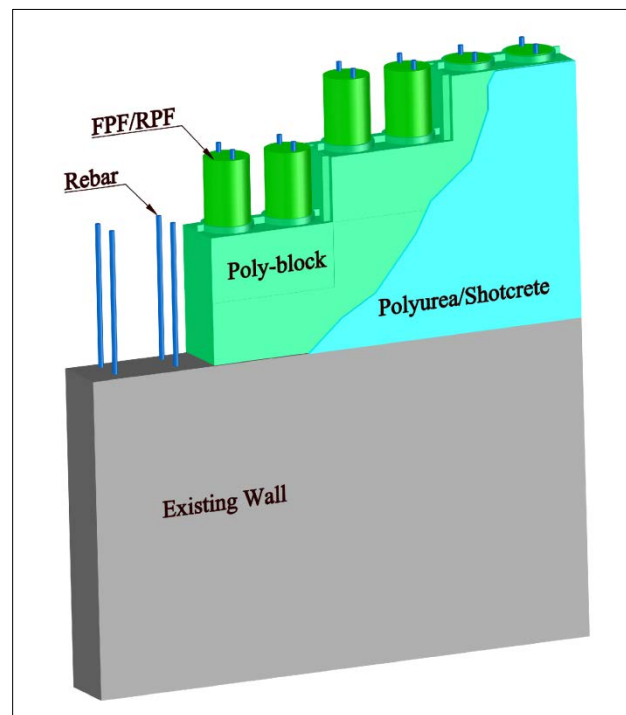
Figure 5.2: Poly-wall/flexi-wall structural system built on existing sound wall

5.2 Scope

This chapter discusses the structural design procedure for a sound barrier comprised of rigid and flexible polyurathe foam utilizing the results of the experimental and numerical investigations described in the previous chapters. It is focussed on the design of the suprer-structure, which is constructed on a foundation, existing structure or paved

surface. The design of the foundation or the exising structure is oustide the scope of this work. This chapter mainely elaborates the flexural design of the sound barrier under lateral loading considering uniform wind loading under different wind speed conditions. In addition, design guidelines are provided for the case of vertical loading applied to the poly-wall cores, which is called "load-bearing wall". Besed on the parametric numerical analysis, some reduction factors are suggested to account for the effect of vertical loads.

Since poly-wall and flexi-wall are much lighter than conventional walls, earthquake loading does not govern the desig of the wall and hence it is not discussed herin. The impact load is not included herein assuming that the wall is constructed on a berm or is protected from vehicular collision by means of guard rail or Jersey block.

Wind loading is calculated according to the "Canadian highway bridge design codes and standards" (CSA-S6, 2006) which explicty specifies the loading on noise barreirs. The recommended design requiremets in this code are found slightly more critical than National Building Code of Canada (NBCC, 2010) and so was selected as basis for design.

5.3 General features, construction and materials

5.3.1 Height of sound barrier

Sound barriers shall have a minimume effective height which is defined by acoustic study based on site specifications. The stuctural height of the wall is the vertical distance of top of foundaion to the wall top where it is exposed to wind pressure (w). The height above ground shall be measured from top of berm, hill, footing or foundation. The effective heigt of the wall (H) is illustrated in Fig. 5.3.
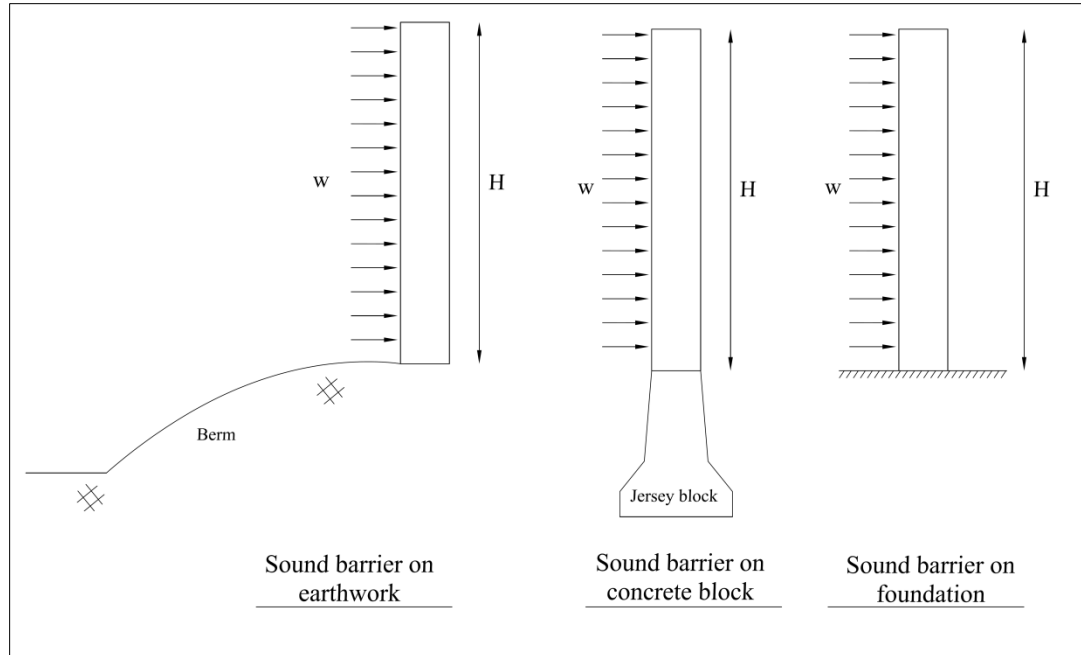
Figure 5.3: Effective height of sound wall (H)

5.3.2 Poly-block placement

The first course of poly-blocks should be placed on a fully-leveled base. To prevent movment of the first course during the injection of material, it shall be epoxied unto the base. Since RPF and LPF are liquids at the time of injection, the first course also needs to be totally sealed to prevent the leakage of liquid out of the block. Where the wall height is less than 1.5 m and LPF is injected into the blocks, other courses of poly-blocks shall be glued togethere as well. This is required to control the dislocation of blocks due to expansion of LPF. The best way to prevent the leakage and dislocation of blocks is to spray a polyurea layer on both surfaces of the wall. This provides sufficent integrity for the formwork and seals most of the seams and joints between the blocks and foundation.

5.3.3 Reinforcement

Rebar sizes of 10M and 15M with f_y=400 MPa (Grade 400R of CSA-G30.18) were used in construction, analysis and design of walls. Using larger size of rebars is not practically possible due the limited space in each core of poly blocks. Where two rebars are required (2x10M or 2x15M), the minimum spacing of rebars shall be 90 mm center-to-center (Fig.

5.4a). Where only one rebar is required, it shall be inserted in the center of the cores (Fig. 5.4b).

5.3.4 Rebars placement

Rebars may either be inserted into the foundation before casting the concrete or be inserted and epoxied to drilled holes in foundation. The former approach is superior and easier in practice if enough rebar's embedment length could be provided in the base. When an existing wall needs to be vertically extended, this method is also applicable. In the experiments conducted in the current study, Hilty epoxy (HIT-HY150MAX-SD), which provides bond strength greater than concrete to steel bond was used to ensure that rebars would not slip. The embedment length of steel rebars for both 10M and 15M was selected to be 220 mm and the performance of the epoxy was found to be completely satisfactory.
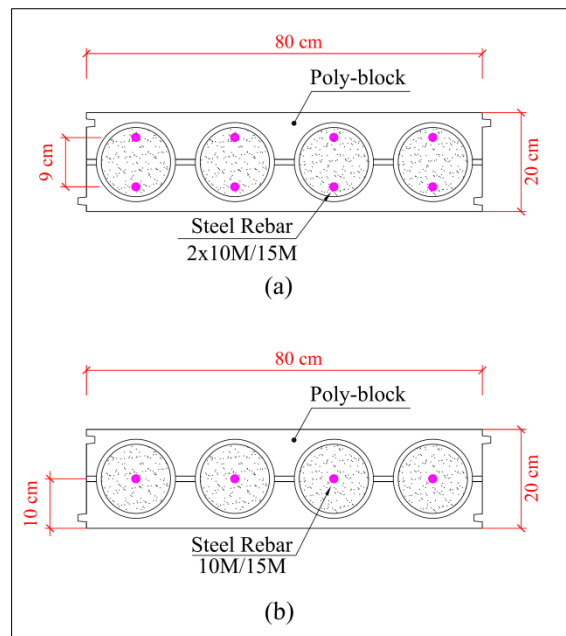
Figure 5.4: Rebars arrangements in poly-block, a) two rebars in each core, b) one rebar in each core

5.3.5 Types of foam

The foams that were employed in construction, analysis and design of poly-wall and flexi-wall are called rigid polyurethane foam (RPF) and light polyurethane foam (LPF). According to the exact measurements, the density of RPF and FPF is equal to 1100 kg/m^3 and 140 kg/m^3, respectively.

Table 5.1 summarizes the strength of each type of foam according to the experimental results that are described in the previous chapters. The authors recommend that resistance factor for both materials is taken equal to 0.65 when these values are used directly in the design of a structure.

5.3.6 Foam injection

Liquid polyurethane foam should be injected into the wall cores continuously. Since the curing time of the foams is very short, any pause in injection may lead to disconnectivity of the cores. The quality of the foams considerably varies with the temperature of the construction environment and the pump pressure. Hence, these parameters should be kept constant during the injection for consistency of the material. It was also found that the size of the injector nozzle alters the characteristics of the foam to some extent.

5.3.7 Polyurea spraying

Polyurea shall be sprayed on all exposed surfaces of the poly-blocks to protect them from abrasion. Properly sprayed polyurea coating seals most of the joints and seams of the poly-blocks. Based on the test observations, in order to obtain a suitable thickness of polyurea, 4 passes of spray on the wall are required. Since polyurea gel-time is about 1 minute for each pass of spray, a specific pattern of spraying should be followed, e.g. 1 pass of spray from bottom to top of the wall, then the same pattern for the other side of the wall and so forth. Following such patterns prevents dripping and accumulation of polyurea on the surfaces of the wall. The main location of leakage is at the connection of the wall and foundation which needs to be fully sprayed and sealed.

Table 5.1: Comparison of mechanical properties of RPF and FPF filler

Type of test	RPF	FPF
Compressive strength (MPa)	20	1.2
Density (kN/m³)	11.1	0.14
Direct tension (MPa)	20	-
Modulus of rupture-flexural (MPa)	9.6	-
Shear strength (MPa)	4.3	-
Bond strength (MPa)	4.5	0.85
Module of elasticity (MPa)	1270	30
Poisson's ratio	0.22	0.3

5.4 Design loads of poly-wall and flexi-wall

5.4.1 Loading

The effects of wind (lateral) load and gravitational (vertical) loads are discussed in this section. Brief explanations of wind loading as well as required data for calculation of wind load included herein are in accordance with the Canadian highway bridge design codes and standards (CSA-S6, 2006).

5.4.2 Wind load

The wind load is applied on the entire frontal surface of a noise barrier as a uniformly distributed load. The wind load (F) per unit length is given by:

$$F = q \, C_e \, C_g \, C_h \, H \tag{5.1}$$

Where q is mean reference wind pressure, C_e is wind exposure coefficient, C_g is gust effect coefficient, C_h is horizontal drag coefficient and H is hight of wall.

The reference wind pressures for some of the large cities of Canada are summarized in Table 5.2 according to Annex 3.1 of the Canadian highway bridge design codes and standards. The 25 years return period is considered for the hourly mean pressure of the wind as the life span of a noise barrier is 25 years (CSA-S6, 2006).

The exposure coefficient, C_e depends on the height of the wall. However, for a superstructure less than 10.0 m high C_e can be taken constant equal to 1.

For a noise barrier, gust effect coefficient, C_g=2.5 and horizontal drag coefficient, C_h=2 (CSA-S6, 2006).

Table 5.2: Reference wind pressures for some of large cities in Canada

City	Wind pressure (Pa)	City	Wind pressure (Pa)
Vancouver	430	Mississauga	435
Victoria	560	Oakville	435
Calgary	455	Ottawa	360
Edmonton	390	Sarnia	415
Regina	385	Toronto	460
Saskatoon	425	London	455
Winnipeg	405	Montreal	365
Burlington	415	Halifax	505
Cambridge	310	Sydney	535
Hamilton	415	St. John's	710

5.4.3 Dead Load

The weight of wall components are included in the analyses of the wall. Other vertical loads such as the weight of attachments and wearing surface shall be included in the design, if applicable. Where the wall act as load-bearing wall, the vertical loads shoud be eaqually distributed on the wall cores. The effect of vertical load on the flexural resistance of the wall is provided using a reduction factor. Only poly-walls (filled with RPF) can be employed as load bearing walls.

5.4.4   Load Combinations of Ultimate Design

The predominant load combination for ultimate limit state (ULS) design includes dead (gravitational) and wind load as specified in the following.

Ultimate limit state $\rightarrow$ (0.9-1.2) Dead+1.5 Wind

Other load combinations may be considered (if applicable) according to Tables 3.1 and 3.2 of Canadian highway bridge design Codes and standards (CSA-S6, 2006).

5.5 Flexural Performance of The Wall under Lateral Loading

5.5.1 Flexural Resistance

Poly-wall and flexi-wall design is conducted following the ULS design procedure according to the requirements of the design code (CSA-S6, 2006). As all loads and resitances are factored in this approach, factored flexural resistance of the entire wall is calculated by considering the resistance factor equal to 0.65 times the ultimate flexural resistance. In the absence of statistical analyses this value conservatively estimates the practical strength of RPF considering all source of error in productions and applications. This value These values (summerized in Table 5.3) were obtained based on the average experimental and numerical results described in the previous chapters. The flexural resistance of each type of wall is presented for a unit length of wall, which contains five reinforced cores. The flexural stiffness (EI) of an equivalent cantilever beam of each case is also shown in Table 5.3.

Table 5.3: Lateral resistance of poly-wall and flexi-wall for a unit length

Type of wall and reinforcement	Maximum flexural resistance (kN.m)		Equivalent flexural stiffness, EI (kN.m^2)
	Unfactored	Factored (0.65%)	
Poly-wall reinforced with 1x15M	8.4	5.5	41.0
Poly-wall reinforced with 2x10M	15.6	10.2	179.0
Poly-wall reinforced with 2x15M	36.3	23.6	306.0
Flexi-wall reinforced with 2x10M	12.5	8.1	82.0
Flexi-wall reinforced with 2x15M	18	11.7	117.0

For design of the wall, the base bending moment due to lateral loading is calculated using the load combinations and compared with the factored flexural resistance in Table 6.3 to determine which type of wall and how much reinforcement is sufficent.

5.5.2 Lateral Displacement

The lateral displacement is not a major concern for the sound barriers design, and hence none of the applicable codes and guidelines specify a lateral displacement limit for sound walls. The design of sound barrier is acceptable as long as the wall and its components remain undamaged and the wall maitains its stability under ULS load combinations in accordance with the general principles of ultimate limit state design. For instance, it is indicated in AASHTO LRFD bridge design (AASHTO, 2004) that "tolerable deformation criteria shall be developed based on maintaining the required barrier

functionality, achiving in anticipated service life and the consequence of unacceptable movements".

It is recommended when taller walls are constructed and they are subject of public attention, the lateral deflection is maintained under 3% of the wall height as a measure for potential safety hazard.

In Chapter 3 of the present research, a simplified approach of equivalent cantilever beam is developed and it is shown that the behaviour of the entire wall can be well approximated by this approach. Hence, within the linear range of the wall behaviour, the lateral deflection can be calculated through the elastic solution of a cantilever beam. Given the flexural stiffness (EI) of each type of wall as given in Table 5.3, the lateral displacement of the wall under a uniform wind loading can be approximated by:

$$\Delta_L = \frac{wH^4}{8EI} \tag{5.2}$$

where w is wind pressure, H is height of wall and Δ_L is lateral deflection of wall, as shown in Fig. 5.5. It should be noted that the lateral deflection should be checked under serviceability load conditions with load factor = 1.0 is applied to wind load.
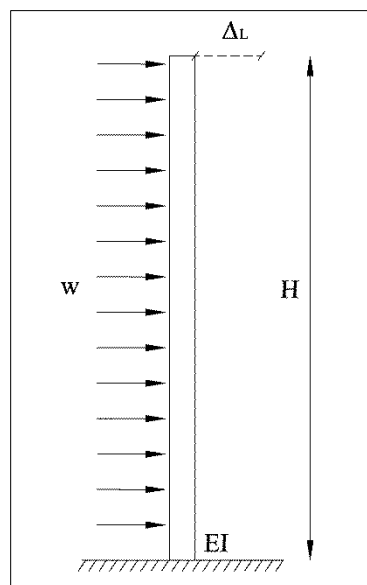
Figure 5.5: Equivalent beam for design of poly-wall and flexi-wall

5.6 Lateral Resistance of Poly-wall under Vertical Load

The aplicability of poly-wall (made of RPF) as a load-bearing wall were also investigated and described in Chapter 3. The usage of flexi-wall (made of LPF) as load-bearing wall is not recommended since LPF cores are compressible under a constant pressure.

Poly-wall cores may carry vertical loads such as dead load of wall attachments or transverse beam at its top. In all cases, the vertical load shall be applied on the cores of the wall to be transferred to the the foundation. The vertical load path should be accurately designed in order to achieve the best lateral performance of the poly-wall. It is recommended that the vertical reinforcements of the poly-wall cores are extended and connected to the member which is transferring vertical load.

A parametric study was conducted to determine the effect of vertical load on the lateral resistance of poly-walls reinforced with 2x10M and 2x15M rebars. For theses analyses, the total vertical (dead) loads were uniformly distributed on the RPF cores at the wall top and a uniform lateral wind load was then applied to the surface of the wall. The analyses were performed for 0, 0.5, 1, 1.5 and 2 MPa vertical pressure on each core and the total lateral resistance of the poly-wall was obtained in each case. The numerical analyses results are summarized in Tables 5.4 and 5.5 and the effect of the vertical load on the lateral resistance is shown as a reduction factor. For instance, 1 MPa pressure on each core of a poly-wall reinforced with 2x10M (equivalent to 76.9 kN for a unit length of the wall) induces 4.6% reduction in lateral resistance of the wall subjected to a uniform wind loading. For both types of reinforcements, the lateral resistance will not decline up to 38.5 kN of vertical load which is equivalent to 0.5 MPa pressure on each core.

Table 5.4: Effect of vertical load on lateral resistance of poly-wall reinforced with 2×10M

Vertical pressure on each core (MPa)	Total vertical load for a unit length (kN)	Factored lateral resistance for a unit length (kN)	Reduction % of lateral resistance
0	0.0	20.3	0
0.5	38.5	20.3	0.0%
1	76.9	19.4	-4.8%
1.5	115.4	18.8	-8.2%
2	153.9	18.1	-12.0%

Table 5.5: Effect of vertical load on lateral resistance of poly-wall reinforced with 2×15M

Vertical pressure on each core (MPa)	Total vertical load for a unit length (kN)	Factored lateral resistance for a unit length (kN)	Reduction % of lateral resistance
0	0.0	47.1	0
0.5	38.5	47.1	0.0%
1	76.9	45.1	-4.6%
1.5	115.4	43.8	-7.5%
2	153.9	42.6	-10.7%

5.7 Example for design of poly-wall and flexi-wall as noise Barrier

Table 5.6 and Table 5.7 demonstrate the preliminary design of poly-wall and flexi-wall for different heights and loading pressures. The design sequence is as followings.

1- Determine the wind pressure relevant to geographical location of the wall (i.e. city) for 25 years return period using Annex 3.1 of Canadian highway bridge design codes and standards (CSA-S6, 2006).

2- From the first column of Table 5.6 find the closest value of wind pressure. The value obtained from the table may be linearly interpolated if not explicitly specified.

3- From the second column of Table 5.6 find the wall height.

4- Columns 5 to 9 of Table 5.6 show the factor of safety for possible design options. It is recommended that an option with factor of safety between 1.5 and 2.5 is chosen.

Example: A 2.25 m high sound barrier is desired to be constructed in Edmonton. The reference wind pressure in Edmonton is equal to 390 Pa. By rounding up the wind pressure to 400 Pa, using columns 7, 8 and 9 of Table 5.6, the possible design options are:

1) Poly-wall reinforced with 2×10M (RPF-2×10M), design factor of safety
   (1.1+1.7)/2=1.4

2) Flexi-wall reinforced with 2×15M (FPF-2×15M), design factor of safety
   (1.2+2)/2=1.6

3) Poly-wall reinforced with 2×15M (RPF-2×15M), design factor of safety
   (2.5+3.9)/2=3.4

The second design option is preferred as it is the safest and most economic and offers the overcapacity ration greater than 1.5. Table 5.7 shows the maximum lateral deflection of at the top of the wall corresponding to Table 5.6.

4) The maximum lateral displacement of the wall for 400Pa wind pressure from Table 5.7 column 8 is approximately equal to
   (84.2+34.5)/2=59.35 mm < 0.03×H=0.03×2200=66 mm → design is satisfactory.

Table 5.6: Preliminary strength design calculation of noise barrier under wind loading

Wind pressure (Pa)	Height of wall (m)	Lateral Wind load (kN)	Factored wind moment (kN.m)	Factor of safety of design for wall				
				RPF-1x15	FPF-2x10	RPF-2x10	FPF-2x15	RPF-2x15
350	1	1.75	1.31	4.2	6.2	7.8	8.9	18.0
	1.5	2.63	2.95	1.9	2.7	3.5	4.0	8.0
	2	3.50	5.25	1.0	1.5	1.9	2.2	4.5
	2.5	4.38	8.20	NA	NA	1.2	1.4	2.9
	3	5.25	11.81	NA	NA	NA	NA	2.0
400	1	2.00	1.50	3.7	5.4	6.8	7.8	15.7
	1.5	3.00	3.38	1.6	2.4	3.0	3.5	7.0
	2	4.00	6.00	NA	1.4	1.7	2.0	3.9
	2.5	5.00	9.38	NA	NA	1.1	1.2	2.5
	3	6.00	13.50	NA	NA	NA	NA	1.7
450	1	2.25	1.69	3.3	4.8	6.0	6.9	14.0
	1.5	3.38	3.80	1.4	2.1	2.7	3.1	6.2
	2	4.50	6.75	NA	1.2	1.5	1.7	3.5
	2.5	5.63	10.55	NA	NA	NA	1.1	2.2
	3	6.75	15.19	NA	NA	NA	NA	1.6
500	1	2.50	1.88	2.9	4.3	5.4	6.2	12.6
	1.5	3.75	4.22	1.3	1.9	2.4	2.8	5.6
	2	5.00	7.50	NA	1.1	1.4	1.6	3.1
	2.5	6.25	11.72	NA	NA	NA	NA	2.0
	3	7.50	16.88	NA	NA	NA	NA	1.4
550	1	2.75	2.06	2.7	3.9	4.9	5.7	11.4
	1.5	4.13	4.64	1.2	1.7	2.2	2.5	5.1
	2	5.50	8.25	NA	NA	1.2	1.4	2.9
	2.5	6.88	12.89	NA	NA	NA	NA	1.8
	3	8.25	18.56	NA	NA	NA	NA	1.3
600	1	3.00	2.25	2.4	3.6	4.5	5.2	10.5
	1.5	4.50	5.06	1.1	1.6	2.0	2.3	4.7
	2	6.00	9.00	NA	NA	1.1	1.3	2.6
	2.5	7.50	14.06	NA	NA	NA	NA	1.7
	3	9.00	20.25	NA	NA	NA	NA	1.2
650	1	3.25	2.44	2.3	3.3	4.2	4.8	9.7
	1.5	4.88	5.48	1.0	1.5	1.9	2.1	4.3
	2	6.50	9.75	NA	NA	1.0	1.2	2.4
	2.5	8.13	15.23	NA	NA	NA	NA	1.5
	3	9.75	21.94	NA	NA	NA	NA	1.1
700	1	3.50	2.63	2.1	3.1	3.9	4.5	9.0
	1.5	5.25	5.91	NA	1.4	1.7	2.0	4.0
	2	7.00	10.50	NA	NA	NA	1.1	2.2
	2.5	8.75	16.41	NA	NA	NA	NA	1.4
	3	10.50	23.63	NA	NA	NA	NA	NA

NA: Not Applicable

Table 5.7: Maximum lateral deflection of noise barrier under wind loading at the wall top

Wind pressure (Pa)	Height of wall (m)	Lateral Wind load (kN)	Maximum lateral displacement of wall top (mm)				
			RPF-1x15	FPF-2x10	RPF-2x10	FPF-2x15	RPF-2x15
	1	1.75	5.5	2.7	1.2	1.9	0.7
	1.5	2.63	27.7	13.5	6.2	9.5	3.6
350	2	3.50	87.5	42.7	19.7	30.2	11.4
	2.5	4.38	NA	NA	48.0	73.7	27.9
	3	5.25	NA	NA	NA	NA	57.9
	1	2.00	6.3	3.0	1.4	2.2	0.8
	1.5	3.00	31.6	15.4	7.1	10.9	4.1
400	2	4.00	NA	48.8	22.5	34.5	13.1
	2.5	5.00	NA	NA	54.9	84.2	31.9
	3	6.00	NA	NA	NA	NA	66.2
	1	2.25	7.0	3.4	1.6	2.4	0.9
	1.5	3.38	35.6	17.4	8.0	12.3	4.7
450	2	4.50	NA	54.9	25.3	38.8	14.7
	2.5	5.63	NA	NA	NA	94.7	35.9
	3	6.75	NA	NA	NA	NA	74.4
	1	2.50	7.8	3.8	1.8	2.7	1.0
	1.5	3.75	39.6	19.3	8.9	13.6	5.2
500	2	5.00	NA	61.0	28.1	43.1	16.3
	2.5	6.25	NA	NA	NA	NA	39.9
	3	7.50	NA	NA	NA	NA	82.7
	1	2.75	8.6	4.2	1.9	3.0	1.1
	1.5	4.13	43.5	21.2	9.8	15.0	5.7
550	2	5.50	NA	67.1	30.9	47.4	18.0
	2.5	6.88	NA	NA	NA	NA	43.9
	3	8.25	NA	NA	NA	NA	91.0
	1	3.00	9.4	4.6	2.1	3.2	1.2
	1.5	4.50	47.5	23.2	10.7	16.4	6.2
600	2	6.00	NA	NA	33.7	51.7	19.6
	2.5	7.50	NA	NA	NA	NA	47.9
	3	9.00	NA	NA	NA	NA	99.3
	1	3.25	10.2	5.0	2.3	3.5	1.3
	1.5	4.88	51.4	25.1	11.6	17.7	6.7
650	2	6.50	NA	NA	36.5	56.0	21.2
	2.5	8.13	NA	NA	NA	NA	51.9
	3	9.75	NA	NA	NA	NA	107.5
	1	3.50	10.9	5.3	2.5	3.8	1.4
	1.5	5.25	NA	27.0	12.4	19.1	7.2
700	2	7.00	NA	NA	NA	60.3	22.9
	2.5	8.75	NA	NA	NA	NA	55.8
	3	10.50	NA	NA	NA	NA	NA

NA: Not Applicable

5.8 Shear design

Flexural failure is the predominant mode of failure of poly-wall and flexi-wall. It is due the fact that the aspect ratio of the wall (height over thickness) is always over 4 in practice and it is categorized as a flexural beam (ACI318-08, definition of deep beam). However, out-of-plane shear shall be also investigated for the case of non-uniform load applied to the wall as shown in Fig. 5.6. Soil pressure, unsynchronized wind load, abrupt change in height of the wall or other construction around the wall may induce non-uniformity in the lateral load distribution. For such cases, a tie beam needs to be incorporated into the wall as illustrated in Fig. 5.7 in order to connect all the RPF/LPF cores. In essence, the tie beam is a horizontal core, which consists of polyurethane filler and steel rebars. Its stiffness can be calculated similar to the vertical cores considering its boundary conditions. The tie beam enhances the shear capacity of the entire wall and also helps to distribute the load among the wall cores.
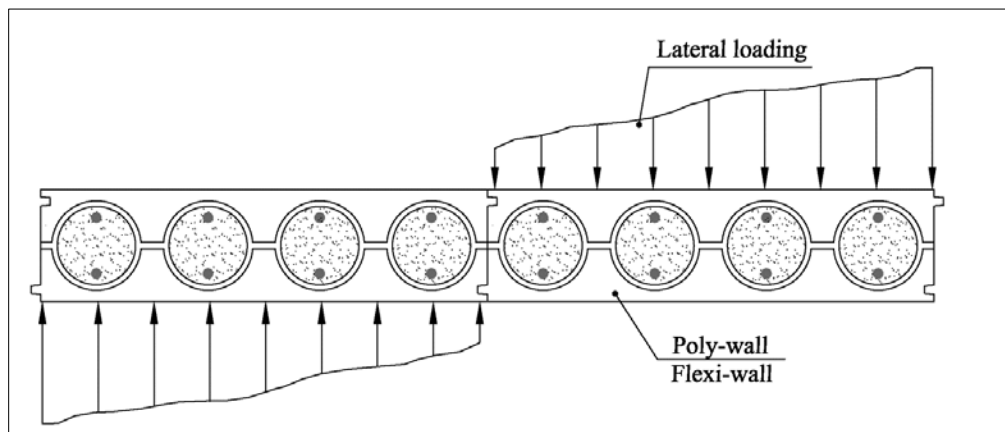
Figure 5.6: Non-uniform lateral loading on the wall

Shear capacity of the wall should be calculated where the out-of-plane shear stress of the wall exceeds the factored shear capacity of the poly-block at a shear plane. According to performed studies shear capacity of light foams in a plane perpendicular to foam rise is the half of its compressive capacity (Witkiewicz et al., 2006). As compressive capacity of poly-block is equal to 0.5 MPa, the shear capacity of the block in out-of-plane shear can be assumed 0.25 MPa.
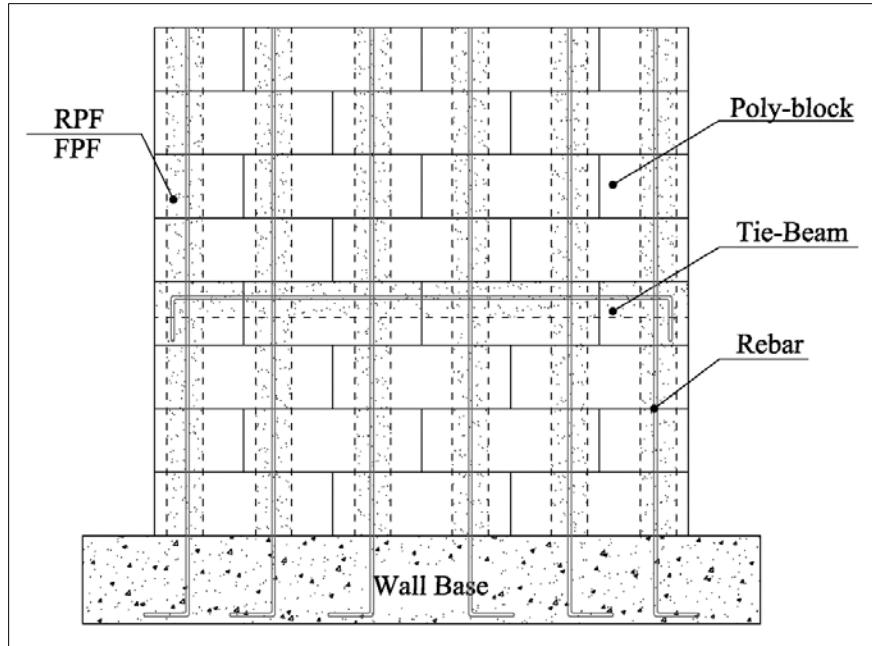
Figure 5.7: Non-uniform lateral loading on the wall

For example for a 1m heigh wall which includes 5 poly-blocks, shear failure occures once at least 2 blocks fail in a shear manner. Given the dimensions of poly-blocks and not considering polyurea shear strength, shear capacity of 2 blocks (V_b) equals to:

V_b=(block shear areas×shear strength)= 2×[200×200 mm]×0.25 MPa/1000=20 kN.

If the factored out-of-plane shear force exceeds 65% of this value (V_{rb}=13.5 kN) a tie beam is required to enhance the shear capacity of the wall.

As shown in Fig. 5.7 at least one rebar is requred to be embedded in the horizontal tie. Shear capacity (V_{rs}) of a 10M rebar according to ACI 318-08 can be calculated as follows:

$$V_{rs}=\varphi_s \, f_y \, A_v=0.9\times400\times78.5/1000=28.2 \ kN \tag{5.3}$$

where φ_s is resistance factor, f_y=400 MPa is steel yeild strength and A_v is area of steel rebar. Total factored shear capacity in this example for a wall with 1 meter height is equal to:

$$V_r = V_{rb} + V_{rs} = 13.5 + 28.2 \text{ kN} = 31.7 \text{ kN} \tag{5.4}$$

5.9 Common defects of the wall

The application of liquid polyurethane foam as a structural core of a building as well as application of polyurea coating as a finishing layer of such a wall system has never been reported in the literatures. Due to limited experience working with this material and their application, some issues arose during the foam injection and polyurea spraying which are listed in followings.

1. According to experimental observations, once foams were not continuously injected, a big crack appeared in the wall core as a result of pause in injection. As shown in Figs. 5.8 and 5.9, the top portion of the core was not properly connected to the bottom part since the bottom part has already cured. This happened once an assembly of three poly-blocks incontinuesly filled due to a leakage of the bottom block.

   Similarly, a crack may develop in the cores due to the leakage of foam. If the liquid foam leaks during injection, an excessive expansion occurs to fill the volume of leaked liquid, which results in creating a crack in the cores.

2. The application of foam liquids in construction should be done with extra caution. Although spraying polyurea on the surface of poly-blocks seals up most of joints and seams between the blocks and foundations, even a small pore may cause leakage. The expansion of liquid foam results in opening tiny holes, which subsequently causes more leakage. In the experimental phase of the current study, all joints were sealed using epoxy and silicon; however, as shown in Fig. 5.10 the leakage was inevitable. This affects the wall quality in terms of aesthetic and reliability aspects.

Figure 5.8: Crack in wall cores due to a puase in injection

Figure 5.9: Crack in wall cores due to leakage

Figure 5.10: leakage of the liquid foam

3. The expansion of foam, particularly FPF, may detach the blocks as displayed in Fig. 5.11. The blocks should be properly glued where high expansion is expected. This can be achieved by filling all the wall cores simultaneousely to avoid unsymmetric expansion in the cores

4. The temprature of liquid foam during the injection should be regularly checked, especially once RPF is injected to the walls.According to the experimental observations, if the temprature of RPF mix exceeds 65^0C the blocks may inflate or deform as shown in Fig. 5.12. High temprature and expansive pressure of foam induce a deformation in poly-blocks.

5. Polyurea layer is the finishing surface of the wall. Therefore, its qulity should be closely monitored for aesthetic aspect of the wall. During the experimental phase of the current study, it was obsereved that working temprature and pressure of the pump influenced the characteristics of polyurea. Low pressure and tempreture increased the polyurea gel time and resulted in dripping and accumulation of the polyurea as shown in Fig. 5.13.

Figure 5.11: Block separation due to expansion of the FPF

Figure 5.12: Wall inflation due to excessive heat

Figure 5.13: Polyurea dripping on the wall surface

5.10 Recommendations for construction

The structural performance and quality of the wall completely depend on the construction procedure. The main underlying assumption of the described design procedure is homogeneity of the material. As the construction issues were specified in the previous section, if the described construction approach is not accurately followed, the quality of RPF cannot be achieved and consequently the expected structural performance will not be obtained. Hence, according to the experimental experience below recommendations should be considered during the construction of the wall.

- The quality of RPF and LPF mixtures significantly varies with temperature and pressure variation. These two parameters should be kept constant during the injection of foam.

  Variability of these parameters may result in sever inhomogeneity of the material and less lateral resistance.

- The liquid foams should be continuously injected to the blocks. This is the key point in construction of poly-wall and flexi-wall since wall cores lose their integrity and split in parts if injection is paused. The disconnectivity of cores will

considerably reduce the strength and stiffness of the wall which is against the assumption of the design procedure.

- It is recommended that where the wall is exposed to public, a thick layer of polyurea is applied since sharp objects may puncture the surface of the wall. A layer of shotcrete is a good alternative to polyurea especially where FPF foam is injected. This is due to the fact that shotcrete enhances the stiffness and lateral strength of the wall in addition to superficial resistance. Fig. 5.14 displays a sound wall consists of concrete cores and poly-blocks which are covered by a shotcrete layer.

Figure 5.14: Utilization of Poly-block with concrete cores in construction project of West Los Angeles Community College (Lexicon website)

5.11 Summary and conclusions

A procedure was described in this chapter to design poly-wall/flexi-wall system as a noise barrier. Construction method, structural system and different loading condtions were dicussed and some recommendations for reliability of the wall system were made. According to the provided design data the following conclusion can be made.

1. The main failure mechanism of the poly is flexral mode. Since the aspect ratio of the wall (height/thickness) is practically gretear than 4, it always behave similar to a flexural beam. The described experimental obserevations in the previous

chaptesrs reaffirm this conclusion as all the full-scale wall models failed in a flexural manner due to a lateral loading.

2. According to the Tables 5.3, 5.6 and 5.7, the proposed wall system is constructable with an acceptable range of height in most of the cities of Canada. The provided design examples showed that if a suitible type of wall and reinforcement arrangement is selected, the lateral stength and deflection of the wall agains wind loading will be sufficent according to the building codes requirements.

3. The structural defects which were observed and reported in this chapter, emphasize the fact that the quality control of the material is a key point in the application of the wall. Tempreture of the mix liquid, pump pressure and continouse injection should be closely monitored during the construction phase, since they all termendously affect the mechanical properties of the wall.

5.12 References

American Association of State Highway and Transportation Officials (AASHTO) (2004). AASHTO LRFD Bridge Design Specifications, 3rd ed. Washington, DC.

ACI 318-08 (2005). Building Code Requirements for Structural Concrete and Commentary. ACI Committee 318. Structural Building Code, American Concrete Institute, Farmington Hills, MI, USA.

Canadian Standard Association. (2006). "CAN/CSA-S6-06 Canadian Highway Bridge Design Code." Mississauga, Ontario, Canada.

Canadian Standard Association. (2009). "CAN/CSA-G30.18-09 Carbon Steel Bars for Concrete Reinforcement", Mississauga, Ontario, Canada.

NBCC. (2005). "National Building Code of Canada", National Research Council of Canada (NRC), Ottawa, Canada.

The Lexicon Company Ltd., *http://www.lexiconbuildingsystems.com*, January, 2015.

Witkiewicz, W., and Zieliński, A. (2006). "Properties of the Polyurethane (Pu) Light Foams. "Advances in Materials Science, 6(2), 35-52.

Chapter 6

Conclusions and Future Works

6.1 Summery and conclusions

The application of polyurethane products in accelerated construction of noise barriers was investigated in this research. Extensive numerical and experimental analyses were conducted to establish the structural performance of the walls using polyurethane products. Poly-wall comprised of poly-blocks, rigid polyurethane foam (RPF) and polyurea coating was proposed, developed and investigated for construction of new sound barriers. For this purpose, mechanical behavior of RPF was characterized by performing tensile, compression, modulus of elasticity, Poisson's ratio, flexural, shear, pull-out, cyclic and long-term creep tests which totals over 100 specimen tests. Five full-scale walls were also fabricated and their lateral resistances in lateral static and cyclic loading were established.

Flexi-wall comprised of poly-blocks, light polyurethane foam (LPF) and polyurea coating was also proposed, developed and investigated for construction of extension to existing sound barriers. For this purpose 8 compression and pull-out tests were carried out on LPF to characterize its mechanical properties for the wall design. Then, three full scale walls were fabricated and their lateral resistances in static and cyclic loading were established similar to poly-wall.

A detailed 3D finite element model of the wall components were simulated and then calibrated with specimen test results. All calibrated elements were put together and a sophisticated 3D finite element model of both poly-wall and flexi-wall were developed including all interfaces and element contacts. Finally results of the finite element analyses were compared with the obtained results of full scale wall experiments. The analyses were furthered by investigation of structural behavior of both poly-wall and flexi-wall under different lateral and vertical loading conditions. The results of all FE and

experimental analyses provided a base to develop a complete design guideline of both proposed wall system.

The following conclusion can be drawn according to the outcomes of the study.

1- Conducted acoustic tests has proved a high Sound Transmission Class rating for the proposed wall system and confirmed the suitability of the proposed wall system as a noise barrier.

2- Applicability and constructability of the poly-wall and flexi-wall in accelerated construction of sound walls were proved through an extensive experimental program. The combination of poly-block, polyurea and polyurethane filler was found very compatible and simple in practice.

3- Mechanical Properties of RPF are completely comparable to other engineering materials such as concrete. The results illustrated that RPF is a competent alternative to conventional material for specific applications.

4- Polyurea coating demonstrated an excellent abrasion resistance according to the standard tests.

5- Structural behaviour of poly-wall under static and cyclic lateral load was found completely satisfactory. This wall system can be built in road side construction easier, faster and less obstructive than other types of wall.

6- Numerical model developed for all components of the wall as well as full-scale poly-wall and flexi-wall illustrated fairly good agreements with the corresponding experimental data.

7- Results of parametric studies indicated that vertical loading has negligible effects on lateral strength of poly-wall up to 0.5 MPa for both types of reinforcement. Reduction factors of lateral strength of poly-wall due to vertical load were established for design application.

8- The equivalent beam models of the poly-wall and flexi-wall were verified with the numerical outcomes and a set of design tables was provided accordingly. Theses tables may be employed to design and calculate the lateral displacement of the walls with reasonable accuracy.

9- The lateral resistance of flexi-wall was achieved highly acceptable for noise barrier renewal. The cyclic response of flexi-wall although is not as adequate as poly-wall, will be quite decent for the short extension of existing barriers.

10- The main failure mechanism of the poly-wall and flexi-wall is flexral mode. Since the aspect ratio of the wall (height/thickness) is practically gretear than 4, it always behave similar to a flexural beam.

11- The described experimental obserevations in the previous chaptesrs reaffirm that the first deterioration occures at the conncetion of the wall and foundation. Therefore, a proper connection should be cautiousely built as recommended for the walls.

12- According to the provided design tables, the proposed wall system is constructable with an acceptable range of height in most of the cities of Canada. The provided design examples showed that if a suitible type of wall and reinforcement arrangement is selected, the lateral stength and deflection of the wall agains wind loading will be suffcent according to the building codes requirements.

13- The structural defects which were observed and reported in this chapter, emphasize the fact that the quality control of the material is a key point in the application of the wall. Tempreture of the mix liquid, pump pressure and continouse injection should be closely monitored during the construction phase, since they all termendously affect the mechanical properties of the wall.

6.2 Recommendations for future research

Some further studies might be useful in the application of polyurethane products in construction.

1- Combine aggregates and RPF to produce a high strength mix with more homogeneous properties.

2- Examine different combination of resin and urethane to find the best temprature and pressure for RPF and LPF injection.

3- Investigate the effects of a tie beam in lateral performance of the wall through full-scale experiments.

4- Conduct a wind load testing using Pneumatic Linear Actuators (PLA) or Wind tunnel testing.

5- Investigate the effect of freez-thaw cycles on mechanical characteritics of the polyurathne foams.

6- Perform a statistical analysis to increase the recommended factor of safetey of the material and therby their reliability.

Curriculum Vitae

Name: Bahman Daee

Post-secondary Education and Degrees:

Civil Engineering, Chamran University
Ahvaz, Iran
2001-2006 B.Sc.

Structural and Earthquake Engineering, TMU of Tehran
Tehran, Iran
2006-2008 M.Sc.

Structural Engineering, Western University
London, Ontario, Canada
2011-2015 Ph.D.

Honours and Awards:

Industrial Postgraduate Scholarship NSERC-IPS
Western University, 2012-2015

Western Graduate Research Scholarship
Western University, 2011-2015

Graduate Research Assistant Scholarship
Western University, 2011-2015

Western Graduate Teaching Assistantship
Western University, 2011-2015

Related Work Experience

Associate Structural Engineer
Giffin Koerth, Toronto, ON
2015-Present

Structural Engineer/ Research Assistant
Poly-mor Canada Inc. London, ON
2012-2015

Lead Structural Engineer
Tehran Raymand Consulting Eng. Tehran, Iran
2008-2011

Structural Engineer
Rahshahr Int. Consulting Eng. Tehran, Iran
2007-2008

Publications:

B. Daee, M.H. El Naggar. "Application of Polyurethane Products in Accelerated Construction of an Innovative Noise Barrier: Experimental study."(2015) "Journal of Composite Materials" (under review)

B. Daee, M.H. El Naggar. "Application of Polyurethane Products in Accelerated Construction of an Innovative Noise Barrier: Numerical study."(2015) "Journal of Construction and building materials" (under review)

B. Daee, M.H. El Naggar. "Application of Flexi-wall in Noise Barriers Renewal."(2015) "Journal of Case Studies in Construction Materials" (under review)

B. Daee, A.A. Aghakouchak. "Assessment of Nonlinear Static Procedures for Determination of Target Displacement in Asymmetric Buildings" Journal of Advances in Structural Engineering, Vol. 15, No. 8, Aug. 2012, pp.1265-1279.

B. Daee, A.A. Aghakouchak. "Code Assessment of Determination of Target Displacement in Non-Linear Static Analysis", 8th International Conference of Civil Engineering, Shiraz ,Iran (Sept. 2008)